Electronic Supplementary Material (ESI) for Journal of Materials Chemistry A.

Supporting Information

Thiophene-Fused Boron Dipyrromethenes as Energy Efficient Near-Infrared Photocatalysts for Radical Polymerizations

Alex Stafford[a], Seth R. Allen[a], Tod A. Grusenmeyer[b], Connor J. O'Dea[a], Laura Estergreen[a], Sean T. Roberts[a]*, Zachariah A. Page[a]*

[a]Department of Chemistry, The University of Texas at Austin, Austin, Texas 78712, United States

[b]Air Force Research Laboratory, Materials and Manufacturing Directorate, Wright-Patterson Air Force Base, OH 45433, USA

Corresponding authors: * roberts@cm.utexas.edu and zpage@cm.utexas.edu

Table of Contents

EXPERIMENTAL DETAILS

Synthesis

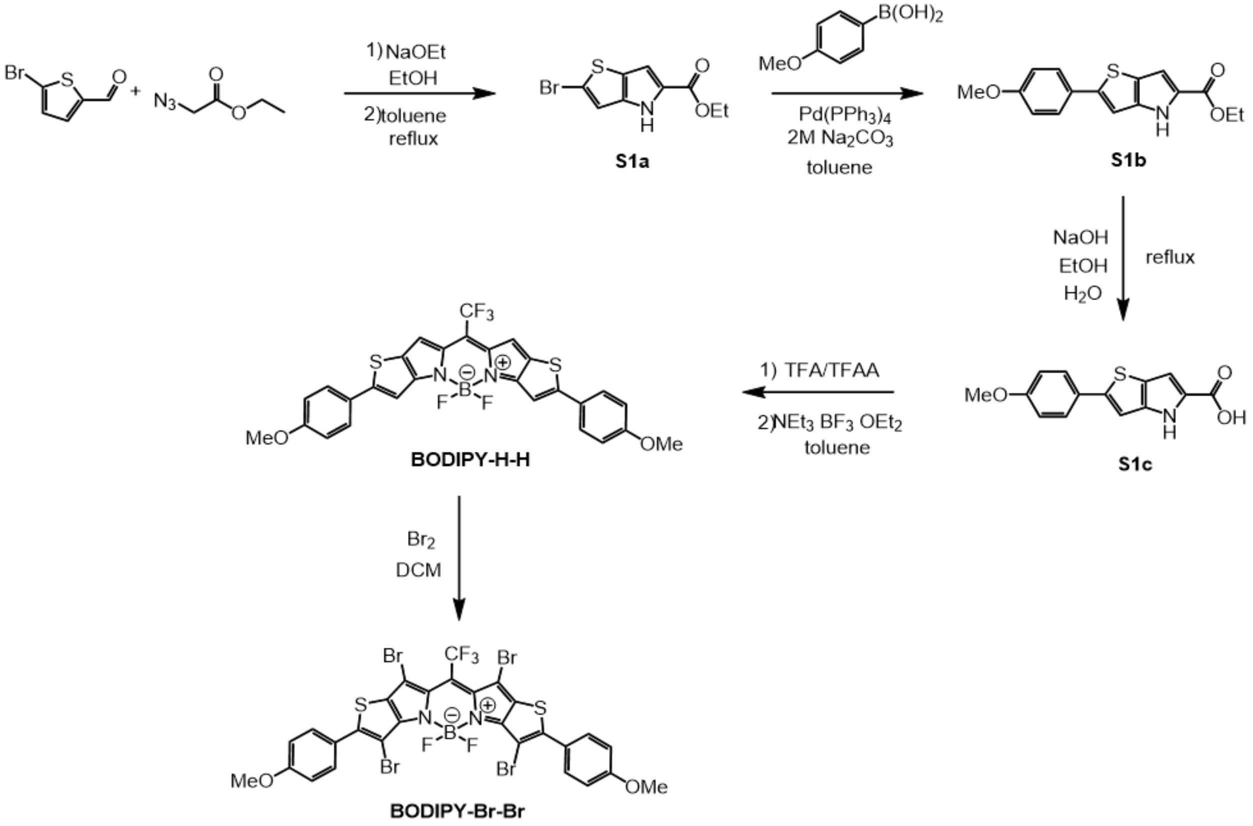

Scheme S1. Synthesis of **BODIPY-H-H** and **BODIPY-Br-Br**.

Synthesis of ethyl 2-bromo-4*H*-thieno[3,2-*b*]pyrrole-5-carboxylate (S1a). Sodium ethoxide (5.0 g, 74 mmol, 4.40 eq.) in 40 mL of ethanol was added dropwise over 20 mins to a mixture cooled in an ice bath of 5-bromothiophene-2-carbaldehyde (3.2 g, 2.0 mL, 17 mmol, 1 eq.) and ethyl 2-azidoacetate (8.0 g, 7.2 mL, 62 mmol, 3.70 eq.) in ethanol (20 mL) in a 250 mL 2-neck round bottom flask equipped with a magnetic stir-bar, inlet adapter, and septum under a nitrogen atmosphere. The mixture was left to stir overnight (16 hr). The reaction was quenched with saturated $NH_4Cl_{(aq)}$ and extracted with ethyl acetate (3 × 30 mL). Solvent was removed under reduced pressure, providing the crude product as a yellow oil. The crude product was used without further purification by dissolving it in 30 mL of toluene and refluxing for 1.5 hr. The mixture was cooled to room temp and the solvent was removed under reduced pressure. The subsequent brown solid was purified via column chromatography (1:10 EtOAc:Hexanes) to yield the desired product as a yellow solid (2.49 g, 54% yield). ^{1}H NMR (400 MHz, $CDCl_3$) δ 9.06 (s, 1H), 7.04 (s, 1H), 7.02 (s, 1H), 4.33-4.39 (q, *J* = 7.1 Hz, 2H), 1.36-1.40 (t, *J* = 7.2 Hz, 3H); ^{13}C NMR (100 MHz, $CDCl_3$) δ 161.9, 139.4, 126.4, 124.9, 116.3, 114.6, 107.5, 61.0, 14.6; IR (ATR): 3270, 3060, 2974, 1677, 1525, 1469, 1444, 1384, 1283, 1181, 1092, 1016, 929, 926, 864, 839, 805, 757, 681 cm^{-1}; HRMS (APCI): exact mass calculated for $C_9H_8BrNO_2S$ $[M+H]^+$ 273.9459, found 273.9533.

Synthesis of ethyl 2-(4-methoxyphenyl)-4*H*-thieno[3,2-*b*]pyrrole-5-carboxylate (S1b). Ethyl 2-bromo-4*H*-thieno[3,2-*b*]pyrrole-5-carboxylate (**S1a**) (700 mg, 2.55 mmol, 1 eq.) , $Pd(PPh_3)_4$ (49.3 mg, 42.6 µmol, 0.0167 eq.), and (4-methoxyphenyl)boronic acid (776 mg, 5.11 mmol 2 eq.) were added to a 100 mL 2-neck round bottom flask equipped with a magnetic stir bar, condenser, inlet adapter, and septum. The atmosphere was removed under reduced pressure and refilled with argon three times. Toluene (10 mL) and 2M Na_2CO_3 (10 mL) were degassed with argon for 10 minutes and added to the round bottom flask, followed by vigorous stirring at 90 °C for 12 hr. After cooling down to room temperature, the reaction mixture was washed with brine (3 × 20 mL) and the organic layer was dried over anhydrous $MgSO_4$, filtered, and concentrated under reduced pressure. The residue was purified via column chromatography (silica, hexane: dichloromethane = 1:2, v/v) to yield a yellow solid (695 mg, 90% yield). ^1H NMR (400 MHz, $CDCl_3$) δ 8.98 (s, 1H), 7.54-7.56 (d, *J* = 8.8 Hz, 2H), 7.11 (s, 1H), 7.07 (s, 1H), 6.92-6.94 (d, *J* = 8.8 Hz, 2H), 4.34-4.39 (q, *J* = 7.1 Hz, 2H), 3.85 (s, 3H), 1.39 (t, *J* = 7.1 Hz, 3H); ^{13}C NMR (100 MHz, $CDCl_3$) δ 161.6, 159.6, 148.1, 141.8, 127.9, 127.7, 127.1, 114.4, 114.2, 107.9, 106.0, 60.6, 55.4, 14.5; IR (ATR): 3305, 2919, 2850, 1667, 1604, 1536, 1510, 1461, 1400, 1275, 1250, 1194, 1110, 1070, 965, 934, 870, 824, 805, 758, 720, 697, 678, 630, 582 cm^{-1}; HRMS (APCI): exact mass calculated for $C_{16}H_{15}NO_3S$ $[M+H]^+$ 302.0773, found 302.0849.

Synthesis of 2-(4-methoxyphenyl)-4*H*-thieno[3,2-*b*]pyrrole-5-carboxylic acid (S1c). Ethyl 2-(4-methoxyphenyl)-4*H*-thieno[3,2-*b*]pyrrole-5-carboxylate (**S1b**) (350 mg, 1.16 mmol 1 eq.) was dissolved in EtOH (10 mL) in a 100 mL round bottom flask equipped with a magnetic stir-bar. Next, sodium hydroxide (0.72 g, 18.1 mmol,15.6 eq.) in water (5 mL) was added to the flask and refluxed for 1 hr. The reaction was cooled to room temperature and then chilled in an ice bath and subsequently acidified with concentrated HCl, resulting in a precipitate, which was filtered, washed with water, and dried under reduced pressure to yield the desired product as a brownish-green solid (274 mg, 86% yield). ^1H NMR (400 MHz, DMSO) δ 11.95 (s, 1H), 7.60-7.62 (d, *J* = 2.0 Hz, 1H), 7.24 (s, 1H), 7.02 (s, 1H), 6.97-7.00 (d, *J* = 8.8 Hz, 2H), 3.79 (s, 3H); ^{13}C NMR (100 MHz, DMSO) δ 162.2, 159.1, 145.8, 142.4, 127.4, 127.0, 126.7, 121.8, 114.6, 107.2, 107.0, 55.3; IR (ATR): 3397, 2921, 2851, 1653, 1606, 1567, 1515, 1502, 1485, 1421, 1404, 1393, 1337, 1294, 1179, 1111, 1032, 1013, 936, 821, 797, 721, 631, 601 cm^{-1}; HRMS (APCI): exact mass calculated for $C_{14}H_{11}NO_3S$ $[M+H]^+$ 274.0460, found 274.0533.

Synthesis of 5,5-difluoro-2,8-bis(4-methoxyphenyl)-11-(trifluoromethyl)-5*H*-4λ^4,5λ^4-thieno[2',3':4,5]pyrrolo[1,2-*c*]thieno[2',3':4,5]pyrrolo[2,1-*f*][1,3,2]diazaborinine (BODIPY H-H)
2-(4-methoxyphenyl)-4*H*-thieno[3,2-*b*]pyrrole-5-carboxylic acid (590 mg, 2.16 mmol, 1 eq.), was dissolved in TFA (20 mL), placed in a 100 mL pressure flask open to air and heated to 40 °C for 15 minutes. The reaction became an intense red color. Subsequently, trifluoroacetic anhydride (6 mL, 42.5 mmol, 19.7 eq.) was added and the flask was sealed and heated to 80 °C with continued stirring for 1 hour. The reaction turned a deep blue color and was allowed to cool to room temperature, followed by pouring it into a saturated aqueous $NaHCO_3$ solution containing crushed ice. The resultant precipitate was then filtered and dried under reduced pressure. The dry solid was then dissolved in toluene (30 mL) in a 250 mL 2-neck round bottom flask equipped with a magnetic stir-bar, inlet adapter, and septum under a nitrogen atmosphere and stirred for 5 min at room temperature. Next, boron trifluoride diethyletherate (2 mL, 15.8 mmol, 7.3 eq.) and NEt_3 (1 mL, 7.17 mmol, 3.32 eq.) were added and the reaction mixture was stirred at 80 °C for 1 hour under a nitrogen atmosphere. The crude mixture was washed with brine (3 × 20 mL), dried with anhydrous $MgSO_4$, filtered, and concentrated under reduced pressure to yield the crude product. Purification via recrystallization in 200 mL of THF:MeOH (1:20) was accomplished by dissolving the crude solid in a small amount of THF (5-10 mL) and then diluting with excess methanol to 200 mL. The flask was subsequently placed in a -20°C freezer for ~16 hours. The desired product was then isolated as a black solid via filtration (213 mg, 17% yield). ^1H NMR (400 MHz, $CDCl_3$) δ 7.68-7.70 (d, *J* = 8.8 Hz, 4H), 7.33 (s, 2H), 7.27 (s, 2H), 6.97-6.99 (d, *J* = 8.8 Hz, 4H), 3.87 (s, 6H); ^{13}C NMR (100 MHz, $CDCl_3$) δ 162.8, 162.0, 128.5, 126.8, 118.3, 114.9, 107.9, 77.4, 55.7, 29.9; IR (ATR): 3368, 2919, 1569, 1536, 1517, 1469, 1413, 1337, 1308, 1284, 1200, 1071, 1026, 970, 955, 918, 826, 800, 759, 732, 673, 595 cm^{-1}; HRMS (APCI): exact mass calculated for $C_{28}H_{18}BF_5N_2O_2S_2$ $[M+Na]^+$ 607.0721, found 607.0712.

Synthesis of 3,7,10,12-tetrabromo-5,5-difluoro-2,8-bis(4-methoxyphenyl)-11-(trifluoromethyl)-5*H*-4λ^4,5λ^4-thieno[2',3':4,5]pyrrolo[1,2-*c*]thieno[2',3':4,5]pyrrolo[2,1-*f*][1,3,2]diazaborinine (BODIPY Br-Br). 5,5-difluoro-2,8-bis(4-methoxyphenyl)-11-(trifluoromethyl)-5*H*-4λ^4,5λ^4-

thieno[2',3':4,5]pyrrolo[1,2-*c*]thieno[2',3':4,5]pyrrolo[2,1-*f*][1,3,2]diazaborinine (**BODIPY H-H**) (60 mg, 0.10 mmol, 1 eq.) was dissolved in CH_2Cl_2 (5 mL) and added to a 100 mL round bottom flask equipped with a magnetic stir-bar. Bromine (0.20 g, 63 µL, 1.2 mmol, 12 eq.) in CH_2Cl_2 (5 mL) was added dropwise and stirred at 40 °C for ~16 hours. The reaction mixture was neutralized with a saturated aqueous Na_2CO_3 solution (20 mL), and the aqueous layer was separated from the organic layer. The aqueous layer was further extracted with diethyl ether (3 × 20 mL) and the combined organic layers were dried over anhydrous Na_2SO_4, filtered, and concentrated under reduced pressure to yield the desired product as a black solid (33 mg, 36% yield). ^{1}H NMR (400 MHz, $CDCl_3$) δ 7.77-7.79 (d, *J* = 8.8 Hz, 4H), 7.01-7.03 (d, *J* = 8.8 Hz, 4H), 3.90 (s, 6H); ^{13}C NMR (100 MHz, $CDCl_3$) δ 162.0, 161.5, 157.0, 155.1, 131.0, 130.4, 129.6, 126.0, 125.2, 114.6, 114.5, 77.4, 55.7; IR (ATR): 2920, 2837, 1597, 1567, 1508, 1452, 1435, 1389, 1356, 1297, 1162, 1117, 1096, 1053, 1025, 985, 954, 754, 730, 598 cm^{-1}; HRMS (APCI): exact mass calculated for $C_{28}H_{14}BBr_4F_5N_2O_2S_2$ [M+H]$^+$ 896.7243, found 896.8773.

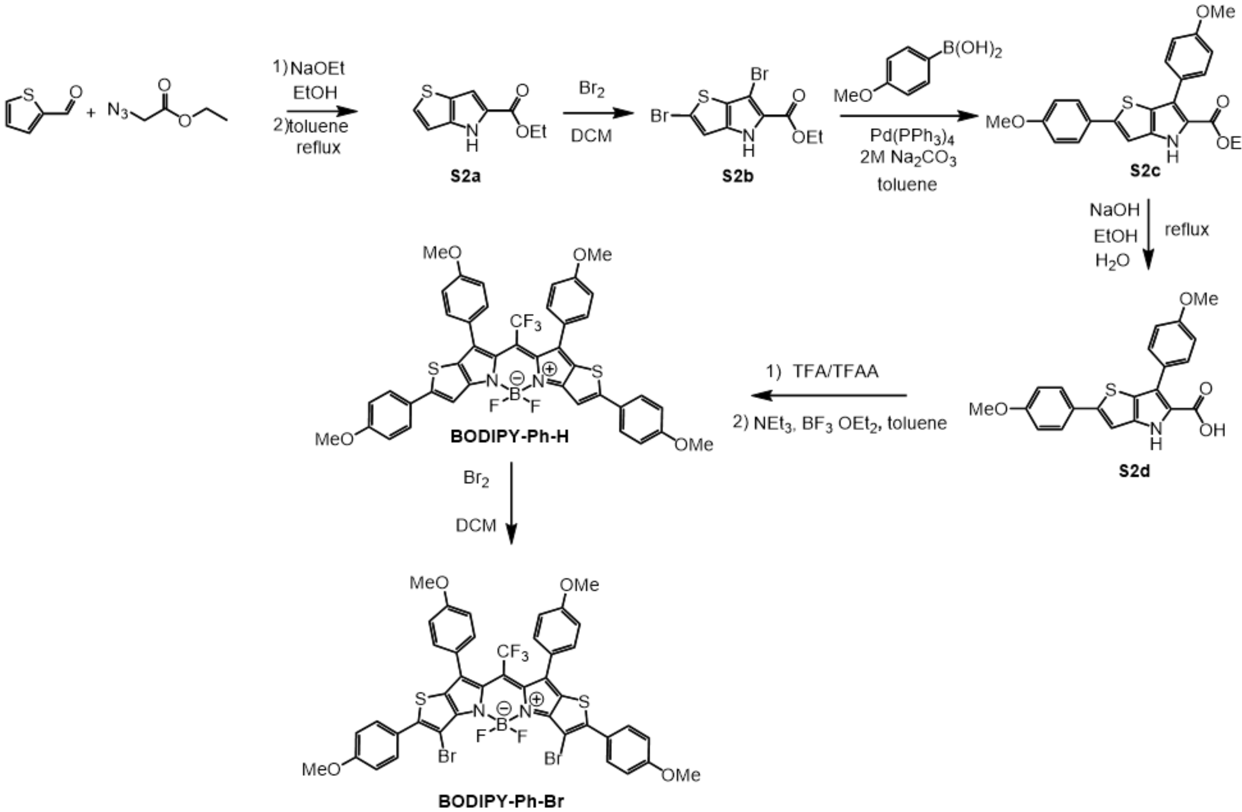

Scheme S2. Synthesis of **BODIPY-Ph-H** and **BODIPY-Ph-Br**.

Synthesis of ethyl 4*H*-thieno[3,2-*b*]pyrrole-5-carboxylate (S2a). Thiophene-2-carbaldehyde (2.4 g, 2.0 mL, 21 mmol, 1 eq.) and ethyl 2-azidoacetate (10 g, 9.1 mL, 79 mmol, 3.7 eq.) was dissolved in ethanol (20 mL) in a 250 mL 2-neck round bottom flask equipped with a magnetic stir-bar, inlet adapter, and septum under a nitrogen atmosphere. The reaction mixture was cooled in an ice bath followed by dropwise addition of sodium ethoxide (6.4 g, 94 mmol, 4.40 eq.) in 40 mL of ethanol over the course of 20 mins. The reaction was allowed to warm to room temperature and stirred for ~16 hours, followed by quenching with saturated aqueous NH_4Cl. The aqueous mixture was extracted with ethyl acetate (3 × 30 mL). The organic layers were combined, dried with anhydrous $MgSO_4$, filtered, and concentrated under reduced pressure. The yellow oil residue was dissolved in 30 mL of toluene and refluxed for 1.5 hours, followed by cooling to room temperature and concentrating under reduced pressure to yield the desired product as an orange solid (1.87 g, 45% yield). ^{1}H NMR (400 MHz, $CDCl_3$) δ 9.11 (s, 1H), 7.32-7.33 (d, *J* = 5.3 Hz, 1H), 7.14-7.15 (d, *J* = 1.7 Hz, 1H), 6.95-6.97 (d, *J* = 5.3 Hz, 1H), 4.34-4.40 (q, *J* = 7.1 Hz, 2H), 1.37-1.41 (t, *J* = 7.1 Hz, 3H); ^{13}C NMR (100 MHz, $CDCl_3$) δ 161.6, 141.2, 129.4, 126.8, 114.3, 111.1, 107.5, 60.7, 14.5; IR (ATR): 3418, 2986, 2958, 1665, 1539, 1475, 1452, 1370, 1305, 1243, 1085, 1017, 868, 761, 726, 688 cm^{-1}; HRMS (APCI): exact mass calculated for $C_9H_9NO_2S$ $[M+H]^+$ 196.0354, found 196.0422.

Synthesis of ethyl 2,6-dibromo-4*H*-thieno[3,2-*b*]pyrrole-5-carboxylate (S2b). Ethyl 4*H*-thieno[3,2-b]pyrrole-5-carboxylate (**S2a**) (200 mg, 1.02 mmol, 1 eq.) was dissolved in 80 mL of CH_2Cl_2 in a 250 mL round bottom flask equipped with a magnetic stir-bar. To the mixture was added dropwise a solution of bromine (327 mg, 106 µL, 2.05 mmol, 2 eq.) in 30 mL of CH_2Cl_2 over 30 minutes. The solution was stirred for an additional 1 hour after complete addition, followed by concentrating under reduced pressure to yield a crude residue. Purification of the residue was accomplished by recrystallization from 40 mL of EtOH:H_2O (1:5) by dissolving in a small amount of EtOH and diluting with H_2O. Filtration provided the desired product as a brown solid (357 mg, 99% yield). ^{1}H NMR (400 MHz, $CDCl_3$) δ 9.17 (s, 1H), 7.03 (s, 1H), 4.37-4.43 (q, *J* = 7.1 Hz, 2H), 1.40-1.43 (t, *J* = 7.1 Hz, 3H); ^{13}C NMR (100 MHz, $CDCl_3$) δ 161.0, 137.8, 127.6, 123.1, 117.2, 115.0, 95.4, 61.4, 14.5; IR (ATR): 3280, 2981, 2901, 1542, 1529, 1476, 1465, 1404, 1386, 1291, 1259, 1193, 1178, 1088, 1036, 1017, 974, 930, 879, 862, 799, 696, 655 cm^{-1}; HRMS (APCI): exact mass calculated for $C_9H_7Br_2NO_2S$ $[M+H]^+$ 351.8564, found 353.8614.

Synthesis of ethyl 2,6-bis(4-methoxyphenyl)-4*H*-thieno[3,2-*b*]pyrrole-5-carboxylate (S2c). Ethyl 2,6-dibromo-4*H*-thieno[3,2-*b*]pyrrole-5-carboxylate (**S2b**) (700 mg, 1.98 mmol, 1 eq.), $Pd(PPh_3)_4$ (38.3 mg, 33.1 µmol, 0.0167 eq.), and (4-methoxyphenyl)boronic acid (904 mg, 5.95 mmol, 3 eq.) were added to a 100 mL 2-neck round bottom flask equipped with a magnetic stir bar, condenser, inlet adapter, and septum. The atmosphere in the flask was removed under reduced pressure and refilled with argon three times. Toluene (10 mL) and 2M Na_2CO_3 (10 mL) degassed with argon for 10 minutes were then added to the round bottom flask, which was then stirred vigorously and heated to 90 °C for 12 hours. The reaction mixture was cooled down to room temperature, washed with brine (3 × 20 mL), and the organic layer was dried over anhydrous $MgSO_4$, filtered, and concentrated under reduced pressure. The resulting residue was purified using column chromatography (silica, hexanes:CH_2Cl_2 = 1:2, v/v). Concentrating the desired band yielded the product as a brown solid (757 mg, 94% yield). ^{1}H NMR (400 MHz, $CDCl_3$) δ 9.05 (s, 1H), 7.69-7.71 (d, *J* = 8.8 Hz, 2H), 7.54-7.56 (d, *J* = 8.8 Hz, 2H), 7.08 (s, 1H), 6.97-6.99 (d, *J* = 8.8 Hz, 2H), 6.92-6.94 (d, *J* = 8.8 Hz, 2H), 4.29-4.34 (q, *J* = 7.1 Hz, 2H), 3.87 (s, 3H), 3.84 (s, 3H), 1.30-1.33 (t, *J* = 7.1 Hz, 3H); ^{13}C NMR (100 MHz, $CDCl_3$) δ 161.5, 159.8, 159.1, 148.5, 140.1, 130.8, 127.9, 127.2, 126.2, 124.5, 120.5, 114.5, 114.3, 113.6, 106.2, 60.6, 55.5, 55.4, 14.5; IR (ATR): 3270, 2982, 2934, 1663, 1607, 1575, 1503, 1464, 1405, 1384, 1283, 1200, 1176, 1111, 1031, 933, 868, 807, 686 cm^{-1}; HRMS (APCI): exact mass calculated for $C_{23}H_{21}NO_4S$ $[M+Na]^+$ 430.1089, found 430.1085.

Synthesis of 2,6-bis(4-methoxyphenyl)-4*H*-thieno[3,2-*b*]pyrrole-5-carboxylic acid (S2d). Ethyl 2,6-bis(4-methoxyphenyl)-4*H*-thieno[3,2-*b*]pyrrole-5-carboxylate (**S2c**) (600 mg, 1.47 mmol 1 eq.) was dissolved in EtOH (10 mL) in a 100 mL round bottom flask equipped with a magnetic stir-bar. Next, sodium hydroxide (1.6 g, 39.8 mmol 27 eq.) in water (5 mL) was added and refluxed for 1 hour. The reaction was cooled to room temperature and then chilled in an ice bath. The mixture was subsequently acidified with concentrated HCl, resulting in a precipitate that was filtered, washed with water, and dried under reduced pressure to yield the desired product as a brownish-green solid (526 mg, 94% yield). ^{1}H NMR (400 MHz, $CDCl_3$) δ 9.13 (s, 1H), 7.70-7.72 (d, *J* = 8.3 Hz, 2H), 7.55-7.57 (d, *J* = 8.6 Hz, 2H), 7.09 (s, 1H), 6.99-7.01 (d, *J* = 8.6 Hz, 2H), 6.92-6.94 (d, *J* = 8.5 Hz, 2H), 3.87 (s, 3H), 3.85 (s, 3H); ^{13}C NMR (100 MHz, DMSO) δ 162.5, 159.2, 158.2, 145.5, 140.1, 130.2, 127.3, 127.2, 126.7, 126.4, 126.2, 125.3, 114.6, 114.4, 113.5, 107.3, 55.3, 55.1; IR (ATR): 3411, 2933, 2837, 1644, 1606, 1573, 1526, 1487, 1452, 1419, 1357, 1292, 1247, 1177, 1113, 1031, 984, 935, 801, 609 cm^{-1}; HRMS (APCI): exact mass calculated for $C_{21}H_{17}NO_4S$ $[M+H]^+$ 380.0878, found 380.0949.

Synthesis of 5,5-difluoro-2,8,10,12-tetrakis(4-methoxyphenyl)-11-(trifluoromethyl)-5*H*-4λ^4,5λ^4-thieno[2',3':4,5]pyrrolo[1,2-*c*]thieno[2',3':4,5]pyrrolo[2,1-*f*][1,3,2]diazaborinine (BODIPY-Ph-H). 2,6-bis(4-methoxyphenyl)-4*H*-thieno[3,2-*b*]pyrrole-5-carboxylic acid (**S2d**) (300 mg, 791 µmol, 1 eq.) was dissolved in TFA (15 mL) in a 100 mL pressure flask open to air and heated to 40 °C for 15 minutes, resulting in an intense green color. The pressure flask was cooled to room temperature, and trifluoroacetic anhydride (4 mL, 28.3 mmol, 35.8 eq.) was added, followed by sealing the flask and heating to 80 °C with continued stirring for 1 hour. The reaction was subsequently cooled to room temperature, quenched with a saturated aqueous solution of Na_2CO_3, and extracted with ethyl acetate (3 × 30 mL). The combined organic layers were washed with water and brine (2 × 20 mL), dried over anhydrous $MgSO_4$, filtered, and concentrated under reduced pressure to provide a crude green solid. The solid was dissolved in anhydrous toluene (30 mL) and added to a 250 mL 2-neck round bottom flask equipped with a magnetic stir-bar, inlet adapter, and septum under a nitrogen atmosphere. Next, NEt_3 (1 mL, 7.17 mmol, 9.07 eq.) was added and the reaction mixture was stirred for 10 minutes at room temperature. $BF_3\cdot OEt_2$ (2 mL, 15.8 mmol, 20.0 eq.) was then added to the reaction mixture, followed by heating to 85°C with continued stirring for 1 hour. Then, the reaction was cooled to room temperature, quenched with water (30 mL), and extracted with CH_2Cl_2 (3 × 30 mL). The combined organic layers were dried with anhydrous $MgSO_4$, filtered, and concentrated under reduced pressure to obtain a crude solid mixture. Purification with recrystallization in 200 mL of THF:MeOH (1:20) was accomplished by dissolving the crude solid in a small amount of THF (5-10 mL) and then diluting to 200 mL with methanol. The mixture was subsequently placed in a -20 ºC freezer for ~16 hours. The desired product was then isolated as a black solid via filtration (74 mg, 12% yield). ^{1}H NMR (400 MHz, $CDCl_3$) δ 7.65-7.67 (d, *J* = 8.8 Hz, 4H), 7.35-7.37 (d, *J* = 8.5 Hz, 6H), 6.95-6.98 (dd, *J* = 8.8, 3.4 Hz, 8H), 3.88 (s, 6H), 3.86 (s, 6H); ^{13}C NMR (100 MHz, $CDCl_3$) δ 162.0, 161.8, 159.9, 157.9, 130.4, 128.3, 127.3, 127.0, 114.8, 113.8, 108.4, 77.4, 55.7, 55.4, 47.4; IR (ATR): 2933, 2837, 1602, 1572, 1517, 1498, 1469, 1409, 1383, 1299, 1249, 1172, 1134, 1091, 1060, 1027, 927, 829, 762, 687, 604 cm^{-1}; HRMS (APCI): exact mass calculated for $C_{42}H_{30}BF_5N_2O_4S_2$ $[M+Na]^+$ 819.1558, found 819.1549.

Synthesis of 3,7-dibromo-5,5-difluoro-2,8,10,12-tetrakis(4-methoxyphenyl)-11-(trifluoromethyl)-5*H*-4λ^4,5λ^4-thieno[2',3':4,5]pyrrolo[1,2-*c*]thieno[2',3':4,5]pyrrolo[2,1-*f*][1,3,2]diazaborinine (BODIPY-Ph-Br). 5,5-difluoro-2,8,10,12-tetrakis(4-methoxyphenyl)-11-(trifluoromethyl)-5*H*-4λ^4,5λ^4-thieno[2',3':4,5]pyrrolo[1,2-*c*]thieno[2',3':4,5]pyrrolo[2,1-*f*][1,3,2]diazaborinine (**BODIPY-Ph-H**) (40 mg, 50 μmol, 1 eq.) was dissolved in CH_2Cl_2 (10 mL) in a 100 mL round bottom flask equipped with a magnetic stir-bar. Bromine (24 mg, 7.8 μL, 0.15 mmol, 3 eq.) in CH_2Cl_2 (5 mL) was then added to the flask while stirring vigorously at 40 °C, followed by continued stirring for ~16 hours. The reaction was cooled to room temperature, quenched with a saturated aqueous solution of Na_2CO_3 and the aqueous layer was extracted with diethyl ether (3 × 30 mL). The organic layers were combined, dried over anhydrous $MgSO_4$, filtered, and concentrated under reduced pressure to yield the desired product as a black solid (40 mg, 83% yield). ^{1}H NMR (400 MHz, $CDCl_3$) δ 7.73-7.75 (d, *J* = 8.8 Hz, 4H), 7.32-7.34 (d, *J* = 8.5 Hz, 4H), 6.96-7.00 (m, 8H), 3.88 (s, 6H), 3.86 (s, 6H); ^{13}C NMR (100 MHz, $CDCl_3$) δ 161.4, 160.2, 159.7, 156.4, 130.9, 130.5, 130.2, 130.0, 129.9, 126.6, 126.4, 114.3, 114.2, 114.0, 77.4, 55.6, 55.5; IR (ATR): 2961, 2917, 2848, 1600, 1571, 1495, 1451, 1438, 1375, 1294, 1256, 1222, 1170, 1143, 1085, 1010, 868, 792, 756, 728, 696, 633 cm^{-1}; HRMS (APCI): exact mass calculated for $C_{42}H_{28}BBr_2F_5N_2O_4S_2$ $[M+H]^+$ 974.9769, found 976.9749.

Summary of Photopolymerizations in Context

Below is a table comparing far-red to NIR light driven polymerizations (>700 nm excitation). Notably, photopolymerization conditions vary considerable and not all factors that influence polymerization efficiency are available from prior reports. Factors include monomer composition, photocatalyst and coinitiator concentrations, spectral profile of light source used and its overlap with the absorption profile of the photocatalyst used, incident light intensity, and sample dimensions (particularly thickness given light attenuation). As such, direct comparisons between prior examples and those presented herein can be difficult make from this table, but it provides a state-of-the-art and encourages future systematic studies to better compare across different photosystems for light-driven polymerizations.

Table S1. Comparative Table Summarizing Far-Red to NIR Light Induced Polymerizations

r_p (M/s) [t_{max} (s)]	λ_{ex} (nm)	I_{ex} (mW/cm^2)	PC	[PC] (mM)	Coinitiators (CoI)	[CoI] (mM)	Mon.	Ref
- [20]	805	1200	Cyanine 1d	6.6	Iodonium 2d	41.8	TMPTA	S1
- [233]	785	400	SQ_1	0.1 wt%	4-dppba, $Ar_2I^+PF_6^-$ BlocBuilder MA	3wt% 2wt% 2wt%	Mix-MA	S2
- [155]	785	400	SQ_2	0.1 wt%	4-dppba, $Ar_2I^+PF_6^-$ BlocBuilder MA	3wt% 2wt% 2wt%	Mix-MA	S2
- [140]	785	400	SQ_3	0.1 wt%	4-dppba, $Ar_2I^+PF_6^-$ BlocBuilder MA	3wt% 2wt% 2wt%	Mix-MA	S2
- [262]	785	400	SQ_4	0.1 wt%	4-dppba, $Ar_2I^+PF_6^-$ BlocBuilder MA	3wt% 2wt% 2wt%	Mix-MA	S2
- [362]	940	3000	SQ_1	0.1 wt%	4-dppba, $Ar_2I^+PF_6^-$ BlocBuilder MA	3wt% 2wt% 2wt%	Mix-MA	S2
- [288]	940	3000	SQ_2	0.1 wt%	4-dppba, $Ar_2I^+PF_6^-$ BlocBuilder MA	3wt% 2wt% 2wt%	Mix-MA	S2
- [153]	940	3000	SQ_3	0.1 wt%	4-dppba, $Ar_2I^+PF_6^-$ BlocBuilder MA	3wt% 2wt% 2wt%	Mix-MA	S2
- [342]	940	3000	SQ_4	0.1 wt%	4-dppba, $Ar_2I^+PF_6^-$ BlocBuilder MA	3wt% 2wt% 2wt%	Mix-MA	S2
- [118]	785	400	SQm_1	0.1 wt%	4-dppba, $Ar_2I^+PF_6^-$ BlocBuilder MA	3wt% 2wt% 2wt%	Mix-MA	S2
- [211]	785	400	SQm_2	0.1 wt%	4-dppba, $Ar_2I^+PF_6^-$ BlocBuilder MA	3wt% 2wt% 2wt%	Mix-MA	S2
- [>500]	785	400	SQm_3	0.1 wt%	4-dppba, $Ar_2I^+PF_6^-$ BlocBuilder MA	3wt% 2wt% 2wt%	Mix-MA	S2
- [>500]	785	400	SQm_4	0.1 wt%	4-dppba, $Ar_2I^+PF_6^-$ BlocBuilder MA	3wt% 2wt% 2wt%	Mix-MA	S2

- [332]	940	3000	SQm_1	0.1 wt%	4-dppba, Ar$_2$I$^+$PF$_6^-$ BlocBuilder MA	3wt% 2wt% 2wt%	Mix-MA	S2
- [>500]	940	3000	SQm_2	0.1 wt%	4-dppba, Ar$_2$I$^+$PF$_6^-$ BlocBuilder MA	3wt% 2wt% 2wt%	Mix-MA	S2
- [416]	940	3000	SQm_3	0.1 wt%	4-dppba, Ar$_2$I$^+$PF$_6^-$ BlocBuilder MA	3wt% 2wt% 2wt%	Mix-MA	S2
- [417]	940	3000	SQm_4	0.1 wt%	4-dppba, Ar$_2$I$^+$PF$_6^-$ BlocBuilder MA	3wt% 2wt% 2wt%	Mix-MA	S2
- [196]	785	400	Bodipy_1	0.1 wt%	4-dppba, Ar$_2$I$^+$PF$_6^-$ BlocBuilder MA	3wt% 2wt% 2wt%	Mix-MA	S2
- [356]	785	400	Bodipy_2	0.1 wt%	4-dppba, Ar$_2$I$^+$PF$_6^-$ BlocBuilder MA	3wt% 2wt% 2wt%	Mix-MA	S2
- [85]	940	3000	Bodipy_1	0.1 wt%	4-dppba, Ar$_2$I$^+$PF$_6^-$ BlocBuilder MA	3wt% 2wt% 2wt%	Mix-MA	S2
- [405]	940	3000	Bodipy_2	0.1 wt%	4-dppba, Ar$_2$I$^+$PF$_6^-$ BlocBuilder MA	3wt% 2wt% 2wt%	Mix-MA	S2
1.68 [2]	850	40	IRT	1.40	Borate B1	20	ethoxylated BPA dimethacrylate + 10 wt% DMSO	S3
0.66 [10]	740	16	aza-Br	4.74	Borate V HNu 254	4.74 47.4	Isobornyl acrylate	S4
0.038 [>160]	780	40	Bodipy-H-H	4.74	Borate V HNu 254	4.74 47.4	Isobornyl acrylate	*this work*
0.14 [30]	780	40	Bodipy-Br-Br	4.74	Borate V HNu 254	4.74 47.4	Isobornyl acrylate	*this work*
0.071 [35]	850	40	Bodipy-Br-Br	4.74	Borate V HNu 254	4.74 47.4	Isobornyl acrylate	*this work*
0.091 [45]	850	40	Bodipy-Ph-H	4.74	Borate V HNu 254	4.74 47.4	Isobornyl acrylate	*this work*
0.110 [25]	850	40	Bodipy-Ph-Br	4.74	Borate V HNu 254	4.74 47.4	Isobornyl acrylate	*this work*
0.59 [20]	850	60	Bodipy-Ph-H	4.74	Borate V HNu 254	4.74 47.4	2-hydroxyethyl acrylate	*this work*
0.082 [40]	940	50	Bodipy-Ph-H	4.74	Borate V HNu 254	4.74 47.4	Isobornyl acrylate	*this work*
0.19 [20]	850	20	Bodipy-Ph-H	4.74	Borate V HNu 254	47.4 47.4	Isobornyl acrylate	*this work*
0.33 [15]	850	20	Bodipy-Ph-H	47.4	Borate V HNu 254	47.4 47.4	Isobornyl acrylate	*this work*

$\boldsymbol{r}_\mathbf{p}$ = polymerization rate; $\boldsymbol{t}_\mathbf{max}$ = time to maximum monomer conversion; $\boldsymbol{I}_\mathbf{ex}$ = excitation intensity; **PC** = photocatalyst; Sq = Squaraine dye; **[PC]** = photocatalyst concentration; 4-dppba = 4-(diphenylphosphino)benzoic acid; Ar$_2$I$^+$PF$_6^-$ = diphenyliodonium hexafluorophosphate; TMPTA = trimethylolpropane triacrylate; Mix-MA = mixed methacrylate resin; BPA = bisphenol A

Dilute Absorption and Fluorescence Data

UV-vis absorption and emission spectra for the BODIPY dyes were collected in dilute solution (CH_2Cl_2 or toluene). Temperature-dependent absorption data was collected in 1,2-dichlorobenzene, showing no evidence for aggregation under dilute or concentrated conditions. All absorption data was collected within the limits of Beer's Law for three separately prepared samples, with averages ±1 standard deviation from the mean reported.

Table S2. Absorbance data for thiophene-fused BODIPYs in CH_2Cl_2.

BODIPY	λ_{max} (nm)	ε (M^{-1} cm^{-1})
BODIPY H-H	730	161,000 ± 3000
BODIPY Br-Br	765	40,000 ± 2000
BODIPY Ph-H	763	85,000 ± 2100
BODIPY Ph-Br	748	46,000 ± 1000

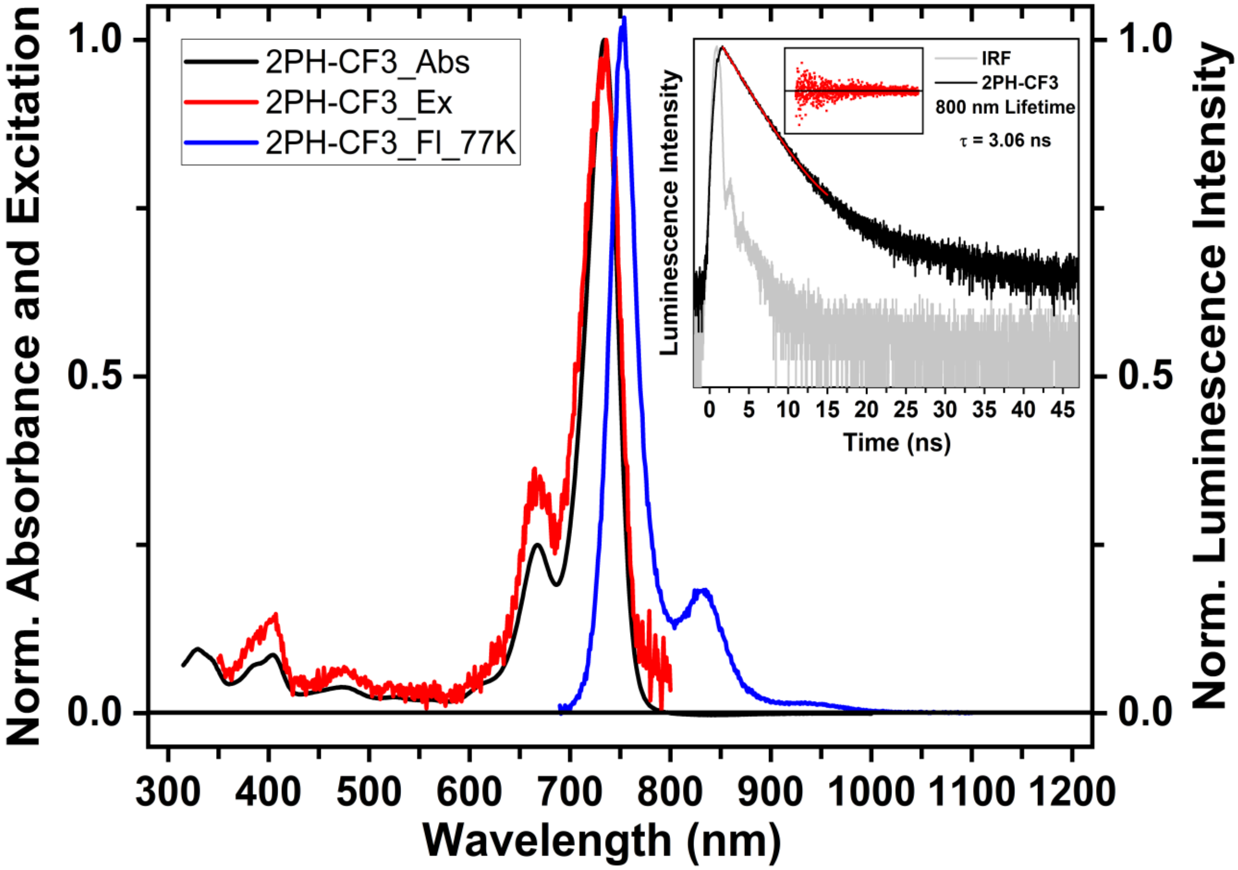

Figure S1. Absorbance and 77K fluorescence spectra of **BODIPY-H-H** in toluene**.** Inset: Fluorescence lifetime of **BODIPY-H-H** collected in toluene.

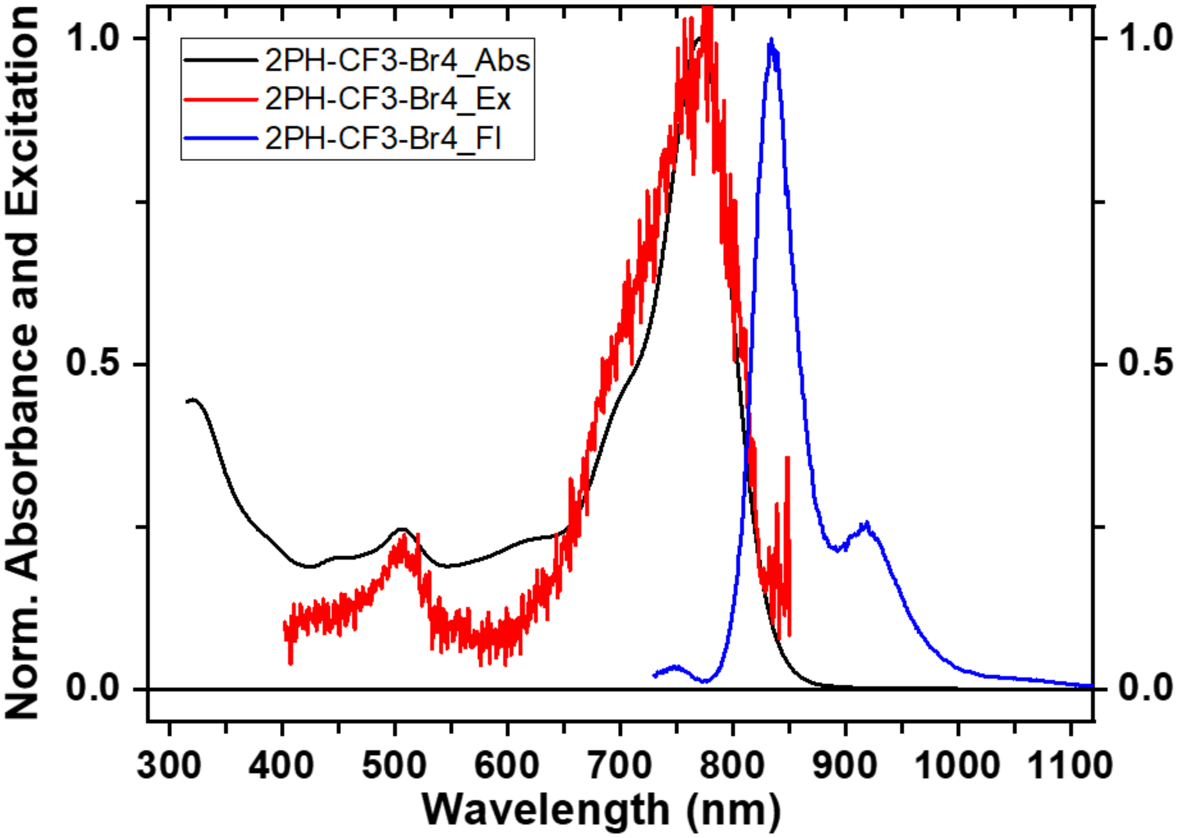

Figure S2. Absorbance and fluorescence spectra of **BODIPY-Br-Br** in toluene.

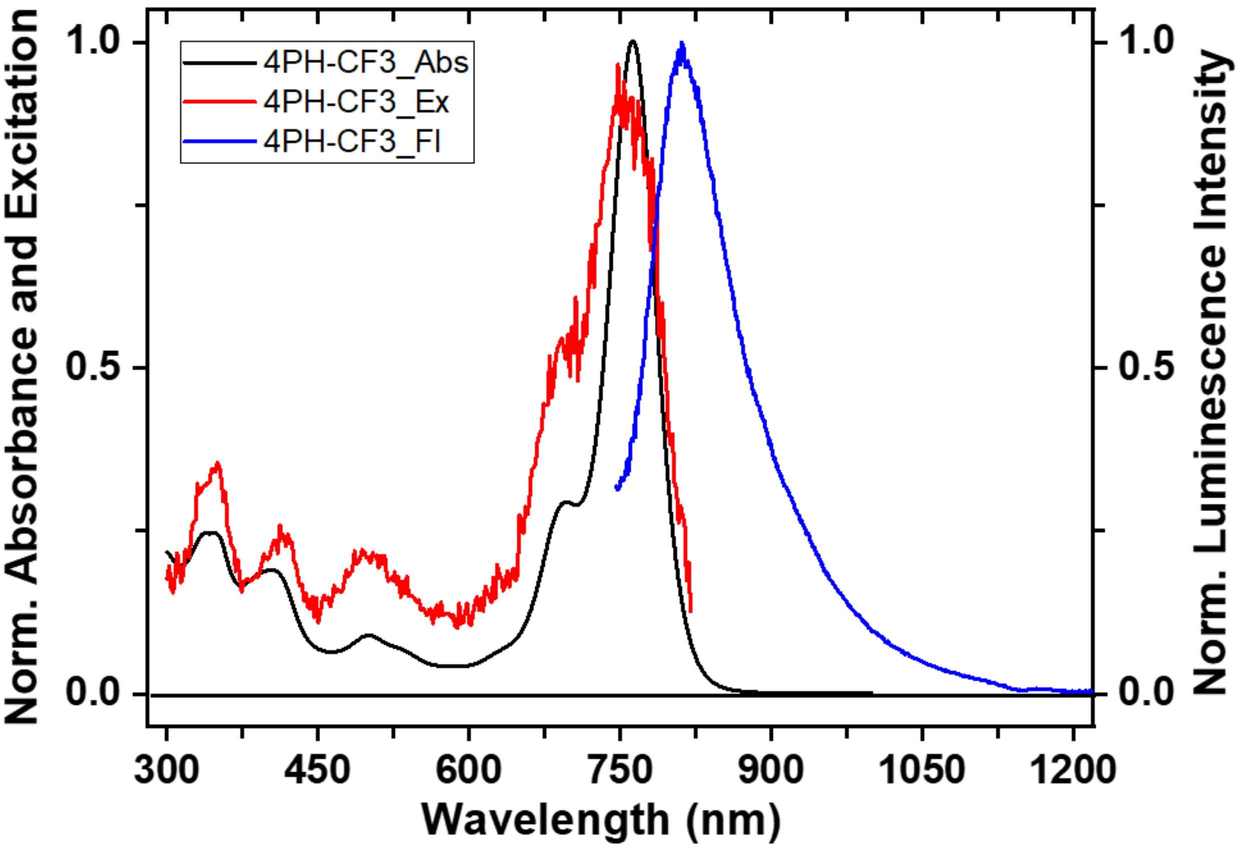

Figure S3. Absorbance and fluorescence spectra of **BODIPY-Ph-H** in toluene.

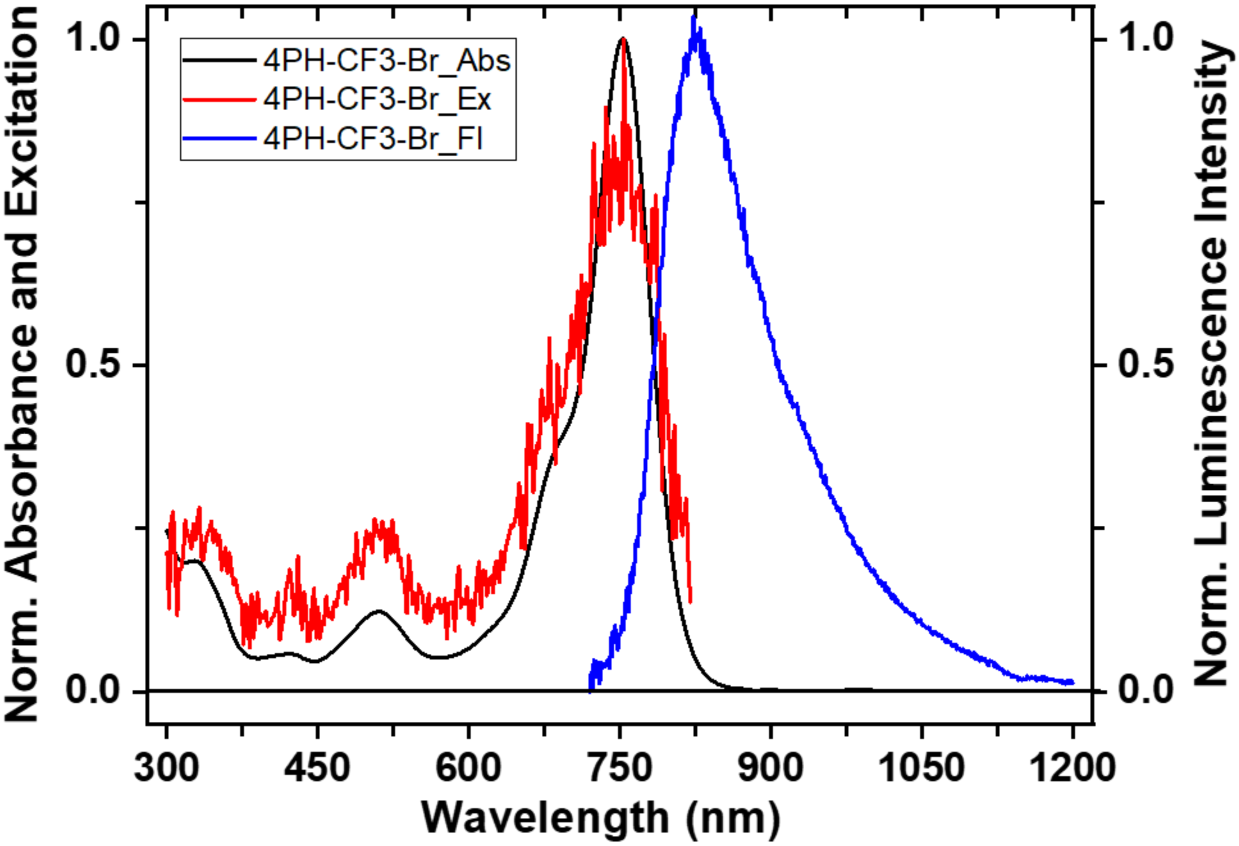

Figure S4. Absorbance and fluorescence spectra of **BODIPY-Ph-Br** in toluene.

Thin-Film Absorption Data

The absorption data for the BODIPY dyes were measured in the resin formulation: 0.1 mol% BODIPY, 0.1 mol% Donor (Borate V) and 1.0 mol% Acceptor (HNu 254) in isobornyl acrylate. Measured extinction coefficients were utilized in the calculation of absorbed LED photons. The resins for UV-vis absorption were placed between glass microscope slides separated by plastic shims of varying thickness. ranging from 13-51 μm (noted color in legends corresponds to a particular thickness). UV-vis absorption spectra were collected using an Ocean Optics Stage RTL-T.

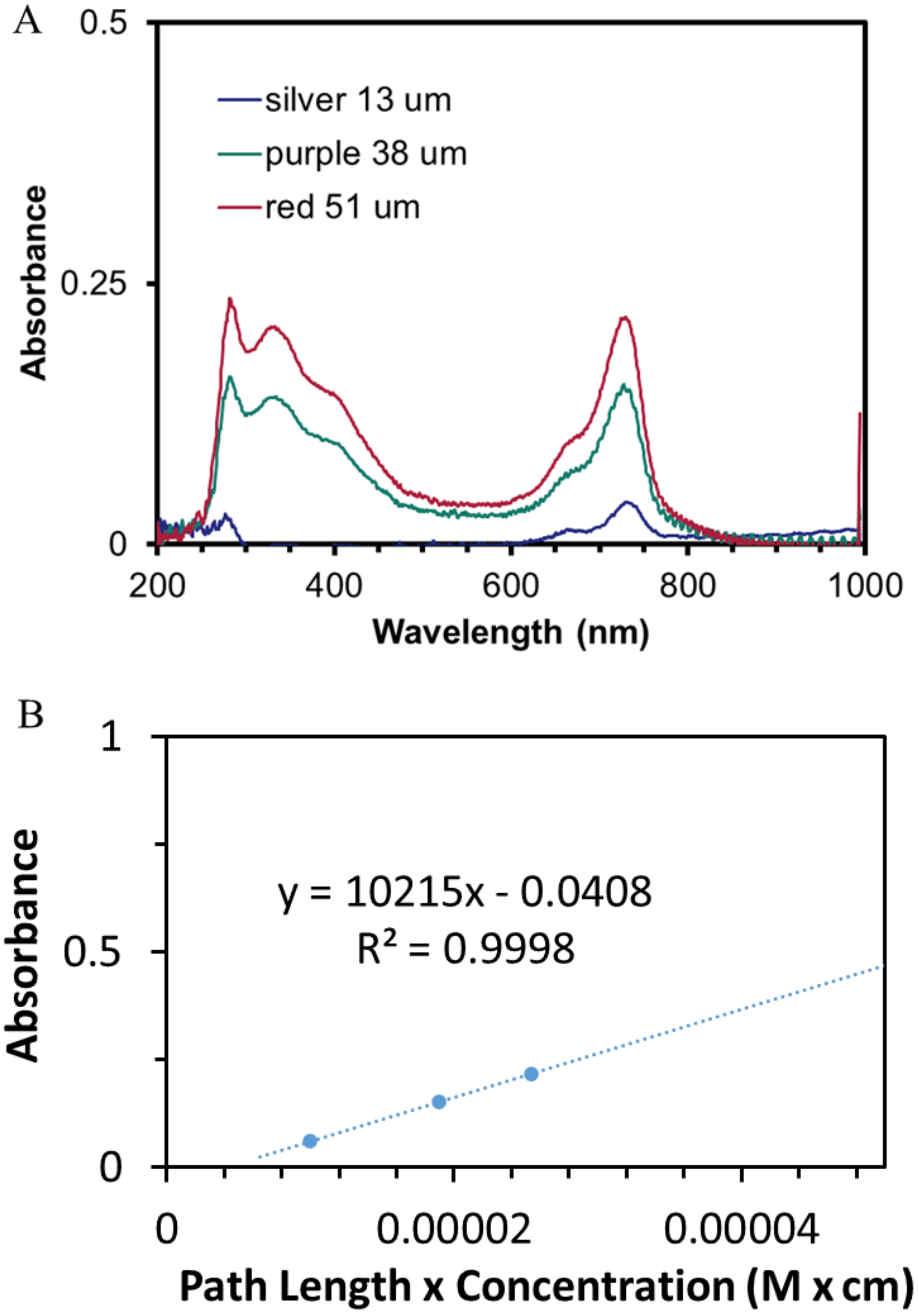

Figure S5. (A) Thin-film absorption data for **BODIPY-H-H**. (B) Corresponding plot used to determine molar absorptivity at the peak absorption wavelength.

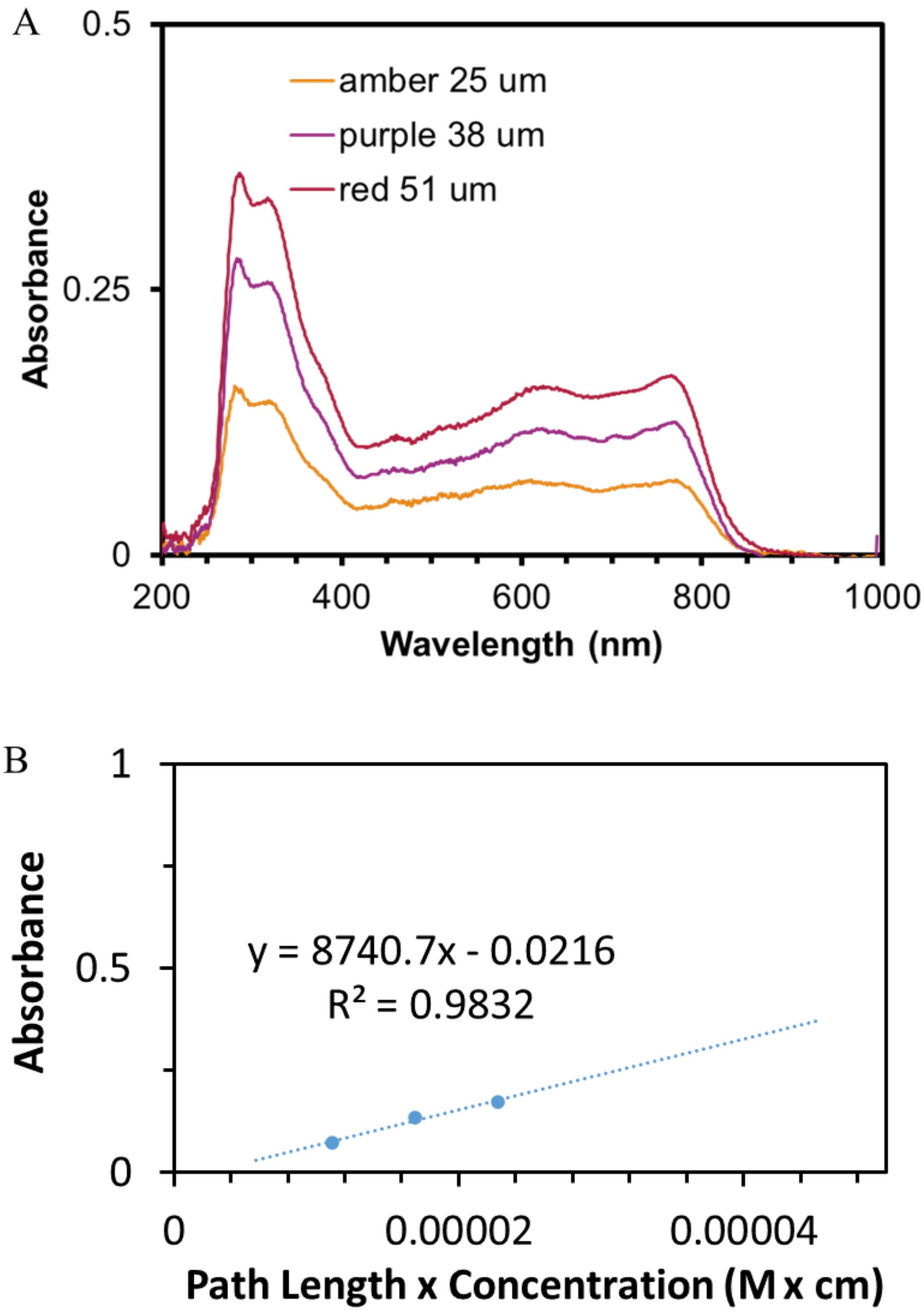

Figure S6. (A) Thin-film absorption data for **BODIPY-Br-Br**. (B) Corresponding plot used to determine molar absorptivity at the peak absorption wavelength.

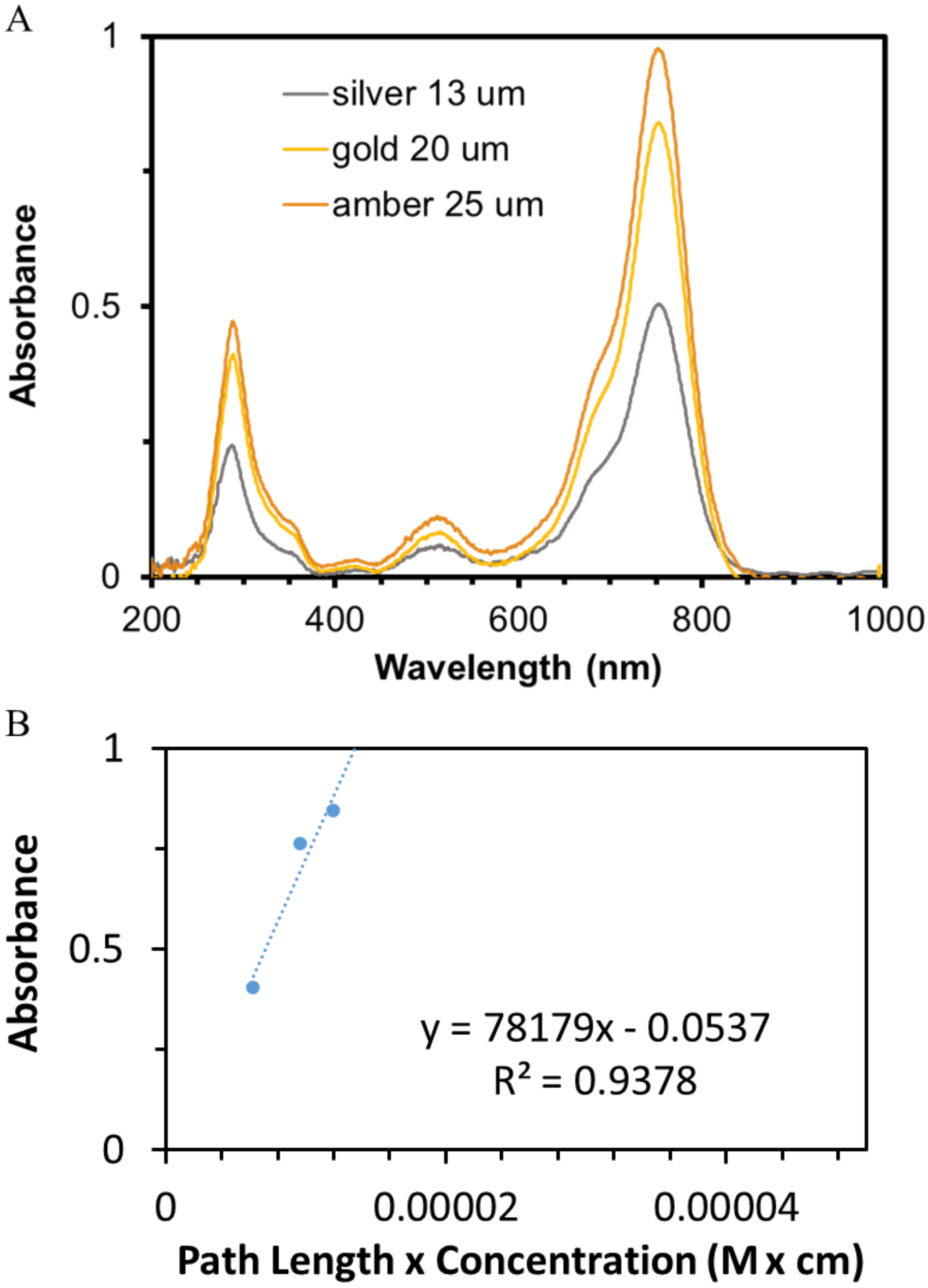

Figure S7. (A) Thin-film absorption data for **BODIPY-Ph-H**. (B) Corresponding plot used to determine molar absorptivity at the peak absorption wavelength.

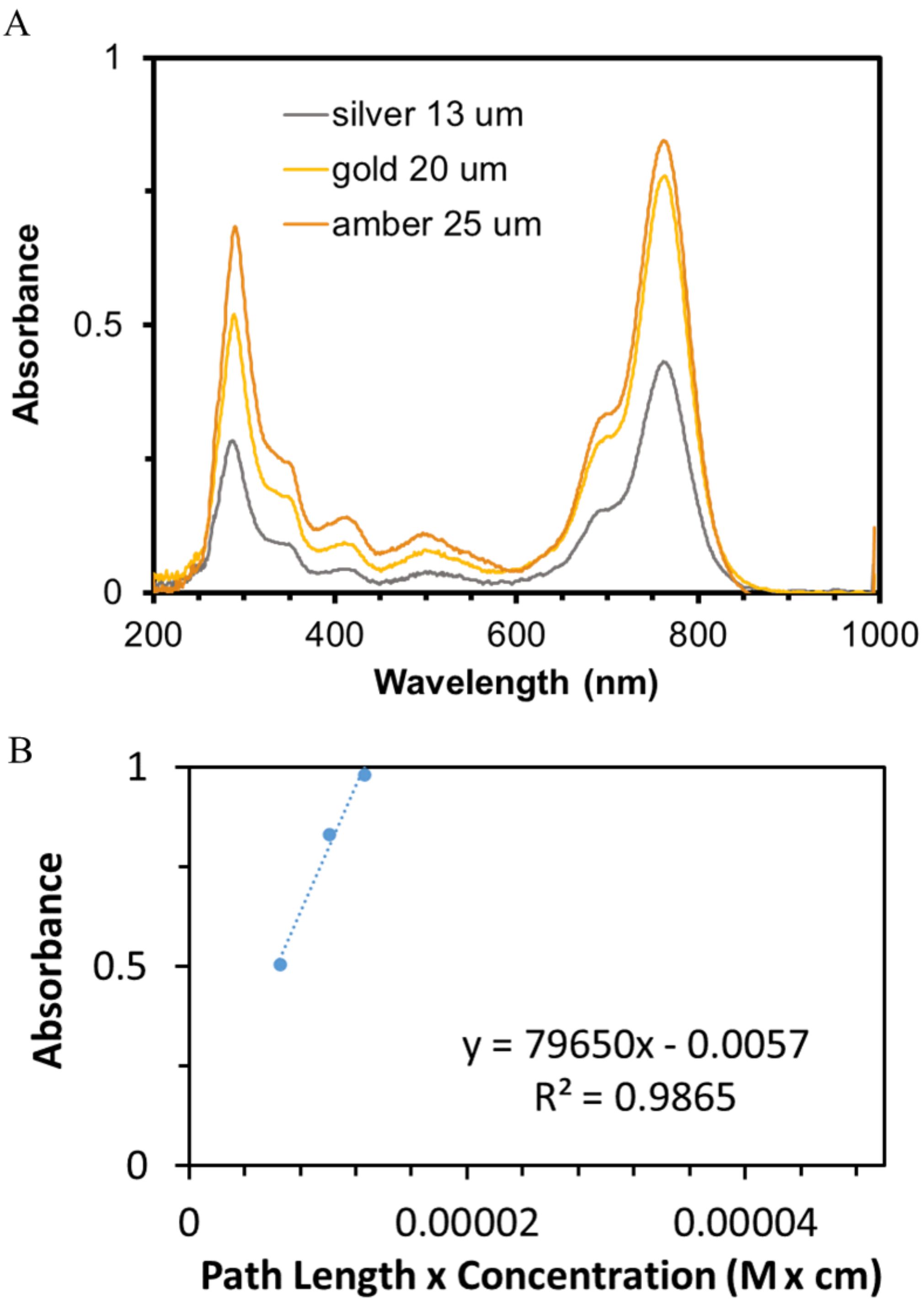

Figure S8. (A) Thin-film absorption data for **BODIPY-Ph-Br**. (B) Corresponding plot used to determine molar absorptivity at the peak absorption wavelength.

Temperature-Dependent Absorption Data

UV-vis absorption for the BODIPY dyes were collected in 1,2-dichlorobenzene showing no evidence for aggregation under dilute or concentrated conditions.

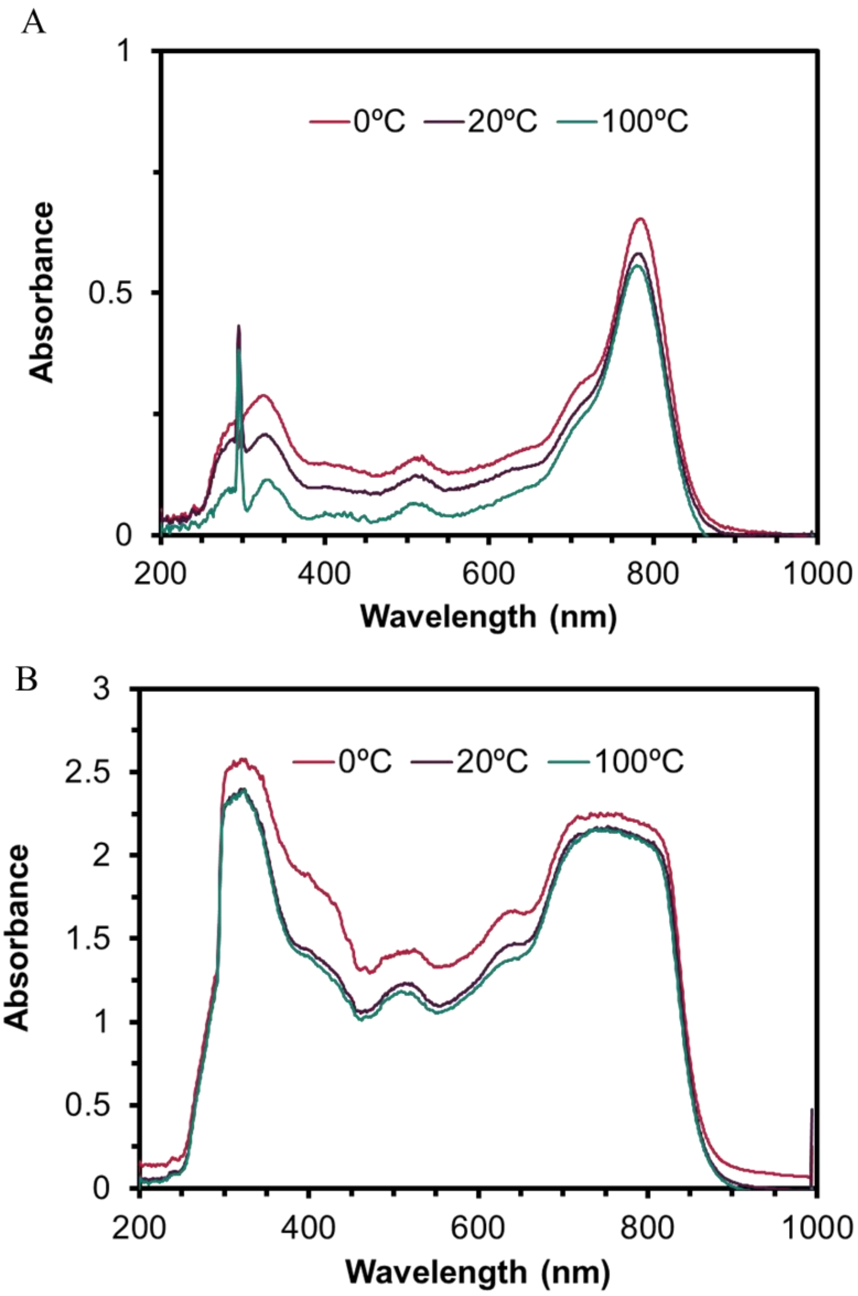

Figure S9. (A) Dilute absorbance spectra and (B) concentrated absorbance spectra of **BODIPY-Br-Br** in 1,2-dichlorobenzene at different temperatures.

Materials

Chemicals: Ethyl azidoacetate (95.0+%), and trifluoroacetic acid (99.0+%) were purchased from TCI America. Dichloromethane (DCM, 99.9%) sodium hydroxide (NaOH, certified ACS), methanol (MeOH, certified ACS), ethanol (EtOH), tetrahydrofuran (THF), and toluene (Certified ACS) were purchased from Fisher Scientific. 2-Thiophene-2-carbaldehyde (98+%) and 5-bromo-2-formylthiophene (≥97.0%) were purchased from VWR. 4-methoxyphenylboronic acid (≥98%) and trifluoroacetic anhydride (≥99%) were purchased from Chem-Impex. Sodium ethoxide (96%), sodium carbonate (98%), and bromine (≥99.8%) were purchased from Alfa Aesar. Triethylamine (≥99.5%) was purchased from Sigma-Aldrich. Boron trifluoride diethyl etherate (98%) was purchased from Oakwood Chemical. Tetrakis(triphenylphosphine)-palladium(0) (99%) was purchased from Strem Chemicals. H-Nu 254, Onium Salt and Borate V were purchased from Spectra Group Limited, Inc. $CDCl_3$ (99.8%) and d6-DMSO (99.9%) were purchased from Cambridge Isotope Laboratories. All chemicals were used as received without additional purification, unless otherwise noted.

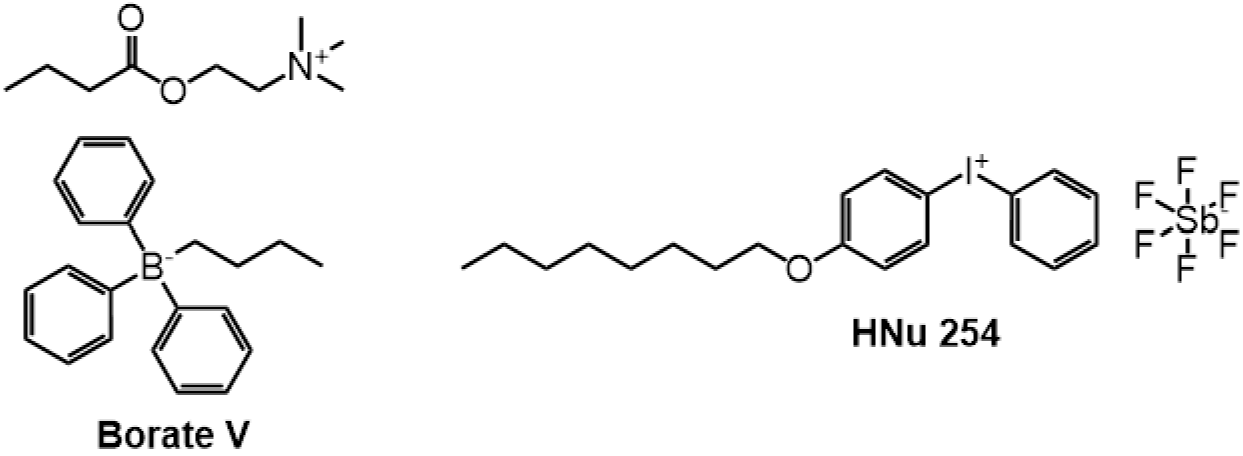

Figure S10. Chemical structures of electron donor (Borate V) and acceptor (HNu 254) co-initiators.

Cyclic Voltammetry Data

Cyclic voltammetry (CV) was performed on the BODIPY dyes in CH_2Cl_2 using 0.1 M Ag/$AgNO_3$ as the reference electrode, glassy carbon as the working electrode and a Pt wire as the counter electrode. Negative and positive potential measurements were done separately, with plots providing the stitched data. Measurements were performed within a nitrogen filled glovebox. Samples were measured in triplicate with averages ±1 standard deviation from the mean reported.

Table S3. Ground state redox potentials of BODIPY dyes in CH_2Cl_2 as measured using CV

BODIPY	E_{ox} **(V)**	E_{red} **(V)**
BODIPY-H-H	0.689 ± 0.002	-0.648 ± 0.005
BODIPY-Ph-H	0.748 ± 0.007	-0.625 ± 0.009
BODIPY-Ph-Br	0.827 ± 0.012	-0.801 ± 0.006
BODIPY-Br-Br	1.073 ± 0.006	-0.285 ± 0.002

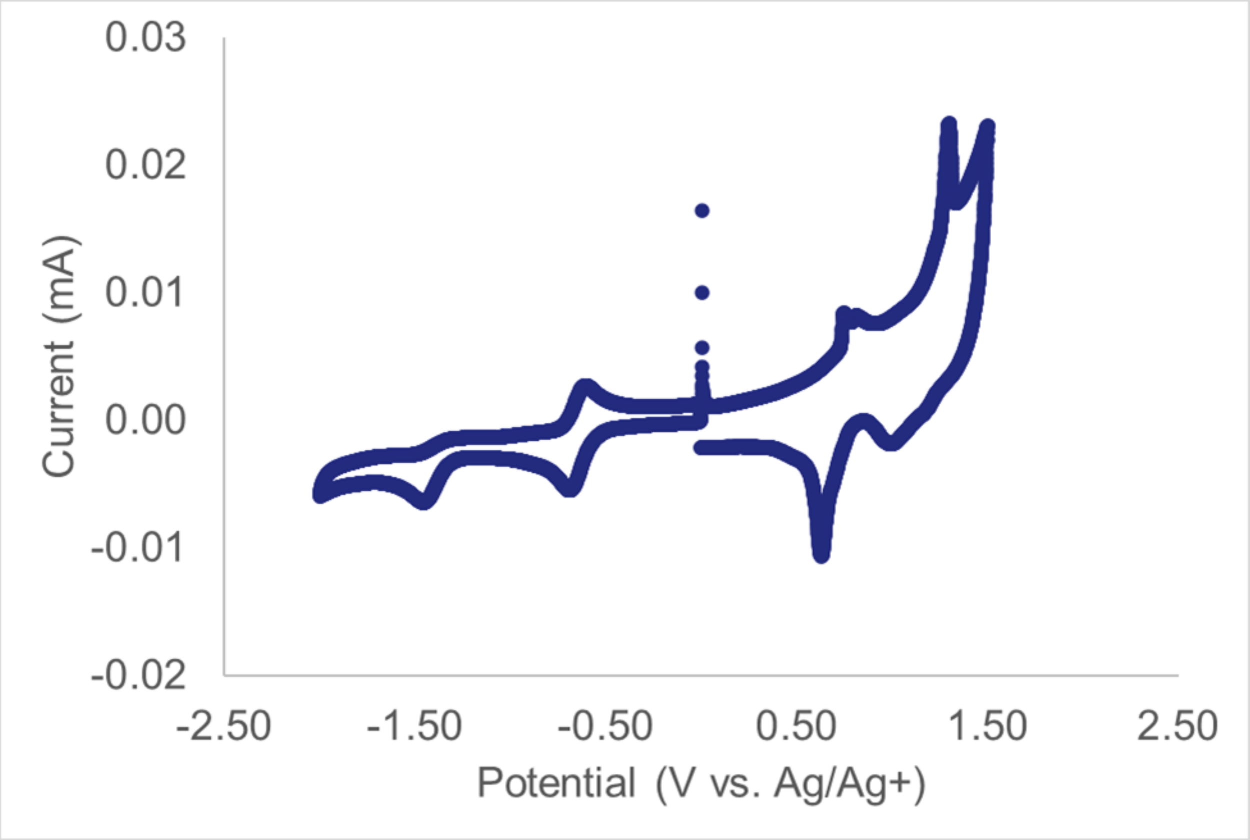

Figure S11. Representative CV trace of **BODIPY-H-H**.

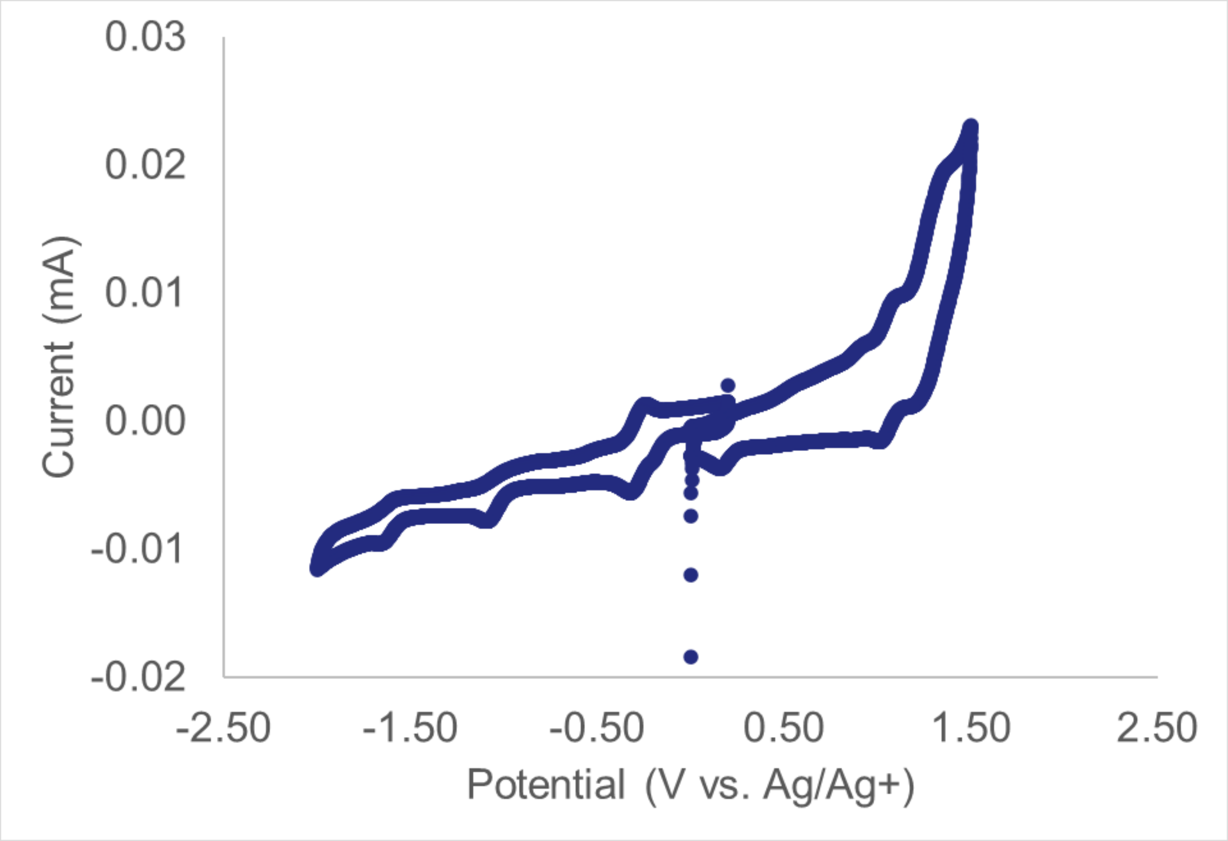

Figure S12. Representative CV trace of **BODIPY-Br-Br**.

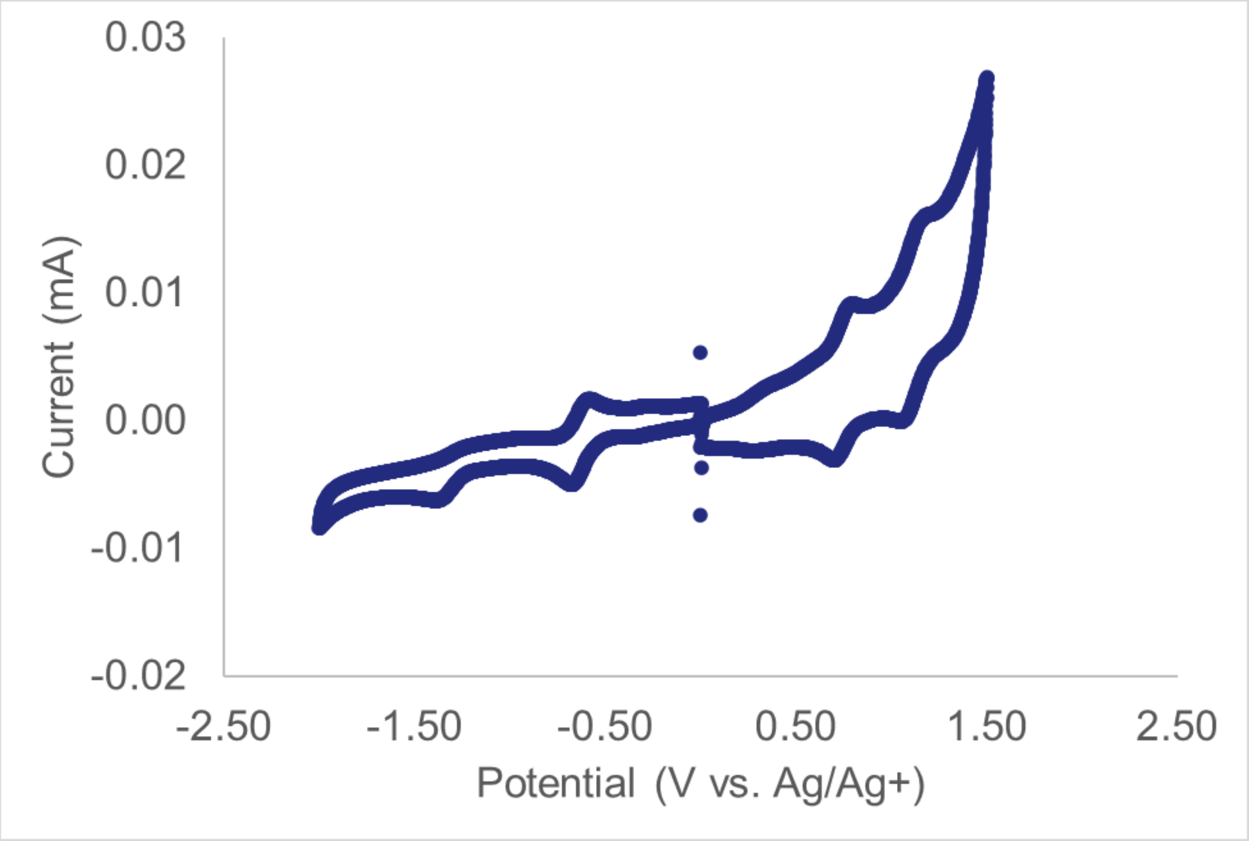

Figure S13. Representative CV trace of **BODIPY-Ph-H**.

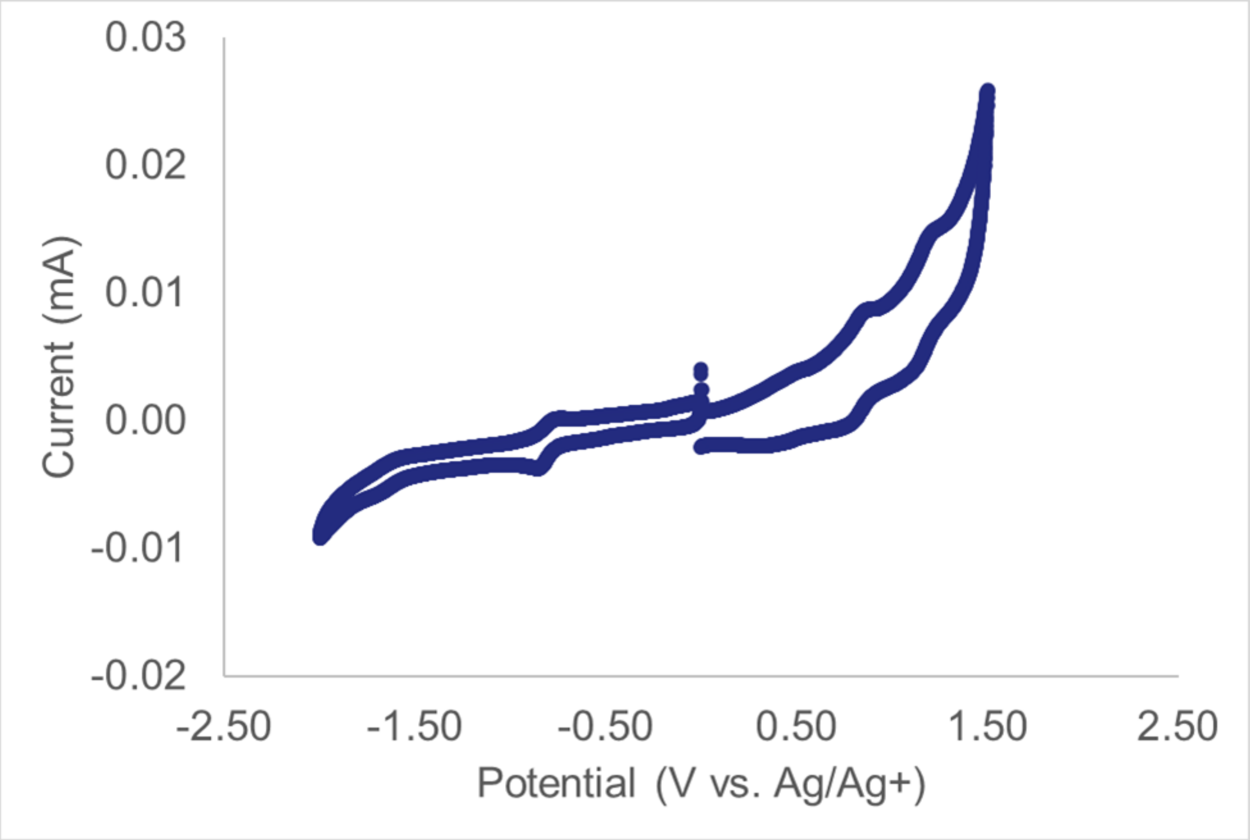

Figure S14. Representative CV trace of **BODIPY-Ph-Br**.

Rehm-Weller Analysis

Photoinduced electron transfer free energies were calculated using the following supplemental equations:

$$E^{*}_{\text{ox}} = E_{\text{ox}} - E_{\text{S1}} \ (\textbf{SE1})$$

where E^{*}_{ox} is the excited state oxidation potential of the photoredox catalyst, E_{ox} is the ground state oxidation potential of the photoredox catalyst, and E_{S1} is the energy of the excited state determined from the intersection of absorbance and emission spectra:

$$E^{*}_{\text{red}} = E_{\text{red}} - E_{\text{S1}} \ (\textbf{SE2})$$

where E^{*}_{red} is the excited state reduction potential of the photoredox catalyst and E_{red} is the ground state reduction potential of the photoredox catalyst.

$$\Delta G_{\text{A}} = E^{*}_{\text{ox}} - E_{\text{red}}\,(\text{A}) + \Delta G^{\text{o}}\,(\varepsilon) \ (\textbf{SE3})$$

where ΔG_{A} is the change in free energy for photoinduced electron transfer from the BODIPY photoredox catalyst to the electron acceptor (HNu 254), $E_{\text{red}}(\text{A})$ is the reduction potential of the electron acceptor[S5] (HNu 254), and $\Delta G^{\text{o}}(\varepsilon)$ is the Born correction term which accounts for the interaction energy between the two radical ions formed after electron transfer. A value of -0.13 eV was used for $\Delta G^{\text{o}}(\varepsilon)$ following reports by Narayanan et. al.[S6]

$$\Delta G_{\text{D}} = E_{\text{ox}}\,(\text{D}) - E^{*}_{\text{red}} + \Delta G^{\text{o}}\,(\varepsilon) \ (\textbf{SE4})$$

where ΔG_{D} is the change in free energy for photoinduced electron transfer from the electron donor (Borate V) to the BODIPY photoredox catalyst, E_{ox} (D) is the oxidation potential of the electron donor[S5] (Borate V), and $\Delta G^{\text{o}}(\varepsilon)$ is the Born correction term which accounts for the interaction energy between the two radical ions formed after electron transfer. A value of -0.13 eV was used for $\Delta G^{\text{o}}(\varepsilon)$ following reports by Narayanan et. al.[S6]

Photopolymerizations with Different Monomers

Photopolymerizations using different monomers were characterized in triplicate with an 850 nm LED and the following resin formulation: 0.1 mol% BODIPY, 0.1 mol% Borate V (donor), and 1.0 mol% Iodonium salt (acceptor).

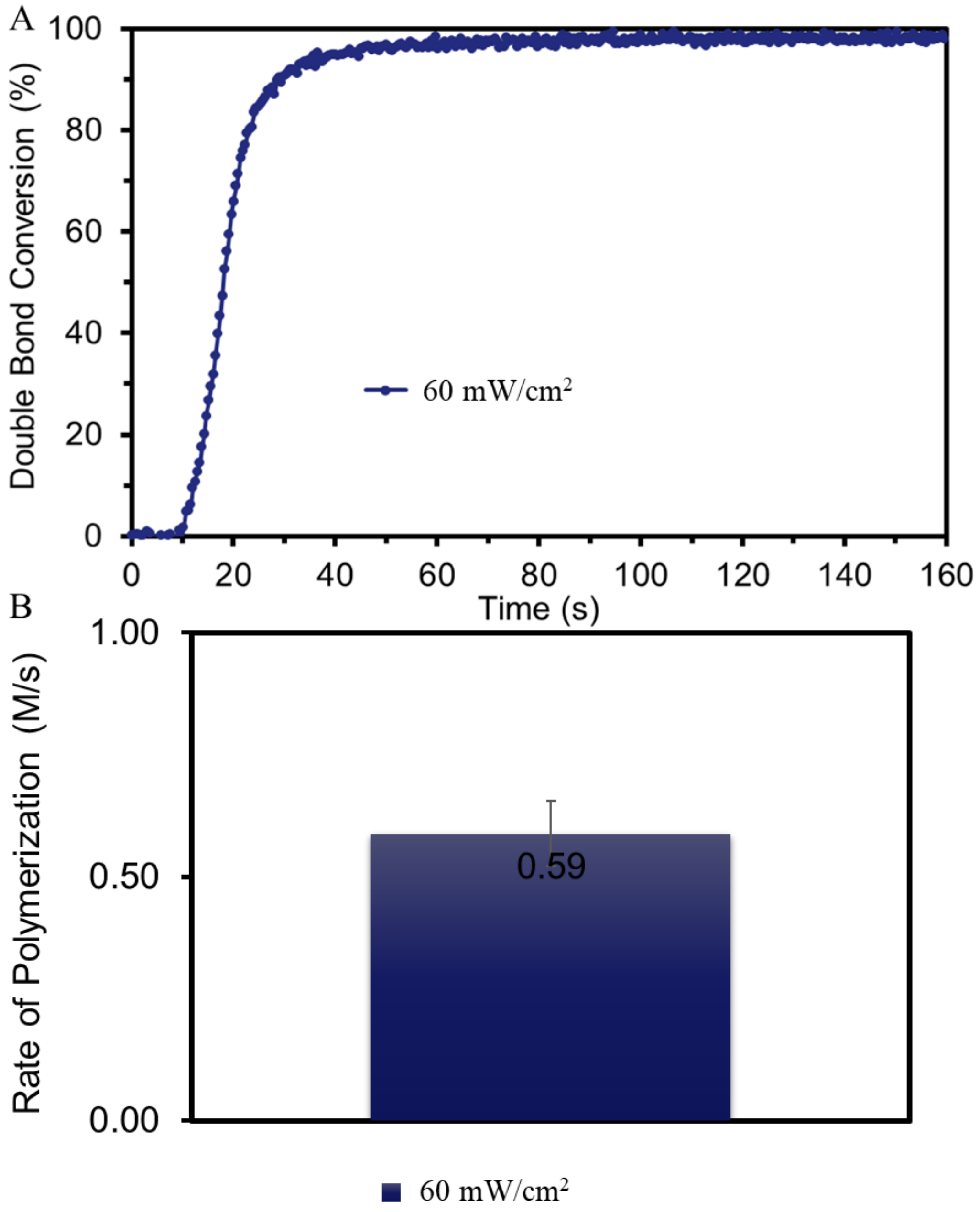

Figure S15. (A) Photopolymerization of 2-hydroxyethyl acrylate (HEA) using **BODIPY-Ph-H**. (B) Rate of photopolymerization in M/s. Error bars represent ± 1 standard deviation from the mean.

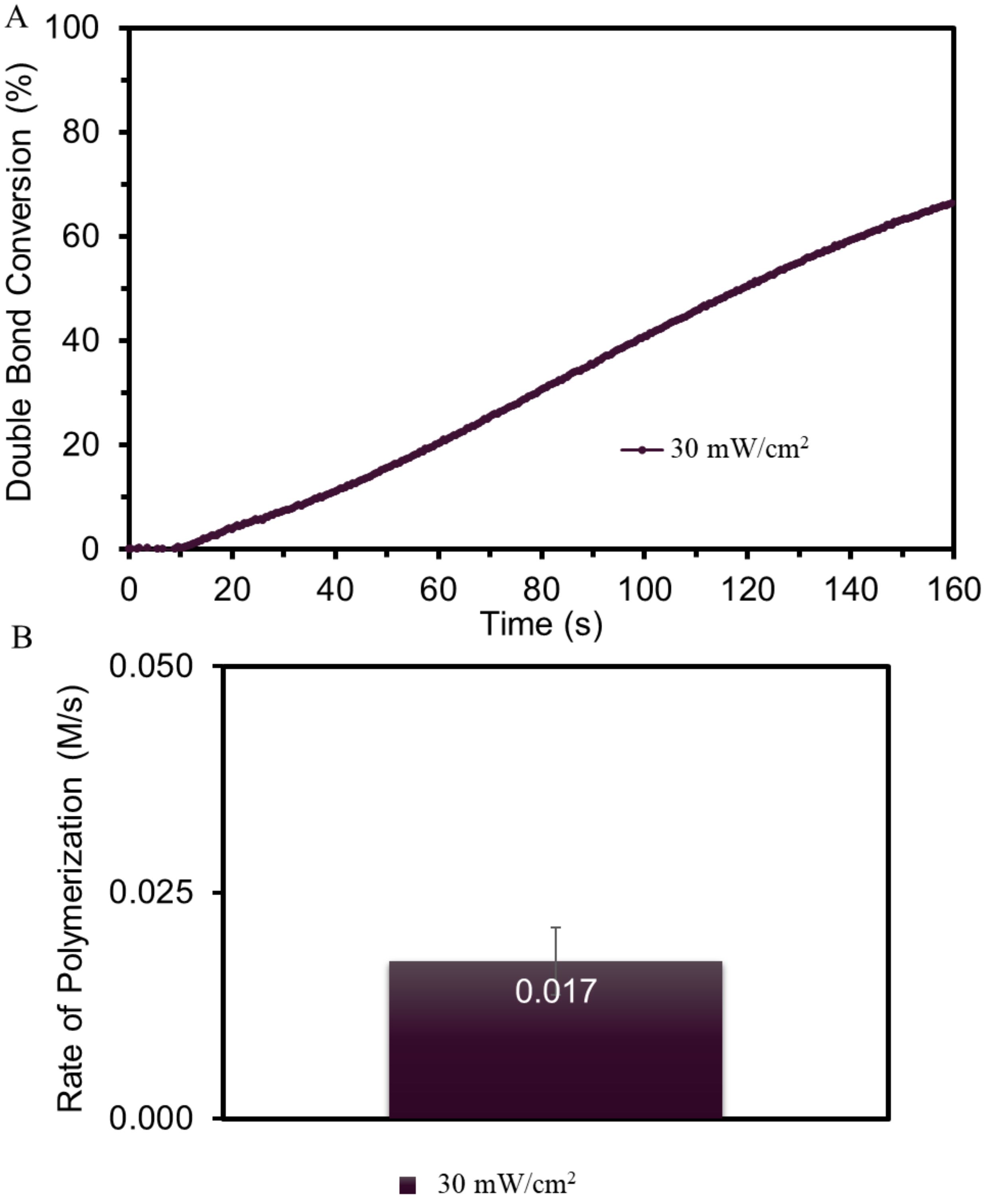

Figure S16. (A) Photopolymerization of carbitol acrylate using **BODIPY-Ph-H**. (B) Rate of photopolymerization in M/s. Error bars represent ± 1 standard deviation from the mean.

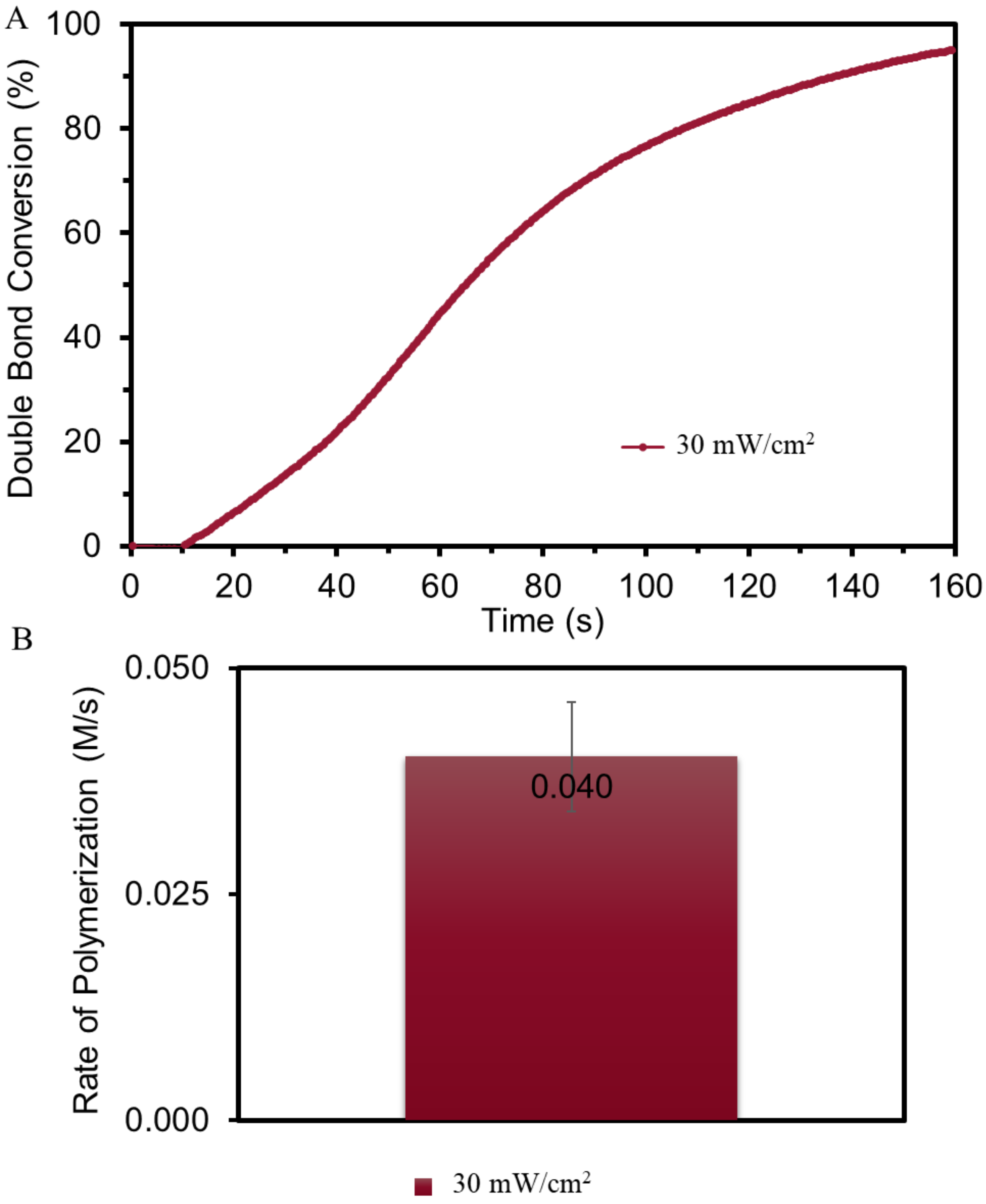

Figure S17. (A) Photopolymerization of 2-phenoxyethyl acrylate using **BODIPY-Ph-H**. (B) Rate of photopolymerization in M/s. Error bars represent ± 1 standard deviation from the mean.

Equipment and Instrumentation

Nuclear Magnetic Resonance (NMR) Spectroscopy. NMR spectra were recorded on an Agilent MR 400 MHz spectrometer utilizing $CDCl_3$ as the solvent. ^1H NMR were carried out coupled and referenced to the $CDCl_3$ chemical shift at 7.26 ppm. ^{13}C NMR were carried out decoupled and referenced to the $CDCl_3$ chemical shift at 77.16 ppm.

High Resolution Mass Spectrometry (HRMS). HRMS was performed on an Agilent Technologies 6530 Accurate-Mass Q-TOF LC/MS using ESI and the data was subsequently analyzed using Agilent MassHunter Qualitative Analysis Software.

Measurement of LED beam area through the ATR crystal. The area of the irradiated region through the ATR crystal was measured using ImageJ to trace the outline of a low intensity LED. The size was determined to be 1.27 mm^2 relative to the total crystal area of 6.92 mm^2 (**Figure S4**).

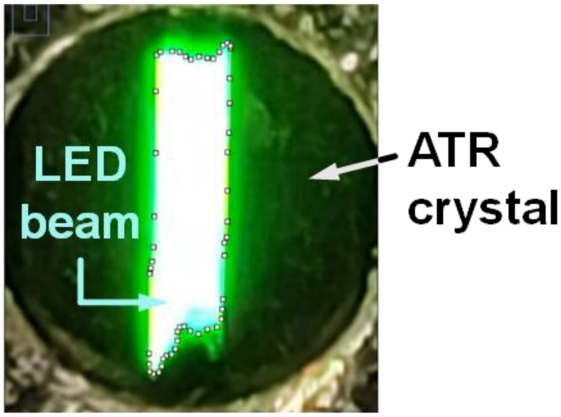

Figure S18. Close-up image of FTIR-ATR crystal with a green LED (530 nm) at low intensity (<0.1 mW/cm^2) used to measure the area of irradiation.

Measurement Area of Incident IR-Beam relative to LED. The measured area of the incident FTIR beam was estimated by placing pieces of Kapton tape on the ATR crystal and monitoring the appearance of a signal originating from the silicone adhesive (**Figure S19A**). The tape was moved stepwise from each side of the crystal until a signal was observed - which appeared sooner when moving the tape inward from the left-hand side of the crystal. Subsequently, two flanking pieces of tape were placed parallel to the LED irradiation zone and moved stepwise toward the center. **Figure S19B** shows the position of the tape before any signal was found and gives a rough estimate of the FTIR-ATR measurement region which is left-of-center and an oval shape due to the cut of the diamond. In effect, the LED intensities reported are conservative values since a portion of the area being measured by the incident IR-beam at a 5 mm aperture is outside the direct LED irradiation area.

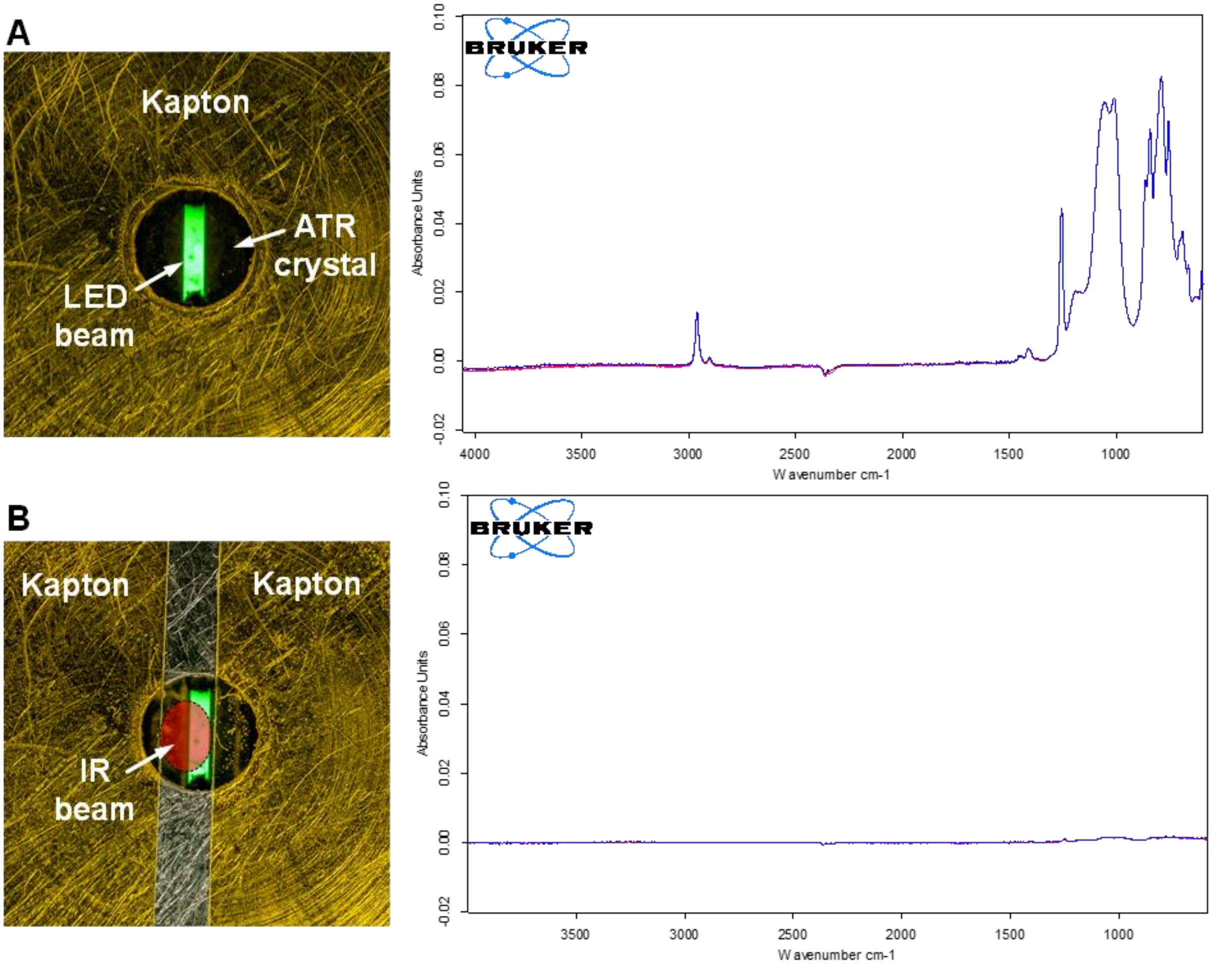

Figure S19. (A) Annotated FTIR-ATR spectrum of crystal fully covered with Kapton tape. (B) Kapton tape flanking the measured region of the crystal. The red oval indicates the estimated area of measurement at a 5 mm aperture.

Real-Time Fourier-Transform Infrared Spectroscopy (RT-FTIR). RT-FTIR was recorded utilizing an INVENIO-R FT-IR Spectrometer from Bruker (**Figure S20**) and controlled via OPUS Spectroscopy Software. A liquid nitrogen cooled (LN-MCT Mid) detector was used for measurements. A modified GladiATR Illuminate ATR accessory[S7] from PIKE Technologies was used to analyze chemical composition and monitor photocuring of liquid resins upon exposure to light. Collimated LED light sources (780 nm-P/N LCS-0780-02-22, 850 nm-P/N LCS-0850-03-22, 940 nm-P/N LCS-0940-02-38) from Mightex Systems along with Lightguide Adapters were utilized to irradiate resins with visible light (see photopolymerization procedure for more details). LED Controller M/N SLC-MA02-U was used with a 3 mm liquid light guide (LLG-3- 4H).

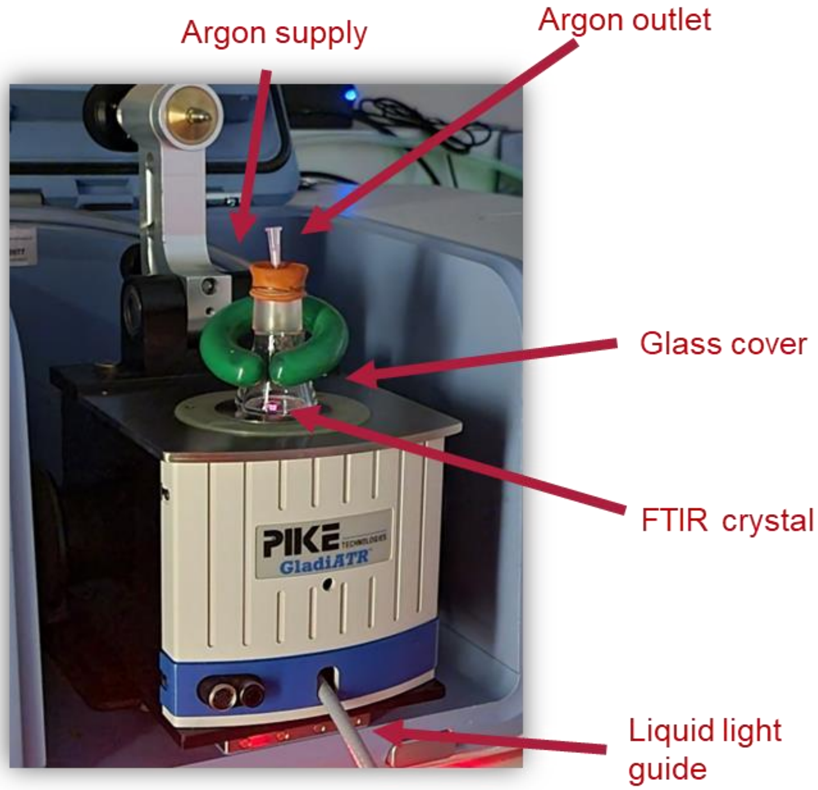

Figure S20. Image of RT-FTIR setup using an ATR configuration with air-free glassware.

Steady-State Optical Characterization. UV-visible absorption spectra were recorded on an Ocean Optics QE PRO-ABS Fiber Optic Spectrometer utilizing deuterium and tungsten halogen light sources (DH-2000-BAL). 600 μm fiberoptic cables (QP600-025-SR) were coupled to the detector with a slit width of 5 μm. Dilute absorption data was collected in acetonitrile and dichloromethane utilizing quartz cuvettes and a qpod sample holder (QNW qpod2e). Thin-film absorption data was collected in the resin formulation utilizing an Ocean Optics Stage RTL-T (see **BODIPY Thin-Film Absorption Data** above).

Electronic Characterization. Cyclic voltammetry (CV) was performed in a nitrogen-filled VAC glovebox using a BioLogic SP-50e potentiostat. A single-compartment three-electrode cell was used with glassy carbon as the working electrode, a platinum wire as the counter electrode, and an $Ag/AgNO_3$ (0.01 M) nonaqueous reference electrode calibrated versus Fc/Fc^+ in 0.1 M tetrabutylammonium hexafluorophosphate ($TBAPF_6$) dichloromethene solutions ($E_{1/2}(Fc/Fc^+) = 0.1$ V vs Ag/Ag^+) with a 0.1 V/s scan rate. Oxidation onsets were utilized to calculate the highest occupied molecular orbital (HOMO) energy level -(4.8 eV – E_{ox}(Ferrocene) + E_{ox}) and reduction onsets to calculate the lowest unoccupied molecular orbital (LUMO) energy level -(4.8 eV –Eox(Ferrocene) + E_{red})[S8].

Light emitting diodes (LEDs). All LEDs used were purchased from Mightex Systems. The product numbers for the three LEDs listed are 780 nm-P/N LCS-0780-02-22, 850 nm-P/N LCS-0850-03-22, and 940 nm-P/N LCS-0940-02-38. The emission profile for each LED was measured using a calibrated UV-Vis Ocean Insight system. Irradiation intensities were measured with a Thorlabs PM100D photometer equipped with a silicon-based photodiode power sensor (S120VC, Thorlabs). Emission profiles were recorded with a QE pro spectrometer, in which the LED was connected to the fiber optic system using a 3 mm 420 – 2000 nm liquid lightguide from Mightex Systems (serial #: LLG-03-59-340-0800-1). A 775 nm longpass filter from ThorLabs (R5000872535-21348) was used with the 850 nm LED to block any visible light emission from the LEDs. Spectral profiles are provided in **Figure S21** below.

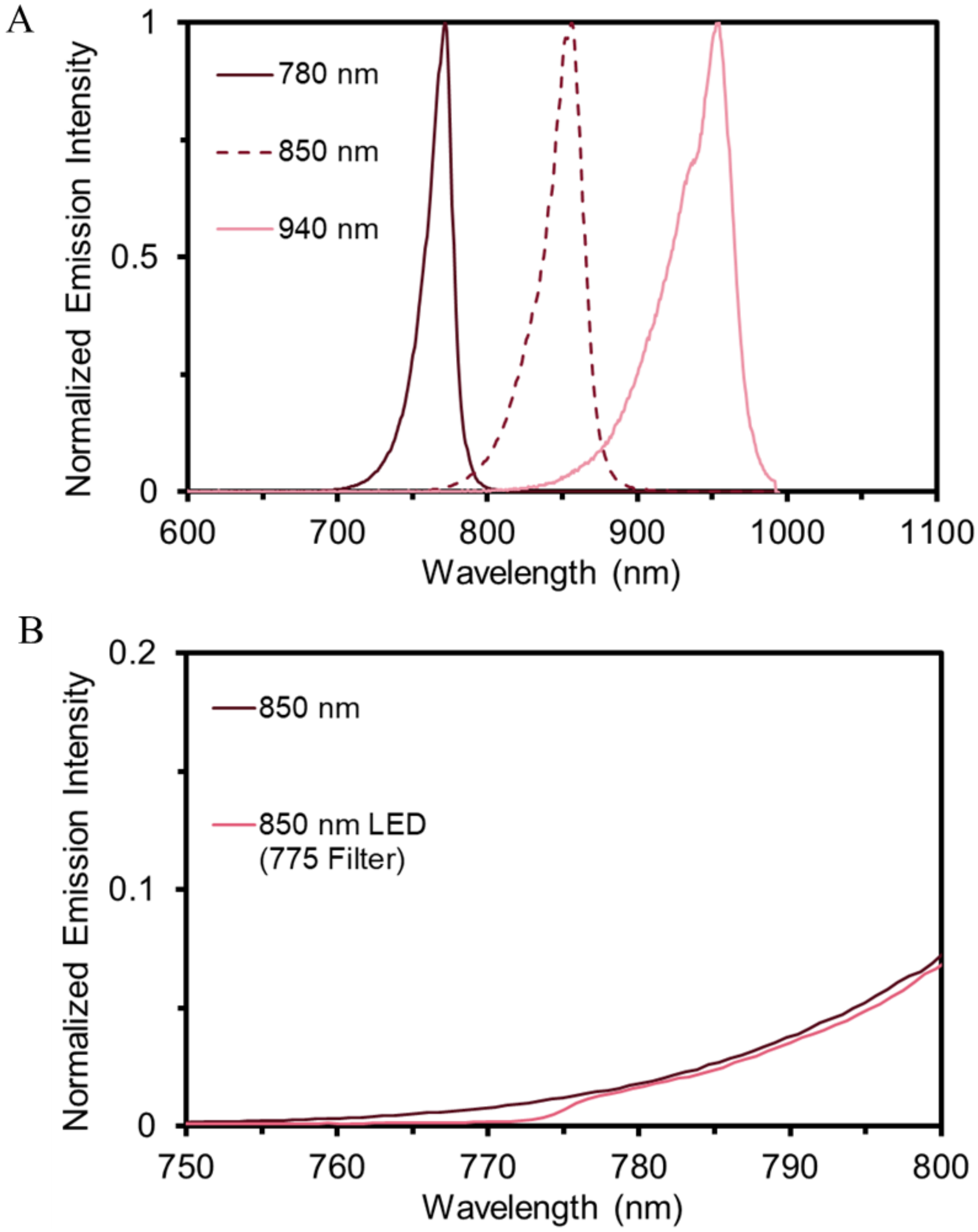

Figure S21. (A) LED emission profiles of near-IR light sources. (B) LED emission profile of 850 nm LED with and without a 775 nm longpass filter.

Photopolymerizations at Variable Intensity

Photopolymerizations were measured in triplicate at varying LED intensities with 780, 850, and 940 nm LEDs, utilizing the resin formulation: 0.1 mol% BODIPY, 0.1 mol% Borate V (donor), and 1.0 mol% HNu 254 (acceptor).

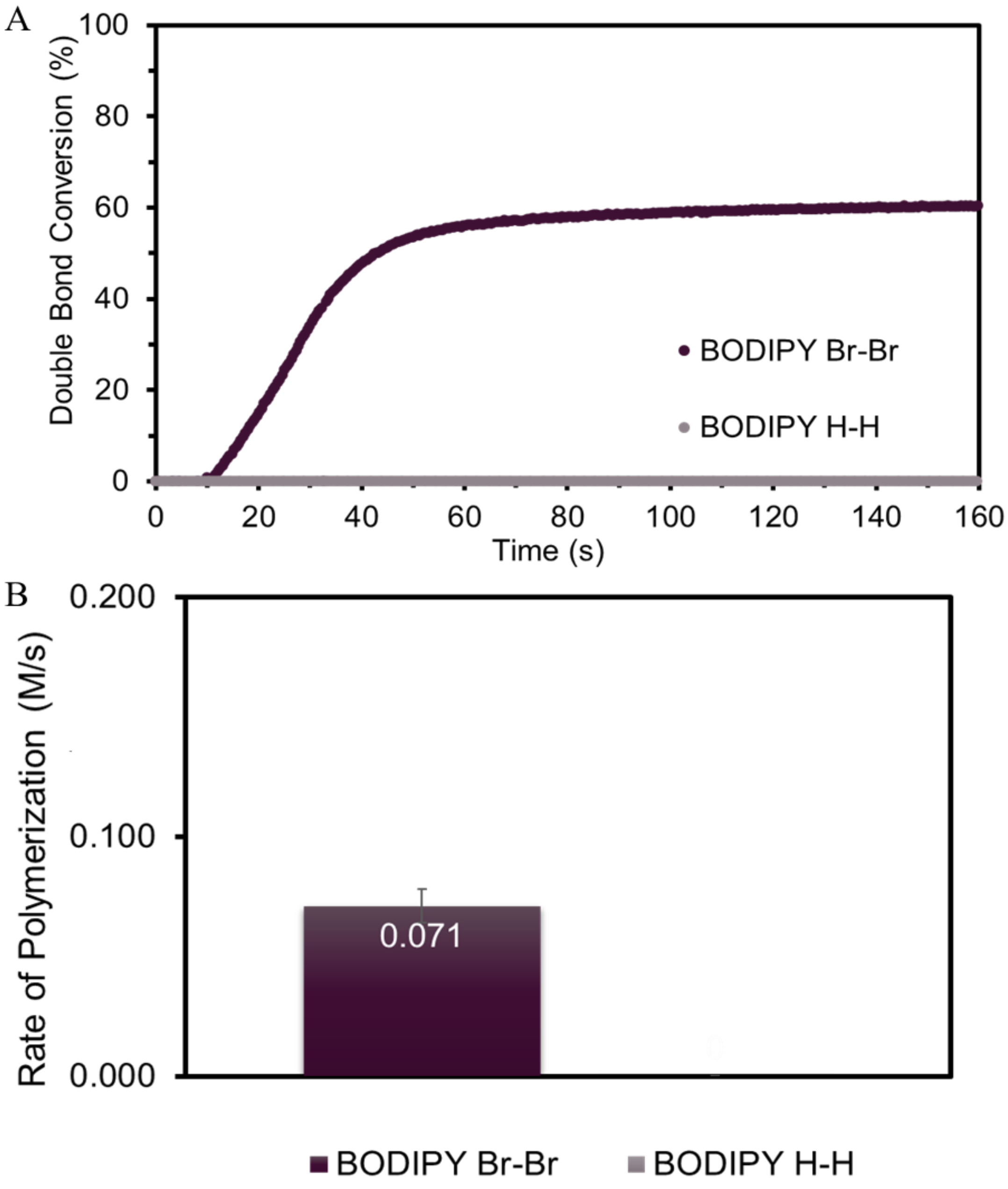

Figure S22. (A) Photopolymerization of isobornyl acrylate with **BODIPY-Br-Br** and **BODIPY-H-H** using an 850 nm LED equipped with a 775 nm longpass filter. The LED intensity was 40 mW/cm^2 (post-filter) using the resin formulation: 0.1 mol% BODIPY, 0.1 mol% Donor, and 1.0 mol% Acceptor. (B) Polymerization rate in M/s under the conditions employed in (A). Error bars represent ± 1 standard deviation from the mean.

The total number of photons absorbed for each photosystem was calculated using the following procedure. The emission profile of each LED was measured using a QE pro spectrometer (**Fig S21**) and equations **SE5** and **SE6** were used to convert the intensity output of the LED (mW/cm^2) (**Fig S23A**) into a photon flux (# of photons/cm$^2\cdot$s) (**Fig S23C**). **Fig S23B** shows the energy of each photon at each wavelength computed using equation **SE5**:

$$E = hc/\lambda \; (\mathbf{SE5})$$

where E is energy (mW), h is Plank's constant (= 6.626×10^{-34}J·s), c is the speed of light (3×10^8 m/s), and λ is wavelength (nm). The intensity of the LED source is given by:

$$I_{\mathrm{LED}} = n \times E/t \; (\mathbf{SE6})$$

where I_{LED} is the LED intensity density in mW/cm^2, n is number of photons, E is energy density of photons (mJ/cm^2), and t is the time in seconds. Dividing the light intensity at each wavelength (**Fig S23A**) by the energy per photon at that wavelength (**Fig S23B**) gives the total # of photons emitted by the LED at each wavelength (**Fig S23C**). If the intensity has a unit of (mW/cm$^2\cdot$nm), we integrate it across the entire emission spectrum in to obtain the total intensity (mW/cm^2). Transmission (T) was calculated using equation **SE7**, followed by the portion of photons absorbed as (1-T).

$$-logT = A = \varepsilon cl \; (\mathbf{SE7})$$

where A is absorption (AU), ε is molar absorptivity (M$^{-1}\cdot$cm-^{1}), c is concentration (M), and l is path length (cm). Multiplying the light intensity by (1-T) provided the number of photons being absorbed at each wavelength by a particular compound (**Fig S23D**). Finally, integrating each curve provided the total photon flux (or number of photons absorbed) for each sample.

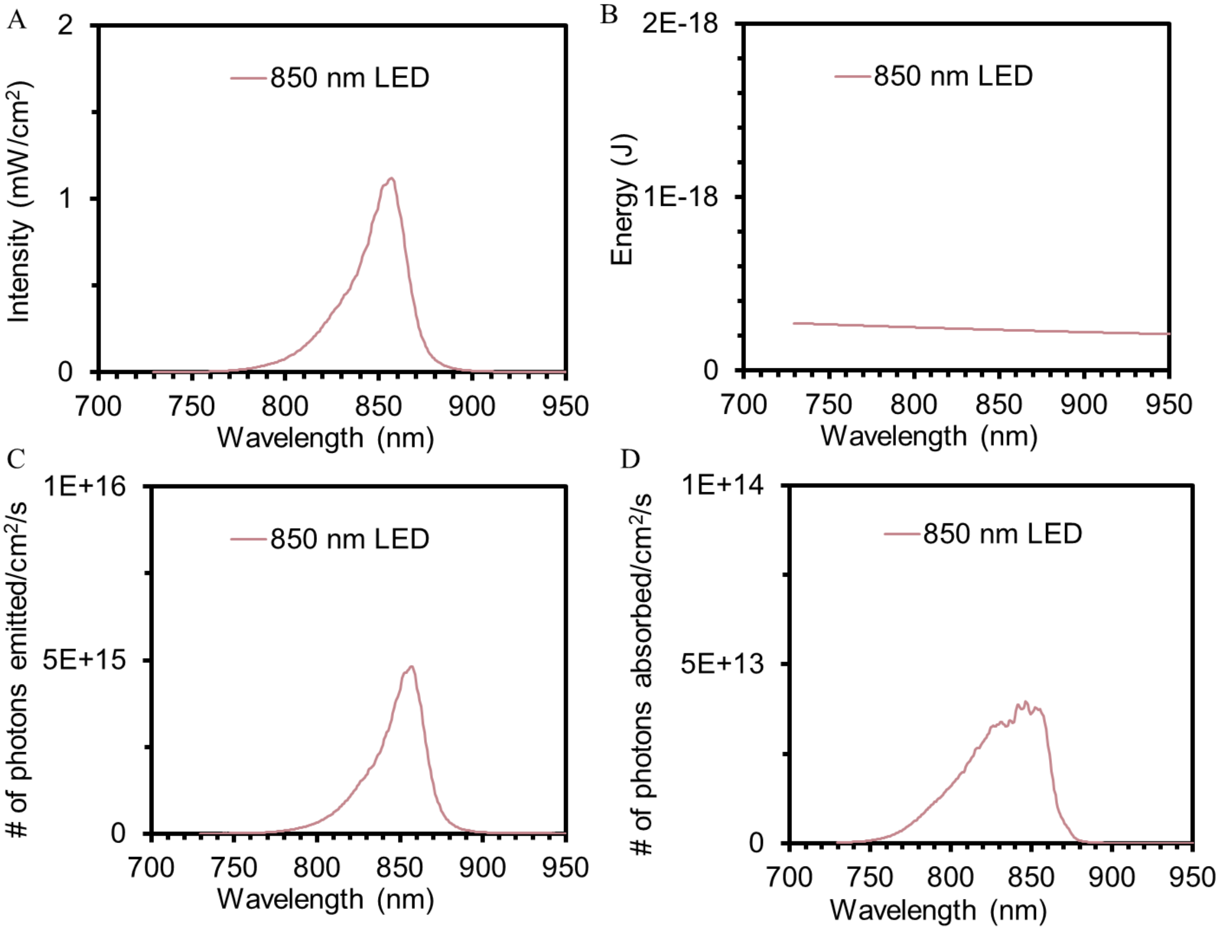

Figure S23. (A) Emission profile of the 850 nm LED at a total intensity density of 40 mW/cm^2. (B) Energy of a photon at the given wavelength of the 850 nm LED. (C) # of photons emitted at each wavelength of the 850 nm LED at 40 mW/cm^2. (D) # of photons absorbed by BODIPY-Ph-H of the 850 nm LED at 40 mW/cm^2.

Table S4. Total # of photons emitted at given LED intensities.

LED Intensity	# of photons/cm^2·s
850 nm (40 mW/cm^2)	1.87 x 10^{17}
850 nm (20 mW/cm^2)	9.32 x 10^{16}
850 nm (10 mW/cm^2)	4.66 x 10^{16}
850 nm (6.6 mW/cm^2)	3.08 x 10^{16}
850 nm (5 mW/cm^2)	2.33 x 10^{16}
850 nm (2.5 mW/cm^2)	1.17 x 10^{16}
780 nm (40 mW/cm^2)	1.65 x 10^{17}
780 nm (20 mW/cm^2)	8.27 x 10^{16}
780 nm (10 mW/cm^2)	4.13 x 10^{16}
780 nm (6.89 mW/cm^2)	2.85 x 10^{16}
780 nm (5 mW/cm^2)	2.07 x 10^{16}
780 nm (2.5 mW/cm^2)	1.03 x 10^{16}

Table S5. Total # of absorbed photons/cm^2·s at given LED intensities.

LED Intensity	BODIPY H-H	BODIPY Br-Br	BODIPY Ph-H	BODIPY Ph-Br
850 nm (40 mW/cm^2)	-	-	2.54 x 10^{15}	1.68 x 10^{15}
850 nm (20 mW/cm^2)	-	-	1.27 x 10^{15}	8.39 x 10^{14}
850 nm (10 mW/cm^2)	-	-	6.34 x 10^{14}	4.19 x 10^{14}
850 nm (6.6 mW/cm^2)	-	-	4.19 x 10^{14}	-
850 nm (5 mW/cm^2)	-	-	3.17 x 10^{14}	2.10 x 10^{14}
850 nm (2.5 mW/cm^2)	-	-	1.59 x 10^{14}	1.05 x 10^{14}
780 nm (40 mW/cm^2)	1.28 x 10^{15}	3.70 x 10^{15}	-	-
780 nm (20 mW/cm^2)	6.39 x 10^{14}	1.85 x 10^{15}	-	-
780 nm (10 mW/cm^2)	3.20 x 10^{14}	9.26 x 10^{14}	-	-
780 nm (6.89 mW/cm^2)	-	6.38 x 10^{14}	-	-
780 nm (5 mW/cm^2)	1.60 x 10^{14}	4.63 x 10^{14}	-	-
780 nm (2.5 mW/cm^2)	8.00 x 10^{13}	2.32 x 10^{14}	-	

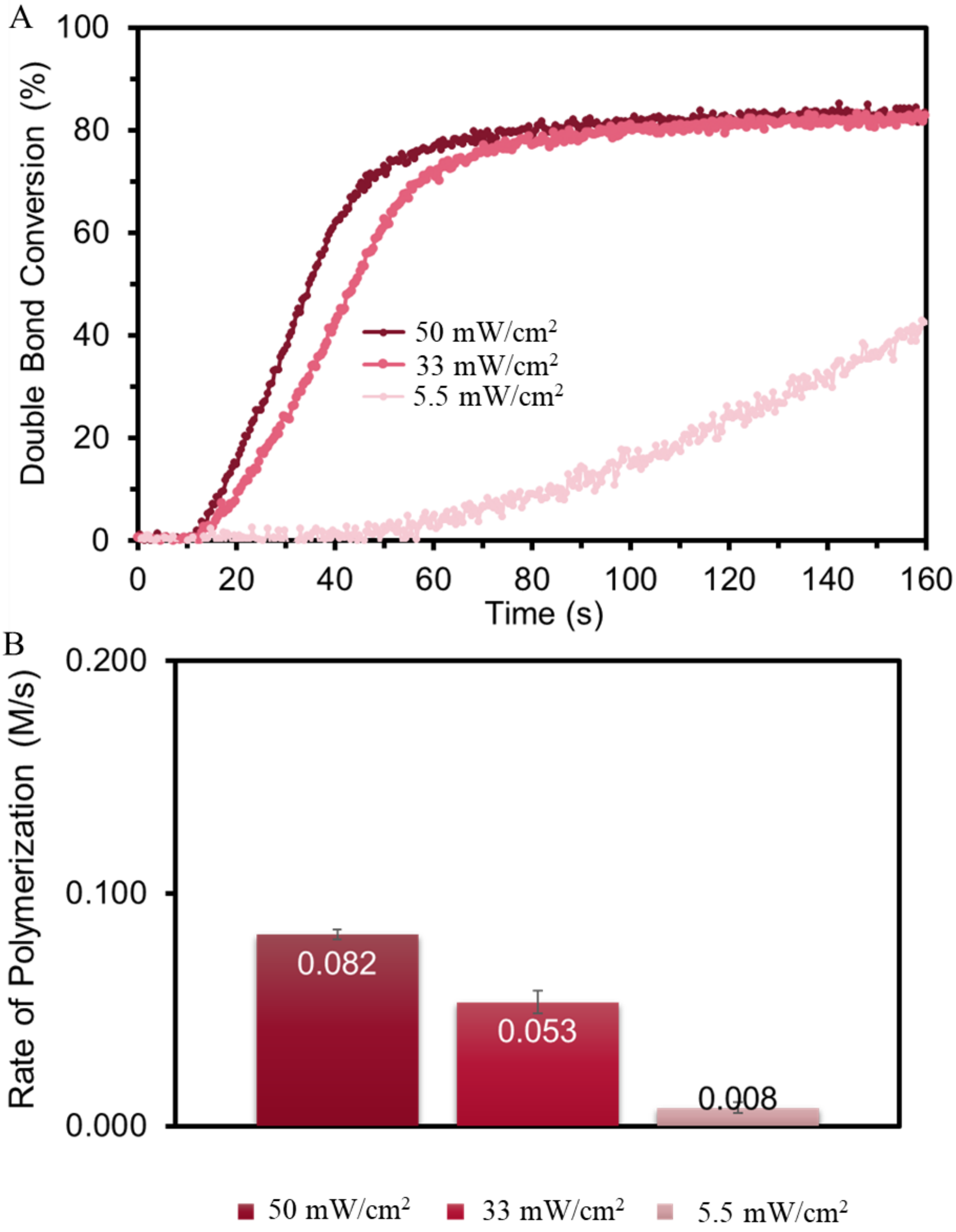

Figure S24. Photopolymerization of isobornyl acrylate with **BODIPY-Ph-H** using a 940 nm LED. (A) Double bond conversion vs. time determined using ATR-FTIR at varying LED intensities. (B) Polymerization rate in M/s at the different LED intensities. Error bars represent ± 1 standard deviation from the mean.

Transient Absorption (TA) Characterization.

Femtosecond time-resolved experiments: A detailed description of our femtosecond TA spectroscopy setup is given in previous reports.[S9,S10] Briefly, a Ti:sapphire regenerative amplifier (Coherent Legend Duo Elite, 4.5 mJ) was employed to produce ~90 fs pulses, centered at 800 nm, with a repetition rate of 3.0 kHz. A fraction of the 800 nm beam was routed into an optical parametric amplifier (Coherent TOPAS-Prime) to produce a 1200 nm signal beam. This 1200 nm beam was then focused into a 3 mm thick c-cut sapphire window to generate supercontinuum probe pulses that spanned a spectral range from ~600 nm to at least ~1120 nm, the upper wavelength limit of the Si CCD detector employed for TA measurements (Teledyne-Princeton Instruments PyLON 100BR). Another portion of the 800 nm beam was directed into a homebuilt noncollinear optical parametric amplifier to produce pump pulses centered at 670 nm. A mechanical chopper was used to adjust the repetition rate of the pump pulses to 1.5 kHz. Each pump pulse had a peak fluence of 120 μJ/cm^2 and the relative polarization between the pump and probe pulses was set to the magic angle of 54.7°.

Nanosecond time-resolved experiments: A fully integrated benchtop TA spectrometer (Magnitude Instruments enVISion) was utilized to record nanosecond TA measurements of the thiophene-BODIPYs. Using the second harmonic of the instrument's internal Nd:YAG laser, the samples were excited with pulsed 532 nm light at a repetition rate of 6 kHz and a pulse energy of 33.3 μJ. The peak fluence of the excitation beam was 114 μJ/cm^2. Photoinduced changes in sample absorption were probed in the visible and shortwave infrared using light produced by a xenon arc lamp. Background photoluminescence produced by the sample during TA measurements was recorded at each time delay and probe wavelength by measuring the sample response in the absence of the probe and was subtracted from recorded TA signals. The instrument response function of the internal detector used is ~5 ns.

Femtosecond TA Spectroscopy. The thiophene-BODIPY derivatives were prepared by dissolving dried powders of each compound in toluene. These sample solutions were stored in 1 mm pathlength cuvettes and degassed with nitrogen prior to experiments. Femtosecond TA spectra of **BODIPY-Br-Br** and **-Ph-Br** are reported in **Fig. 5** in the main text while spectra of **-H-H** and **-Ph-H** are displayed in **Fig. S25**.

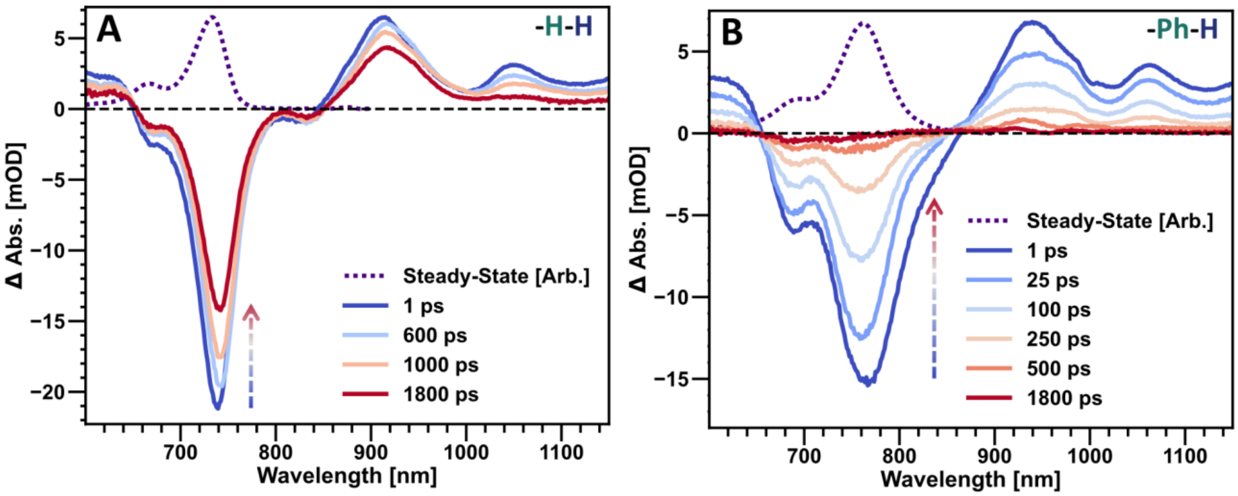

Figure S25. Femtosecond TA spectra of **BODIPY-H-H** (A) and **-Ph-H** (B) recorded in toluene. The steady-state absorption spectrum of each compound (purple dashed) is displayed as well.

Photoexcitation of **BODIPY-H-H** produces a ground state bleach centered at 740 nm concurrent with a prominent stimulated emission band at 815 nm and two excited state absorption features peaked near 900 nm and 1020 nm. This compound does not undergo any significant spectral changes as time progresses, indicating that the first excited singlet state (S_1) of this compound relaxes to its ground state (S_0) and does not produce an observable triplet state (T_1).

Photoexciting **BODIPY-Ph-H** yields a ground state bleach centered at 759 nm that appears in tandem with a stimulated emission shoulder in the vicinity of 820 nm and likewise two excited state absorption bands at 930 and 1060 nm. The stimulated emission and excited state absorption bands decay in parallel and signify the loss of S_1. As these S_1 features are depleted, a weak, positive excited state absorption feature that ranges from ~790 nm to ~1120 nm replaces the stimulated emission with a time constant of 157 ps. This excited state absorption feature also partially consumes the ground state bleach, which blue-shifts its maximum amplitude to ~740 nm. The emergence of these features suggests that some of the initially excited S_1 population evolves to a new state. However, nanosecond TA experiments (*vide infra*) suggest that this state is not T_1, but rather an intermediate state formed en route to T_1.

Global Target Analysis. To characterize the kinetics of S_1 decay and T_1 formation in the thiophene-BODIPY derivatives, global target analysis of the femtosecond TA spectra was performed using Glotaran software.[S11,S12] Each TA dataset $\Delta Abs(t,\ \lambda_{probe})$ was decomposed into linear combinations of basis vectors representing spectrally-distinct states of the system called species-associated decay spectra (SADS) $\{\sigma_n(\lambda_{probe})\}$.

$$\Delta Abs(t,\ \lambda_{probe}) = \sum_n c_n(t)\sigma_n(\lambda_{probe}) \qquad \textbf{(SE8)}$$

SADS contain both positive features due to excited state absorption and negative features that arise from a combination of ground state bleaching and stimulated emission. The time-dependent amplitudes $\{c_n(t)\}$ of the SADS are solutions to the set of sequential first-order rate equations below:

$$\frac{dc_1(t)}{dt} = I_0 - k_1 c_1 \qquad \textbf{(SE9)}$$

$$\frac{dc_n(t)}{dt} = k_{n-1}c_{n-1}(t) - k_n c_n(t), n > 1 \qquad \textbf{(SE10)}$$

I_0 represents the initial photoexcited population created by the pump pulse, and the set $\{k_n\}$ is comprised of first-order rate constants that correspond to the sequential transfer of population from one SADS to the next. For each compound, $\{k_n\}$ and $\{\sigma_n(\lambda_{probe})\}$ were estimated using a non-linear least squares method to minimize discrepancies between experimental and computed spectra. Likewise, the computed spectra were dispersion-corrected and convolved with a Gaussian instrument response function with a full-width at half maximum of ~100 fs to better approximate the experimental data.

Normalized SADS of the four thiophene-BODIPY compounds are displayed in **Figure S26**. Upon photoexcitation, **BODIPY-Br-Br** and **-Ph-Br** transfer a fraction of their excited population to their T_1 state. The T_1 state of these molecules is typified by the absence of stimulated emission and a broad excited state absorption band beginning anywhere from ~780 to ~800 nm and extending to ~1120 nm. The time constant describing the total loss of the S_1 SADS (τ) determined from global target analysis arises from competition between the rate of decay of S_1 to S_0 (k_{S1}) and the rate of T_1 formation via intersystem crossing (k_{ISC}):

$$\frac{1}{\tau} = k_{S1} + k_{ISC} \qquad \textbf{(SE11)}$$

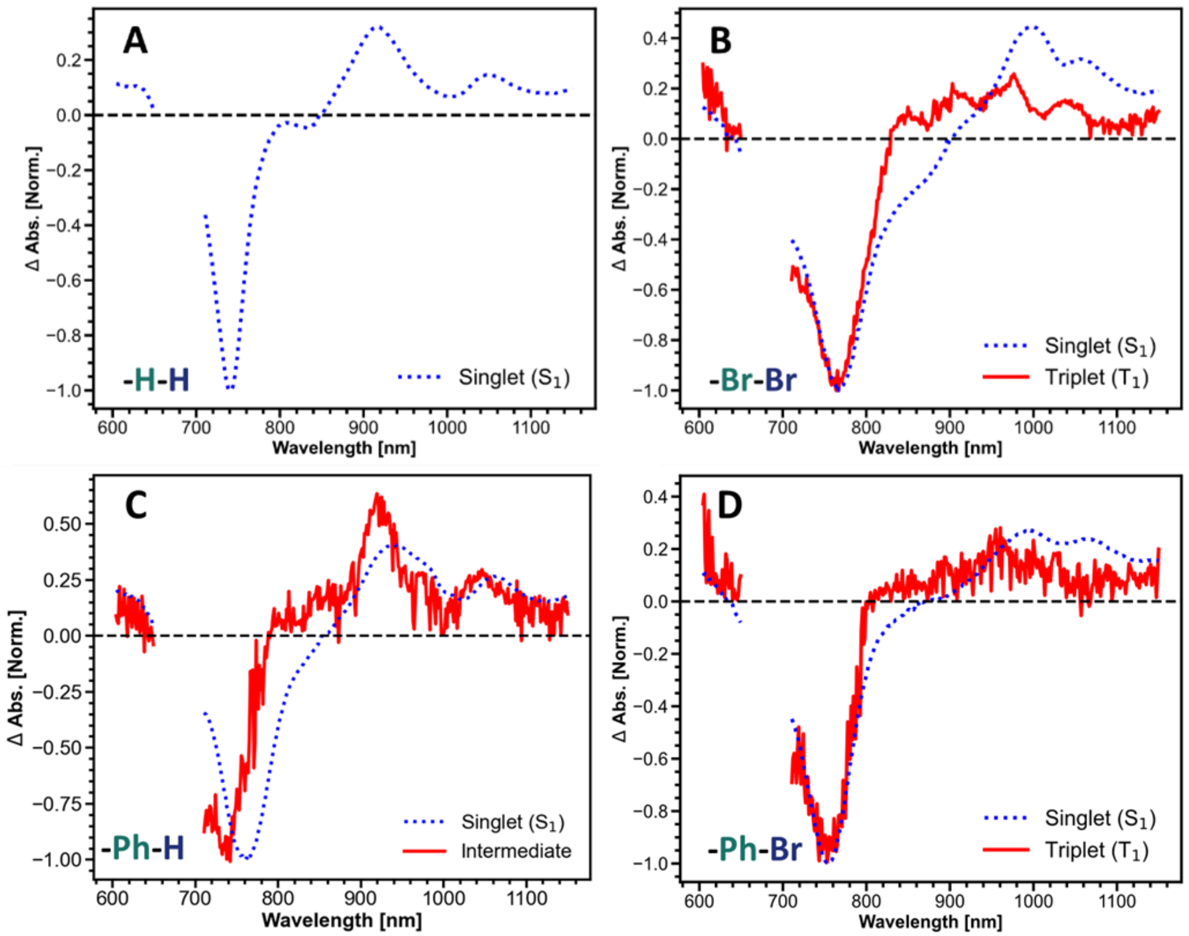

Figure S26. Normalized femtosecond TA SADS of thiophene-BODIPY derivatives corresponding to S_1 and T_1 states: (A) **BODIPY-H-H**, (B) **BODIPY-Br-Br**, (C) **BODIPY-Ph-H**, and (D) **BODIPY-Ph-Br**. Pump scatter in the vicinity of 670 nm has been omitted.

Fig. S27 highlights that as **BODIPY-Br-Br** and **-Ph-Br** undergo ISC to form their respective triplet states, their ground state bleach undergoes negligible spectral evolution. The persistence of the ground state bleach lineshape during triplet formation indicates that it negligibly overlaps with induced absorption features associated with each molecule's T_1 state. Therefore, the triplet yield for these compounds (Φ_T) can be estimated from the percent recovery of the ground state bleach amplitude. Φ_T values of **BODIPY-Br-Br** and **-Ph-Br** were found to be 14% and 5.5%, respectively, as displayed in **Figure 5A** of the main text. Because k_{ISC} is simply the product of $1/\tau$ and Φ_T, k_{ISC} values of 0.372 ns^{-1} and 0.556 ns^{-1} were computed for **BODIPY-Br-Br** and **-Ph-Br**. These results are summarized in **Table S6**.

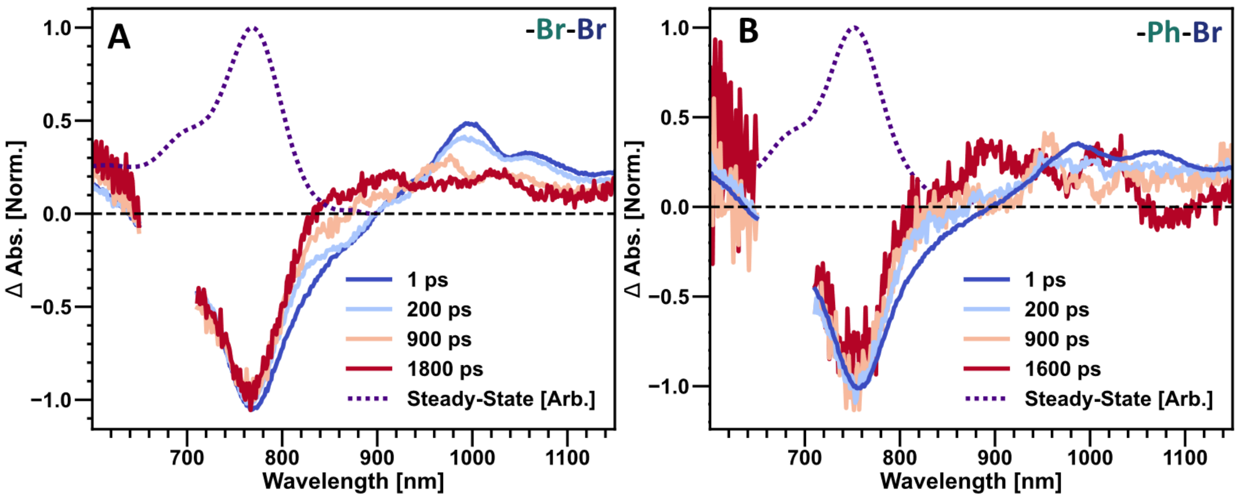

Figure S27. Femtosecond TA spectra of (A) **BODIPY-Br-Br** and (B) **BODIPY-Ph-Br** normalized to the ground state bleach maximum at each time delay. As time progresses, the shape of the ground state bleach of **-Br-Br** and **-Ph-Br** undergo only negligible changes, indicating that the ground state bleach minimally overlaps with induced absorption features from the T_1 state. This minimal overlap allows the triplet formation yield to be estimated from the recovery of the ground state bleach amplitude.

Table S6. Thiophene-BODIPY Triplet Yields and Intersystem Crossing (ISC) rates determined by global target analysis

BODIPY	Φ_T	τ (ps)	k_{ISC} (ns^{-1})	k_{S_1} (ns^{-1})
-Br-Br	0.14	376	0.372	2.29
-Ph-Br	0.055	99	0.556	9.54

Nanosecond TA Spectroscopy. Neat thiophene-BODIPY sample solutions were prepared by dissolving dried powders of each compound in toluene. Solutions containing 10 μM platinum octaethylporphyrin (PtOEP) and 100 μM of thiophene-BODIPY were also prepared. All samples were stored in 1 mm pathlength cuvettes and degassed with nitrogen prior to experiments.

To determine if the evolution observed in the femtosecond TA spectra of **BODIPY-Br-Br**, **-Ph-Br**, and **-Ph-H** was consistent with the formation of T_1, triplet sensitization experiments were performed using PtOEP, a well-studied triplet sensitizer.[S13] Nanosecond TA spectra of toluene solutions containing PtOEP and PtOEP mixed with thiophene-BODIPYs are reported in **Fig. S28**. Following photoexcitation, PtOEP is known to undergo intersystem crossing to form its T_1 state within ~165 fs.[S14] In the spectral range we probe, 600 – 950 nm, this state gives rise to a series of excited state absorption features, with the strongest band appearing in the vicinity of 775 nm. When **BODIPY-Br-Br**, **-Ph-Br**, and **-Ph-H** are added to solutions containing PtOEP, these three bands decay rapidly following photoexcitation of PtOEP. In their place, a negative band centered near 750 nm appears, which can be attributed to the ground state bleach of each thiophene-BODIPY. In **Fig. S29** we compare the rate of decay of phosphorescence detected from PtOEP against the growth of the ground state bleach of each thiophene-BODIPY to determine if these features are correlated. In each case, we indeed find the rate of decay of PtOEP's T_1 state matches that for the growth of the thiophene-BODIPY ground state, indicating triplet energy transfer from PtOEP to each thiophene-BODIPY. This energy transfer allows us to discern from this data the TA spectrum of the T_1 state of each thiophene-BODIPY.

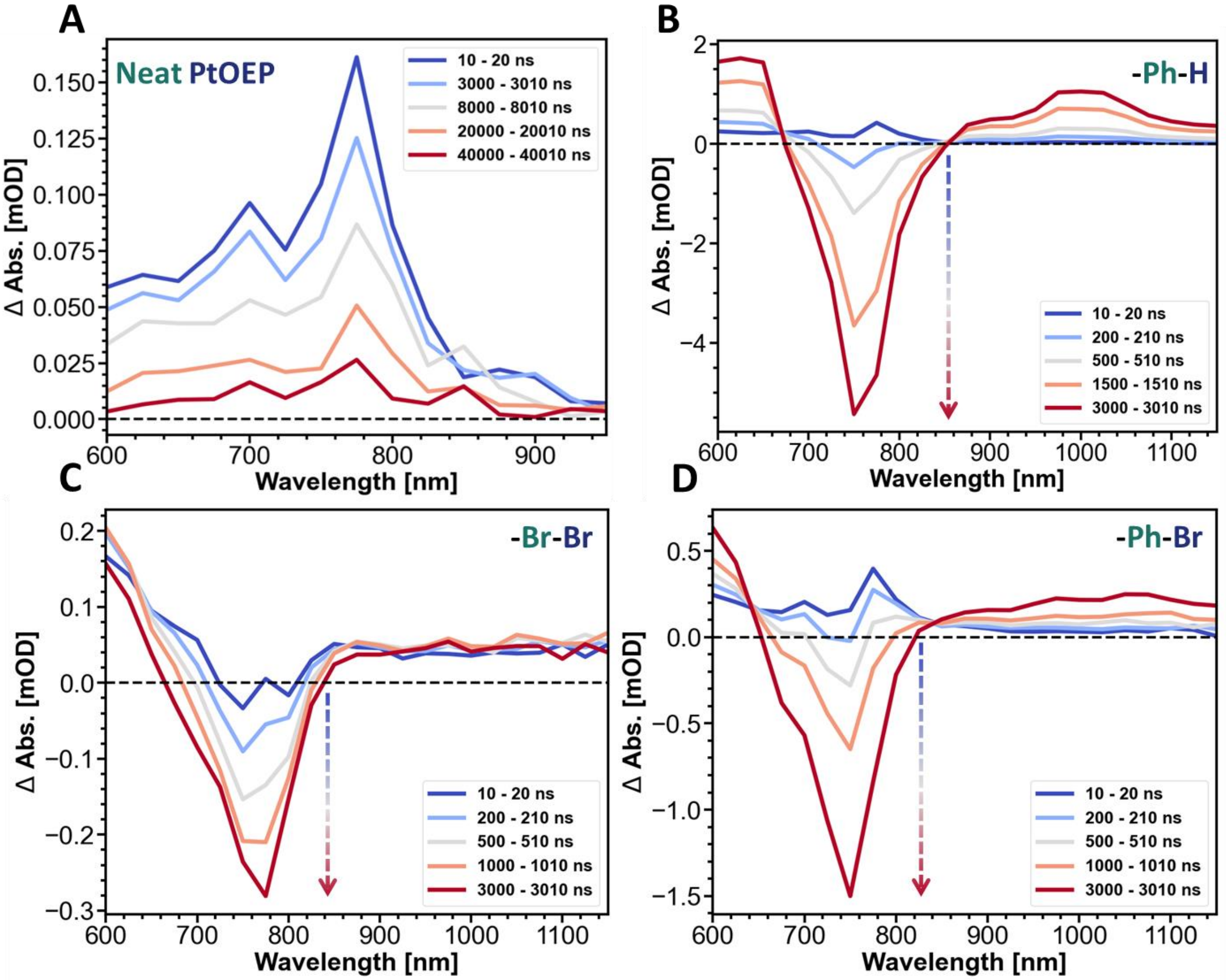

Figure S28. Nanosecond TA spectra of toluene solutions of neat PtOEP (A) and solutions containing 10% PtOEP mixed with **BODIPY-Ph-H** (B), **BODIPY-Br-Br** (C), or **BODIPY-Ph-Br** (D).

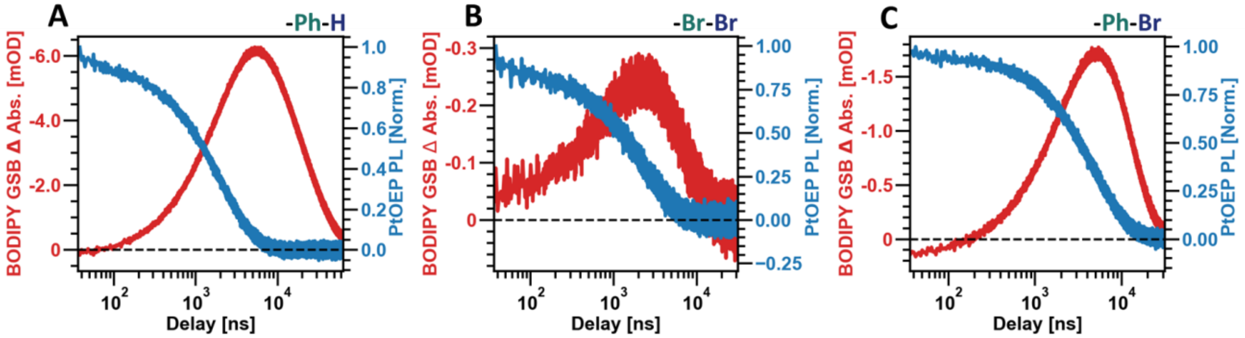

Figure S29. Comparison of the time-resolved phosphorescence decay of PtOEP (blue, λ_{Em} = 650 nm) and the growth of the thiophene-BODIPY ground state bleach (GSB) (red, λ_{probe} = 750 nm) in TA spectra of PtOEP solutions containing **BODIPY-Ph-H** (A), **BODIPY-Br-Br** (B), and **BODIPY-Ph-Br** (C). The correlated decay and growth of these features indicates successful triplet energy transfer from PtOEP to each thiophene-BODIPY.

Fig. S30 compares the PtOEP-sensitized thiophene-BODIPY T_1 spectra to the long-lived SADS obtained from global-target analysis of femtosecond TA measurements. The spectral similarity revealed by these comparisons indicate that T_1 is indeed formed in neat solutions of **BODIPY-Br-Br** and **-Ph-Br** over the course of a few hundred picoseconds (**Figs. S30B** & **S30C**). However, the intermediate state observed in femtosecond TA spectra of **BODIPY-Ph-H** does not appear to be consistent with its T_1 state as the position of its ground state bleach and induced absorption bands do not line up well with the T_1 spectrum extracted from PtOEP sensitization experiments (**Fig. S30A**).

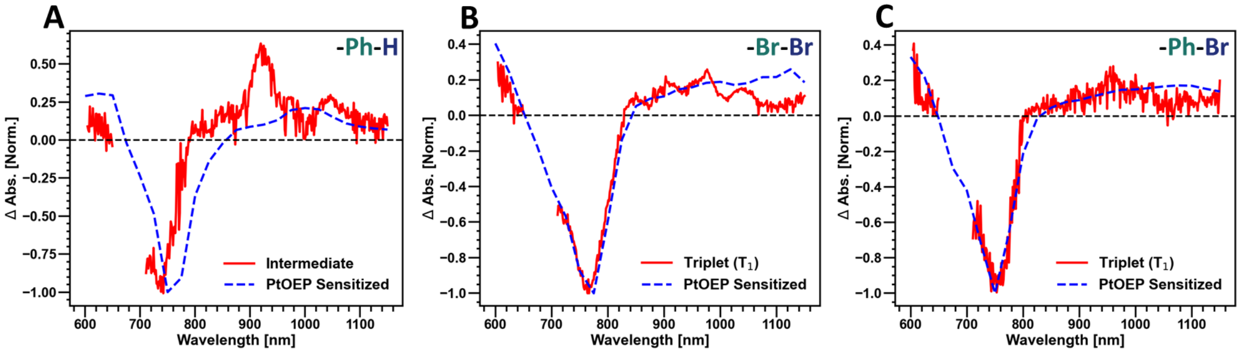

Figure S30. Comparison of long-lived SADS computed from global-target analysis of femtosecond TA spectra (red) and triplet spectra extracted from PtOEP sensitization experiments (blue, dashed) for **BODIPY-Ph-H** (A), **BODIPY-Br-Br** (B), and **BODIPY-Ph-Br** (C).

Nanosecond TA spectra of neat **BODIPY-Br-Br** and **-Ph-Br** were recorded to determine their T_1 lifetime (**Figs. S31A** & **S31B**). To minimize noise, the spectra displayed are averaged over the 10 ns intervals reported in the legend of each subfigure. These spectra are consistent with the PtOEP-sensitized spectra; they contain a ground state bleach in the vicinity of 750 nm and a broad excited state absorption band that ranges from ~800 nm to beyond 1100 nm. A single exponential decay was fit to the 750 nm traces of **BODIPY-Br-Br** and **Ph-Br** (**Figs. S31C** & **S31D**). **BODIPY-Ph-Br** was determined to have a T_1 lifetime of 9.5 μs, which is nearly 8× longer than the 1.2 μs lifetime computed for **BODIPY-Br-Br**. We suspect the shorter lifetime of **BODIPY-Br-Br** relative to **-Ph-Br** arises from enhanced intersystem crossing due to the presence of two additional bromine atoms in its structure.

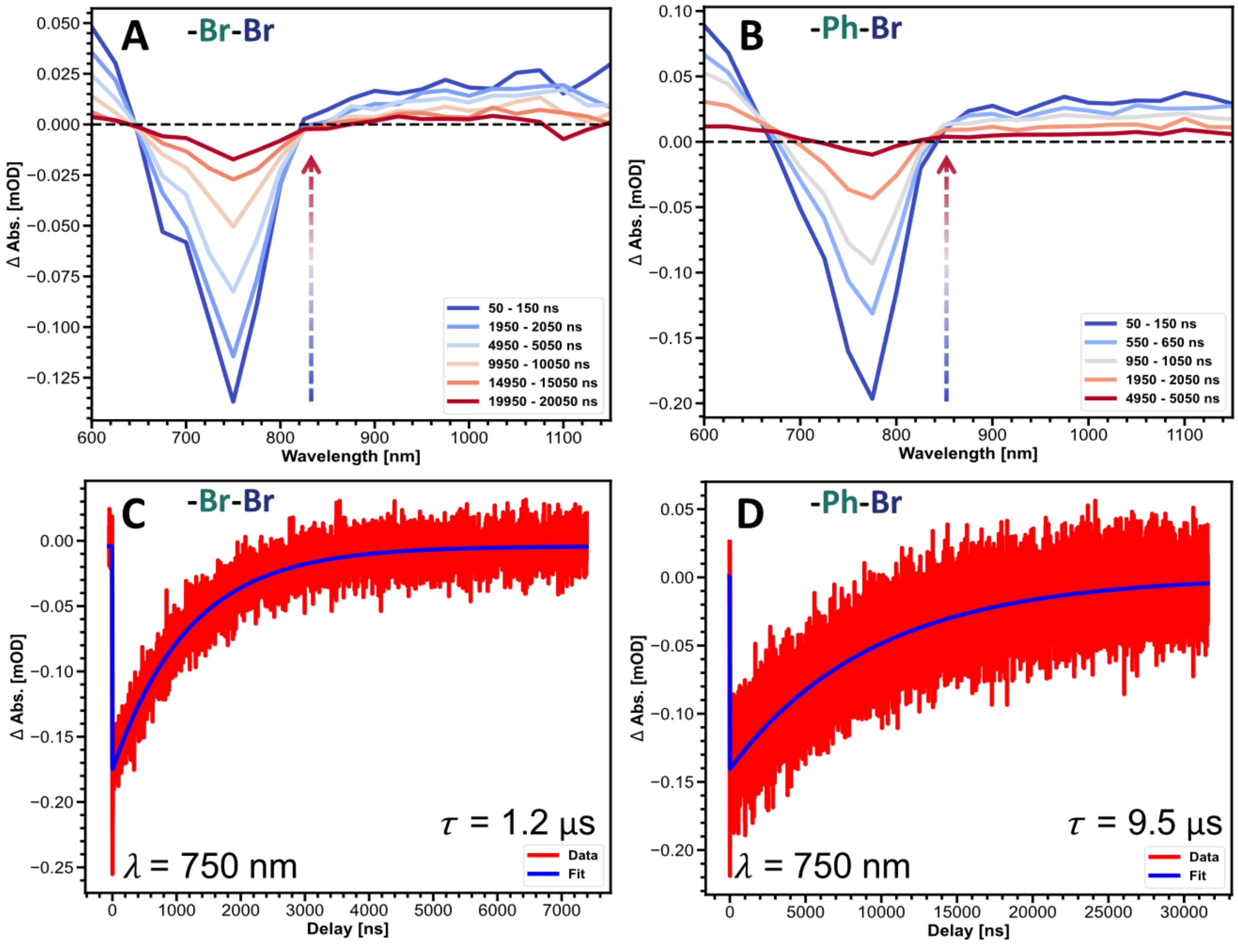

Figure S31. (A & B) Nanosecond TA spectra of **BODIPY-Br-Br** (A) and **BODIPY-Ph-Br** (B) that highlight the decay of the T_1 state of each compound. Spectra are averaged over the time ranges noted in the legend of each figure. (C & D) Decay of the ground state bleach of **BODIPY-Br-Br** (C) and **BODIPY-Ph-Br** (D) at 750 nm. Fitting each trace to an exponential decay yields T_1 lifetimes of 1.2 µs and 9.5 µs for **BODIPY-Br-Br** and **BODIPY-Ph-Br**, respectively.

Nanosecond TA measurements of neat **BODIPY-Ph-H** (**Figs. S32A** & **S32B**) were also collected to determine the fate of the intermediate state observed in femtosecond TA measurements. At delays less than 10 ns, we observe strong excited state absorption features at 775 nm and 850 nm. As these features decay, the ground state bleach of **BODIPY-Ph-H** grows in and reaches a maximum amplitude at ~3 µs. A comparison of the neat **BODIPY-Ph-H** nanosecond TA spectrum observed after 10 µs to the T_1 spectrum acquired from PtOEP-sensitization demonstrates that neat **BODIPY-Ph-H** forms T_1 (**Fig. S32C**). We thus hypothesize that the temporal evolution observed in nanosecond TA measurements of **BODIPY-Ph-H** corresponds to conversion of the intermediate state viewed in femtosecond TA measurements to **BODIPY -Ph-H**'s T_1 state.

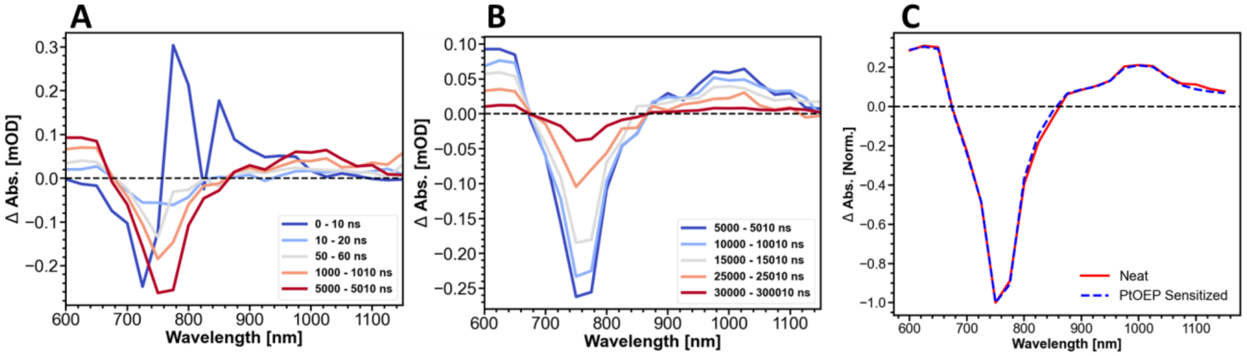

Figure S32. Nanosecond TA measurements of neat **BODIPY-Ph-H** highlighting the growth (A) and decay (B) of its T_1 state. (C) Normalized comparison of the nanosecond TA spectrum of neat **BODIPY-Ph-H** and the T_1 spectrum obtained from PtOEP sensitization experiments (blue, dashed).

To vet this hypothesis, a two-state global-target analysis model was applied to the nanosecond TA data of neat **Ph-H-BODIPY**. This model assumes that an intermediate state formed from S_1 undergoes intersystem crossing to generate T_1. The SADS with the shortest lifetime, SADS 1, bears rough resemblance to the long-lived spectrum observed in femtosecond TA measurements (**Fig. S33A**), and we therefore suspect these spectra represent the same intermediate species. On the other hand, we unequivocally assign SADS 2 to the T_1 state of **Ph-H-BODIPY** spectrum due to its agreement with T_1 spectra obtained from PtOEP sensitization experiments (**Fig. S33B).** While we are unable to assign an origin at this time to the intermediate state, our data shows that it decays with a time constant of 1.6 μs, making k_{ISC} 0.621 μs^{-1}, which is three orders of magnitude slower than the intersystem crossing rates of the brominated species. Furthermore, the lifetime of T_1 (SADS 2) was computed to be 22 μs.

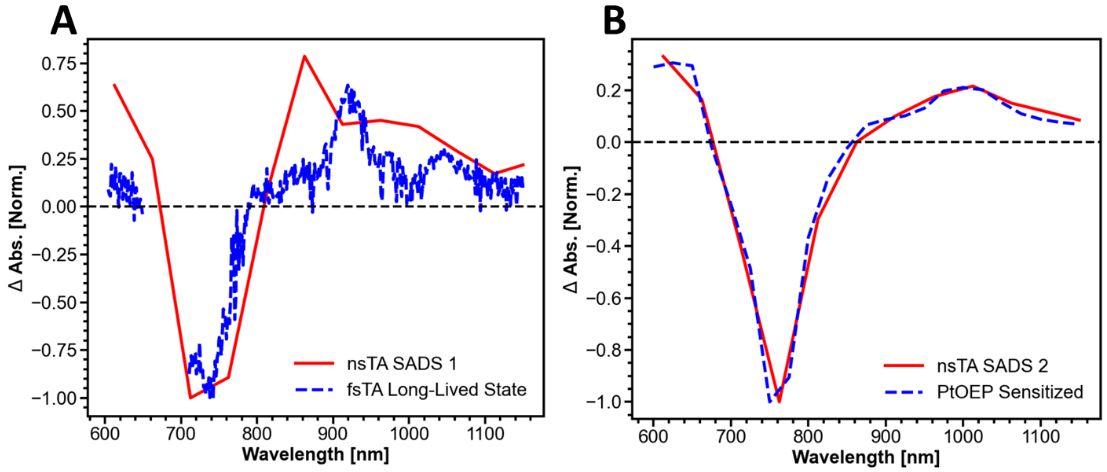

Figure S33. Normalized comparison of the SADS obtained from global-target analysis of nanosecond TA data of neat **BODIPY-Ph-H**. (A) SADS 1 (red) with a lifetime of 1.6 μs is compared to the long-lived component acquired from femtosecond TA experiments (blue, dashed). (B) SADS 2 (red) with a lifetime of 22 μs is compared to the T_1 spectrum extracted from the PtOEP sensitization experiment (blue, dashed).

Optimization of Resin Composition for Photopolymerizations

Photopolymerizations were conducted in triplicate using an 850 nm LED with a 775 nm longpass filter at 20 mW/cm^2. Resin compositions were made at the highest concentration and subsequently diluted to achieve the varying Borate and BODIPY concentrations.

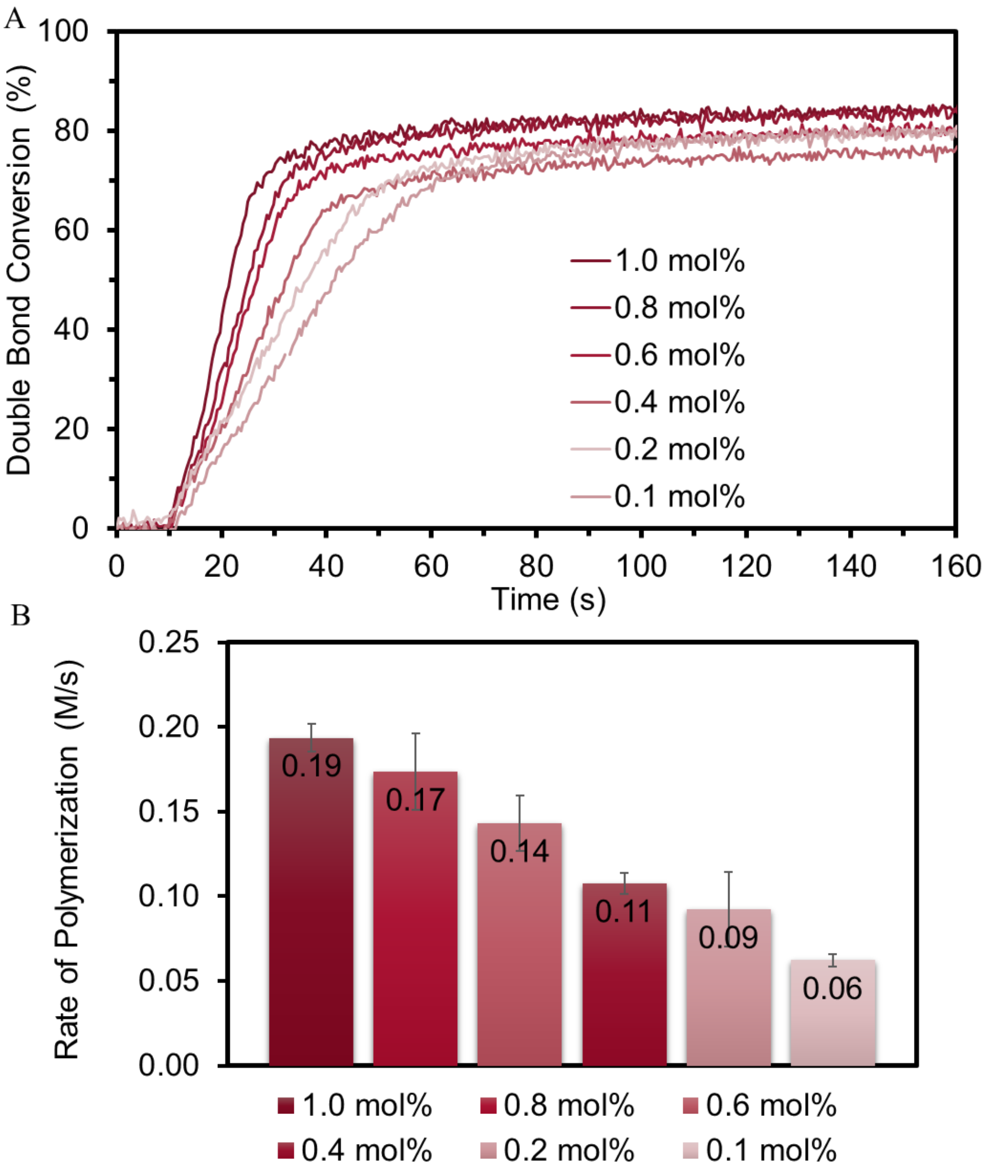

Figure S34. Photopolymerization of isobornyl acrylate with **BODIPY-Ph-H** at varying Borate concentrations using an 850 nm LED with a 775 nm LP filter at 20 mW/cm^2. Resin composition initially made at 0.1 mol% BODIPY, 1.0 mol% Borate V and 1.0 mol% HNu 254 and subsequently diluted, maintaining 0.1 mol% BODIPY and 1.0 mol% HNu 254. (A) Double bond conversion vs time determined using ATR-FTIR at varying Borate concentrations. (B) Polymerization rate in M/s at the different LED intensities. Error bars represent ± 1 standard deviation from the mean.

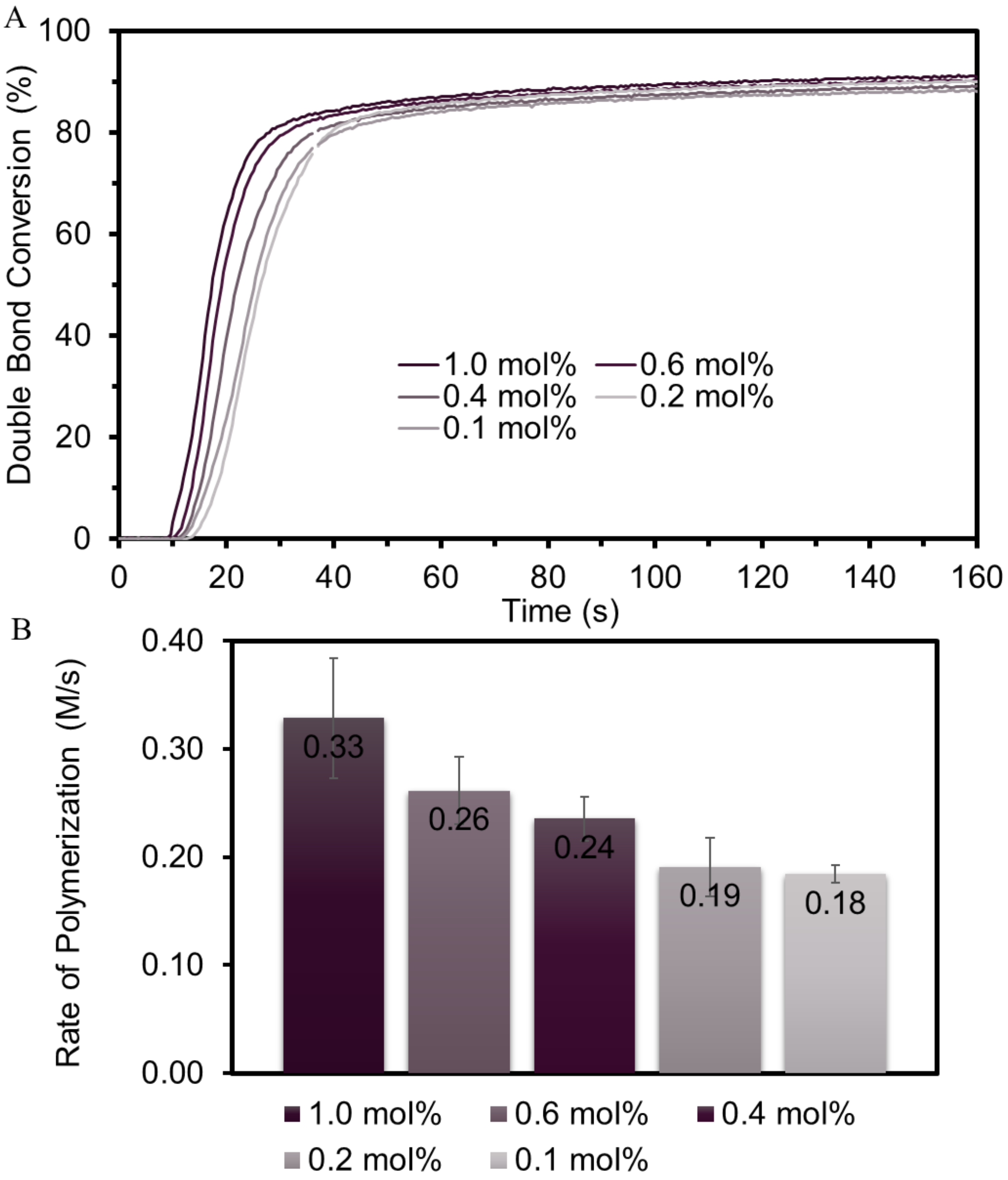

Figure S35. Photopolymerization of isobornyl acrylate with **BODIPY-Ph-H** at varying BODIPY concentrations using an 850 nm LED with a 775 nm LP filter at 20 mW/cm^2. Resin composition initially made at 1.0 mol% BODIPY, 1.0 mol% Borate V and 1.0 mol% HNu 254 and subsequently diluted maintaining 1.0 mol% Borate and 1.0 mol% HNu 254. (A) Double bond conversion vs time determined using ATR-FTIR at varying BODIPY concentrations. (B) Polymerization rate in M/s at the different LED intensities. Error bars represent ± 1 standard deviation from the mean.

Table S7. Rates of Photopolymerization with varying Borate and BODIPY Concentrations. Measurements carried out in triplicate. The concentration of HNu 254 remained at 1.0 mol% for all measurements. The BODIPY-Ph-H concentration was 0.1 mol% for Borate concentration tests while the Borate V concentration was 1.0 mol% for BODIPY-Ph-H concentration tests.

Concentration	**Rate (M/s)**
0.1 mol% Borate V	0.06 ± 0.004
0.2 mol% Borate V	0.09 ± 0.02
0.4 mol% Borate V	0.11 ± 0.01
0.6 mol% Borate V	0.14 ± 0.02
0.8 mol% Borate V	0.17 ± 0.02
1.0 mol% Borate V	0.19 ± 0.01
0.1 mol% BODIPY-H-H	0.18 ± 0.01
0.2 mol% BODIPY-H-H	0.19 ± 0.03
0.4 mol% BODIPY-H-H	0.24 ± 0.02
0.6 mol% BODIPY-H-H	0.26 ± 0.03
1.0 mol% BODIPY-H-H	0.33 ± 0.06

Photopolymerizations at Normalized Photons Absorbed

Photopolymerizations were conducted in triplicate at an equal total number of photons absorbed (**SE5-SE7**, above) using varying LED intensities. With a 780 nm LED, the resin formulation used was: 0.1 mol% BODIPY, 0.1 mol% Borate V (donor), and 1.0 mol% Iodonium salt (acceptor). For ATR measurements, a path length of 2.5 µm was used given an effective angle of 45°, a wavenumber of 808 cm^{-1} (*vide infra*), a refractive index of 2.4 for the ATR crystal (diamond), and a sample refractive index of 1.5 (estimate)[S15].

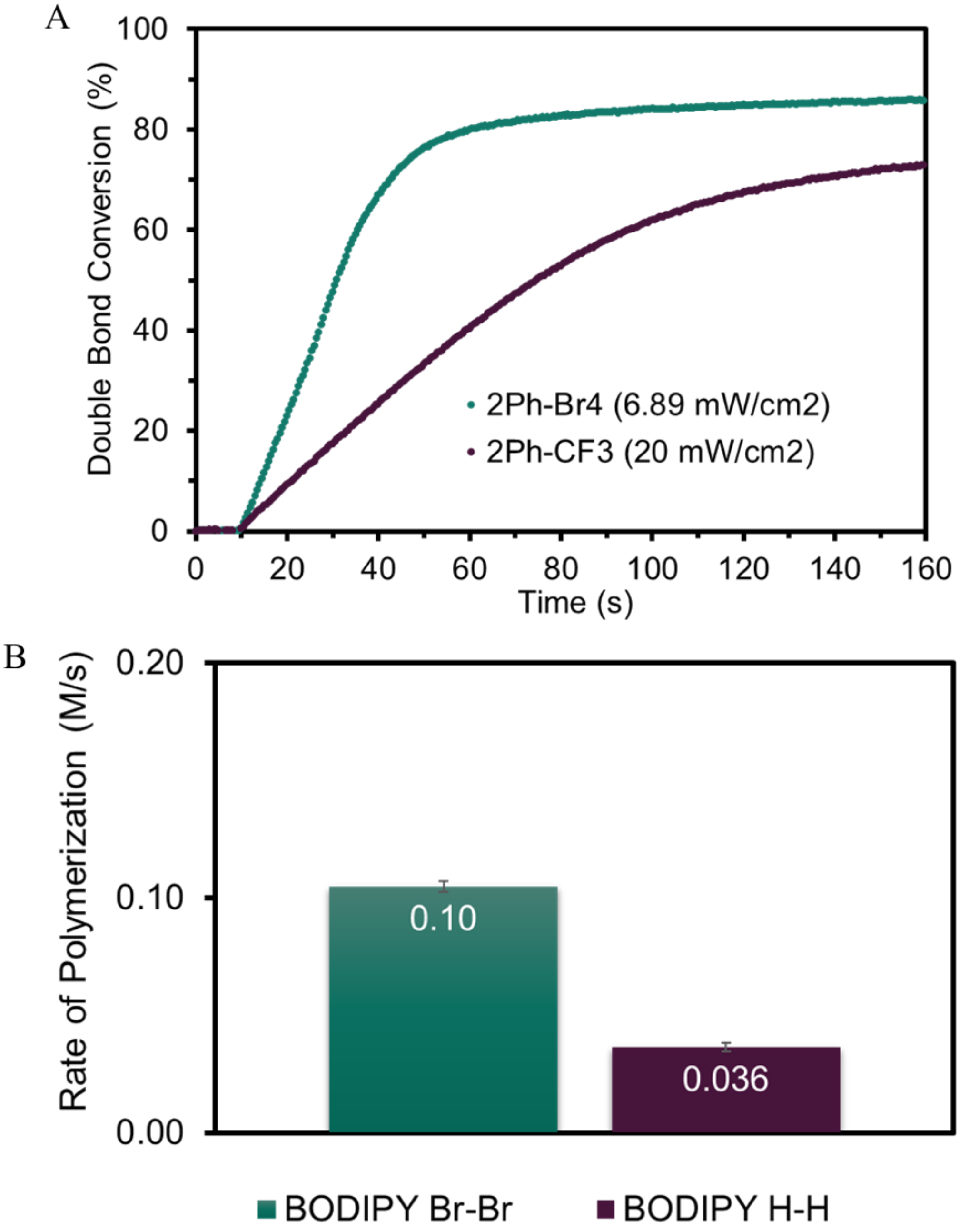

Figure S36. Photopolymerization of isobornyl acrylate with **BODIPY-H-H** and **BODIPY-Br-Br** under conditions wherein each photocatalyst absorbs photons from a 780 nm LED at an equal rate. (A) Double bond conversion vs time determined using ATR-FTIR under these conditions. (B) Polymerization rate in M/s under the conditions employed in (A). Error bars represent ± 1 standard deviation from the mean.

CHARACTERIZATION

^{1}H NMR Data

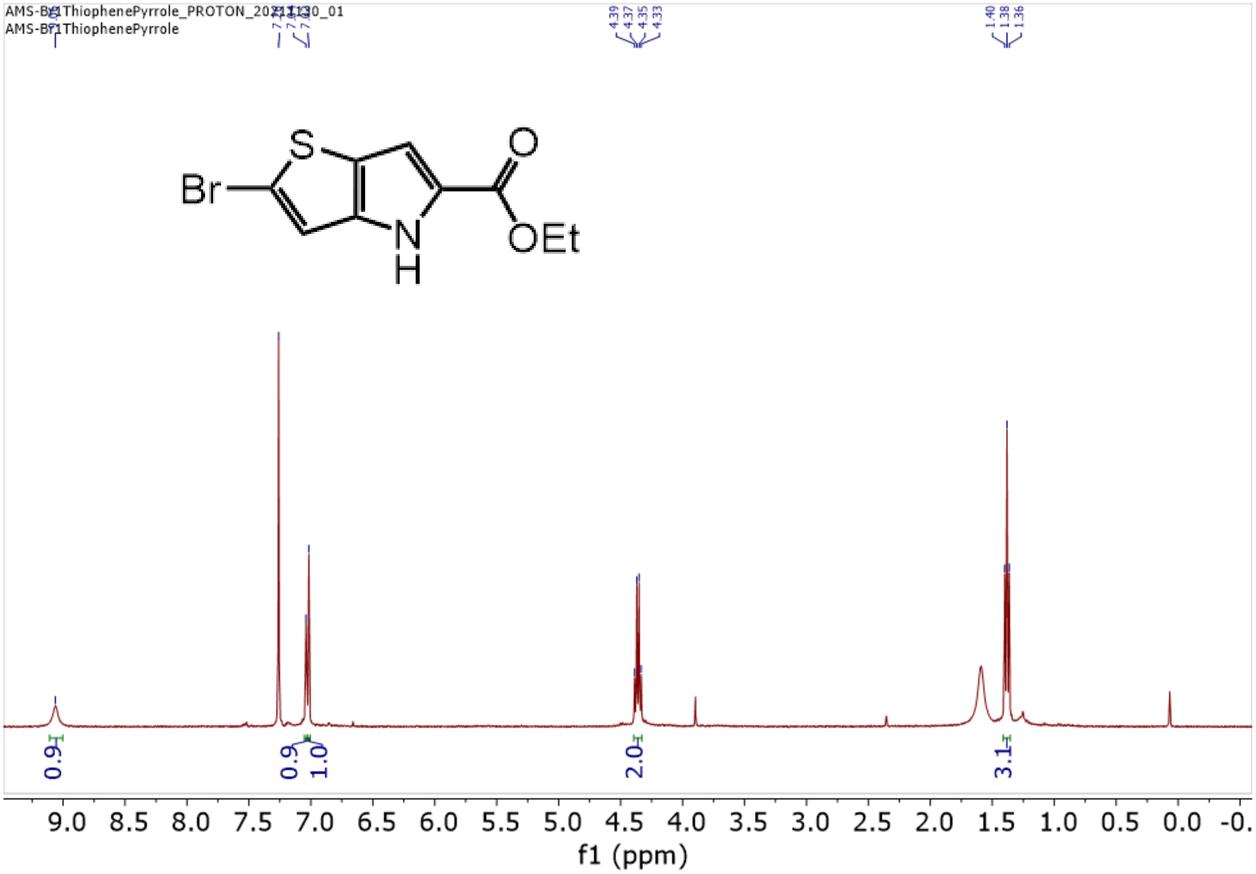

Figure S37: ^{1}H NMR of compound **S1a** in $CDCl_3$

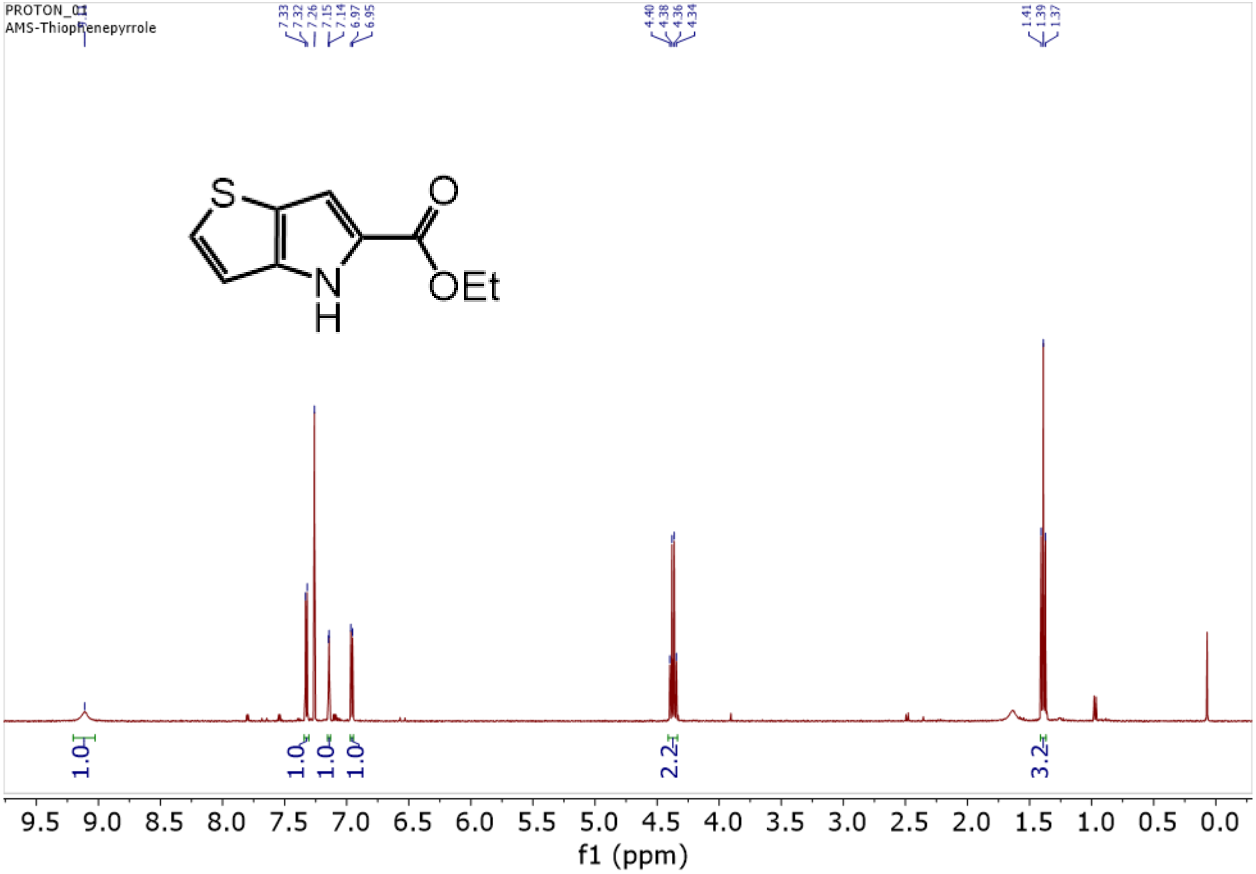

Figure S38: ^{1}H NMR of compound **S2a** in $CDCl_3$

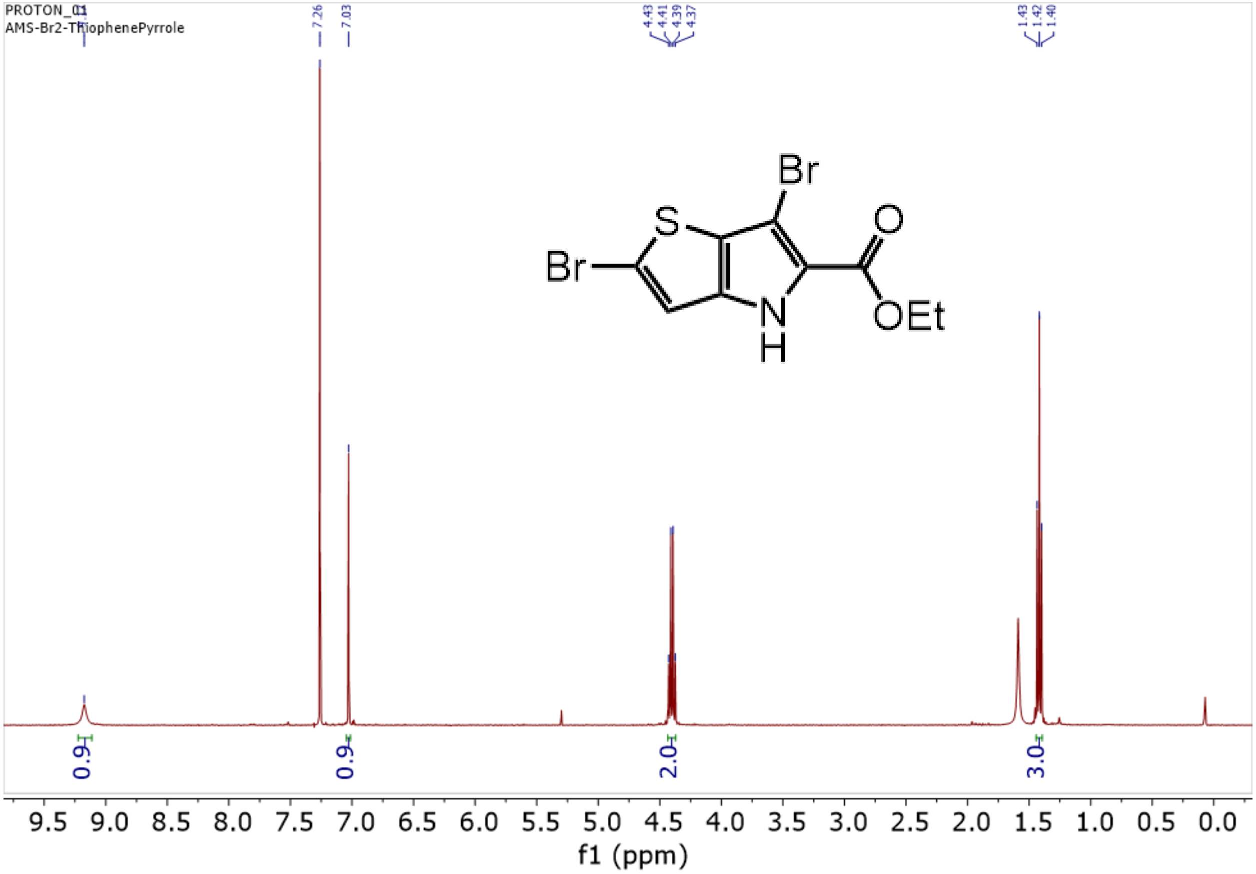

Figure S39: ^{1}H NMR of compound **S2b** in $CDCl_3$

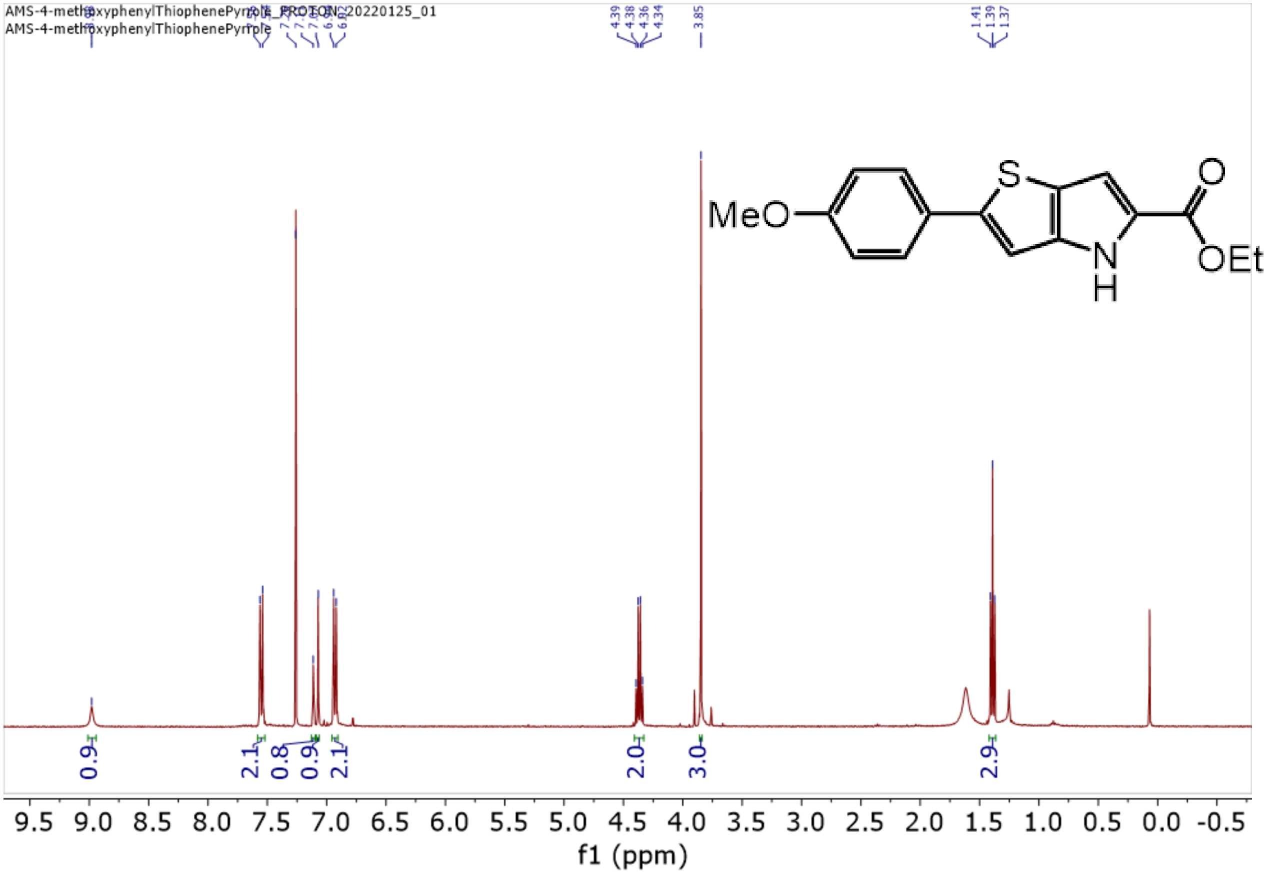

Figure S40: ^{1}H NMR of compound **S1b** in $CDCl_3$

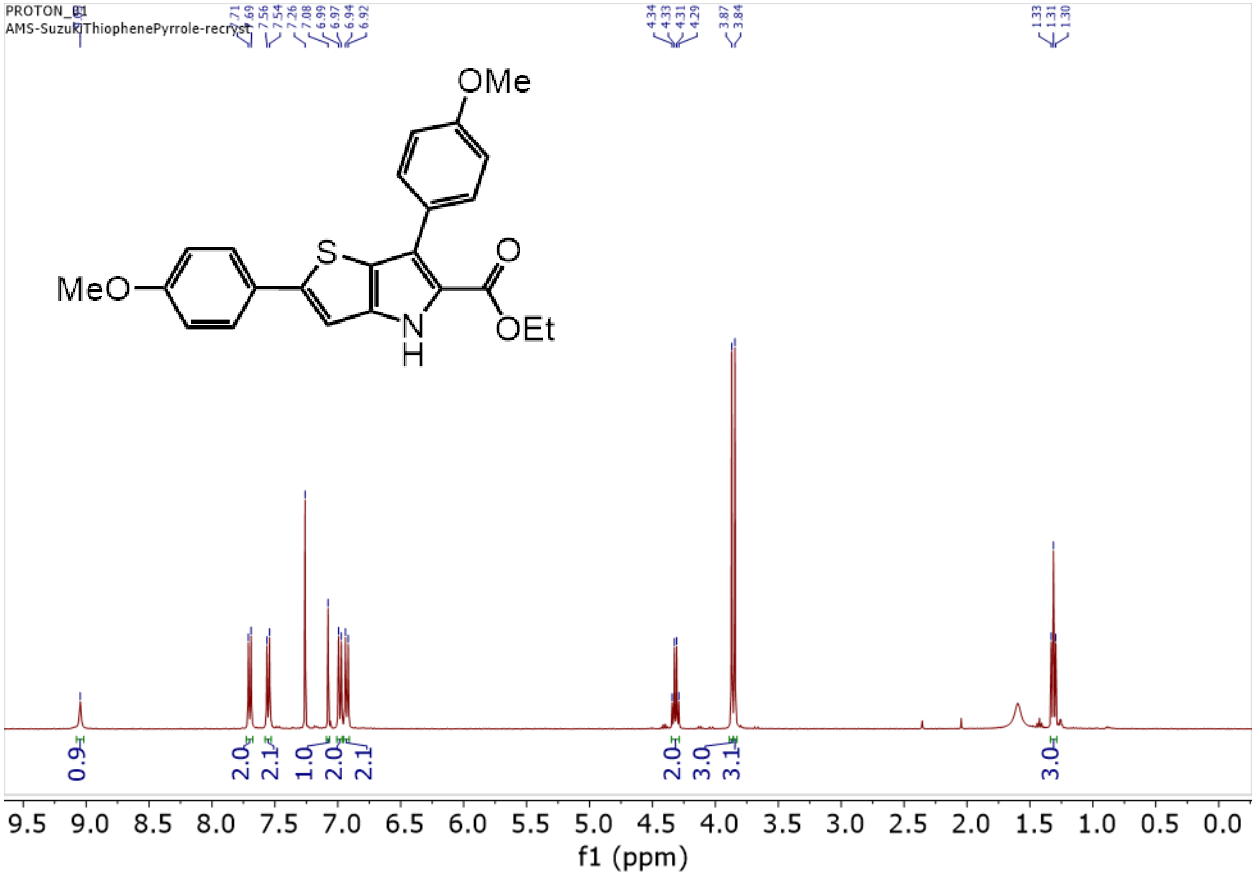

Figure S41: ^{1}H NMR of compound **S2c** in $CDCl_3$

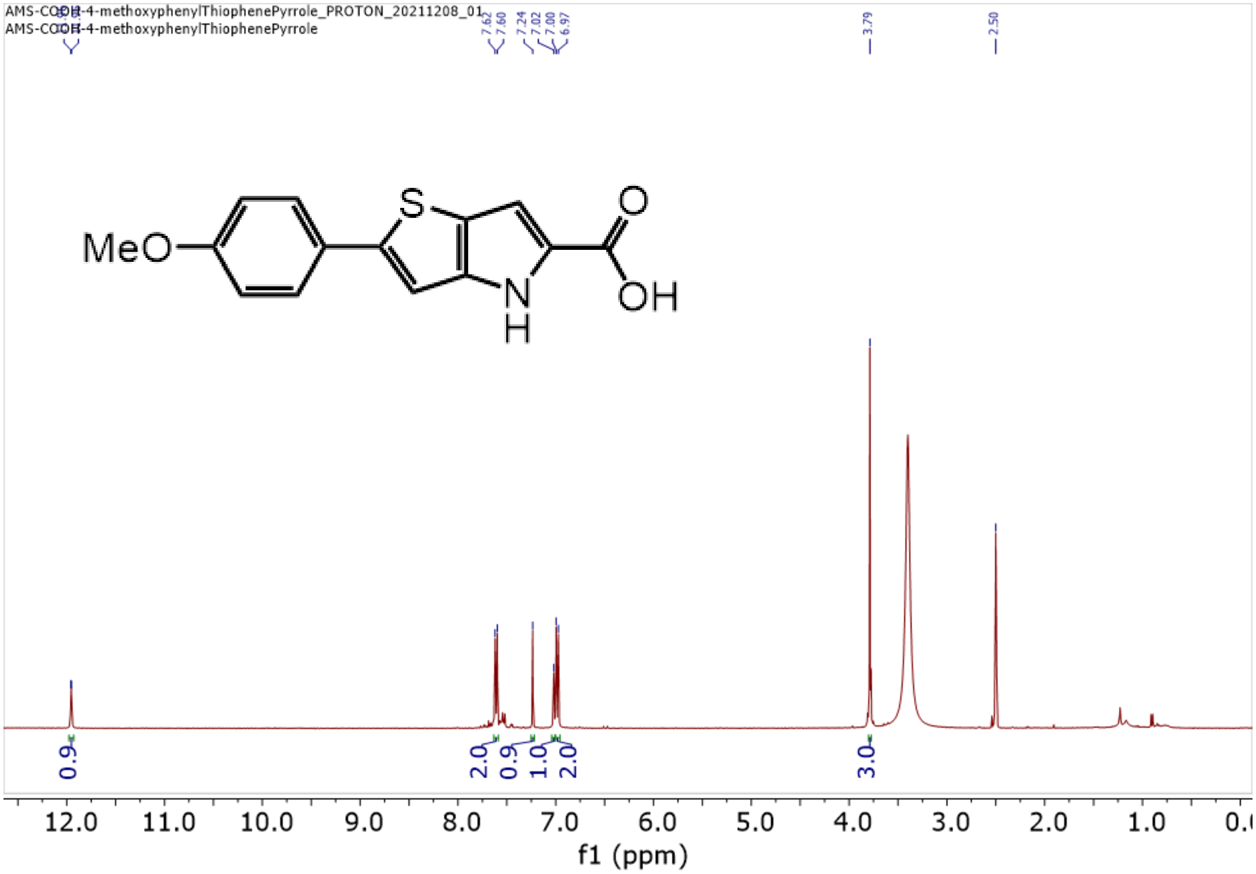

Figure S42: ^{1}H NMR of compound **S1c** in DMSO

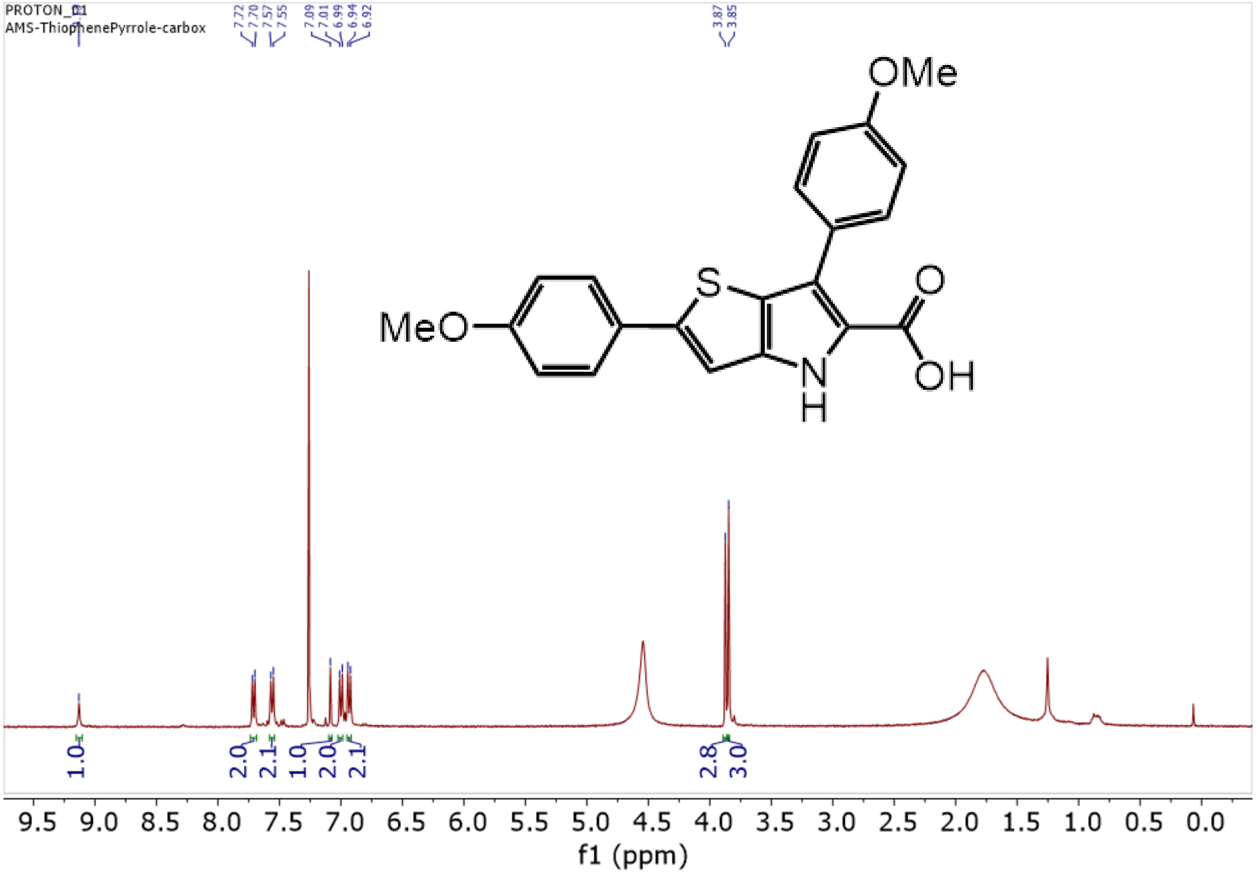

Figure S43: ^{1}H NMR of compound **S2d** in $CDCl_3$

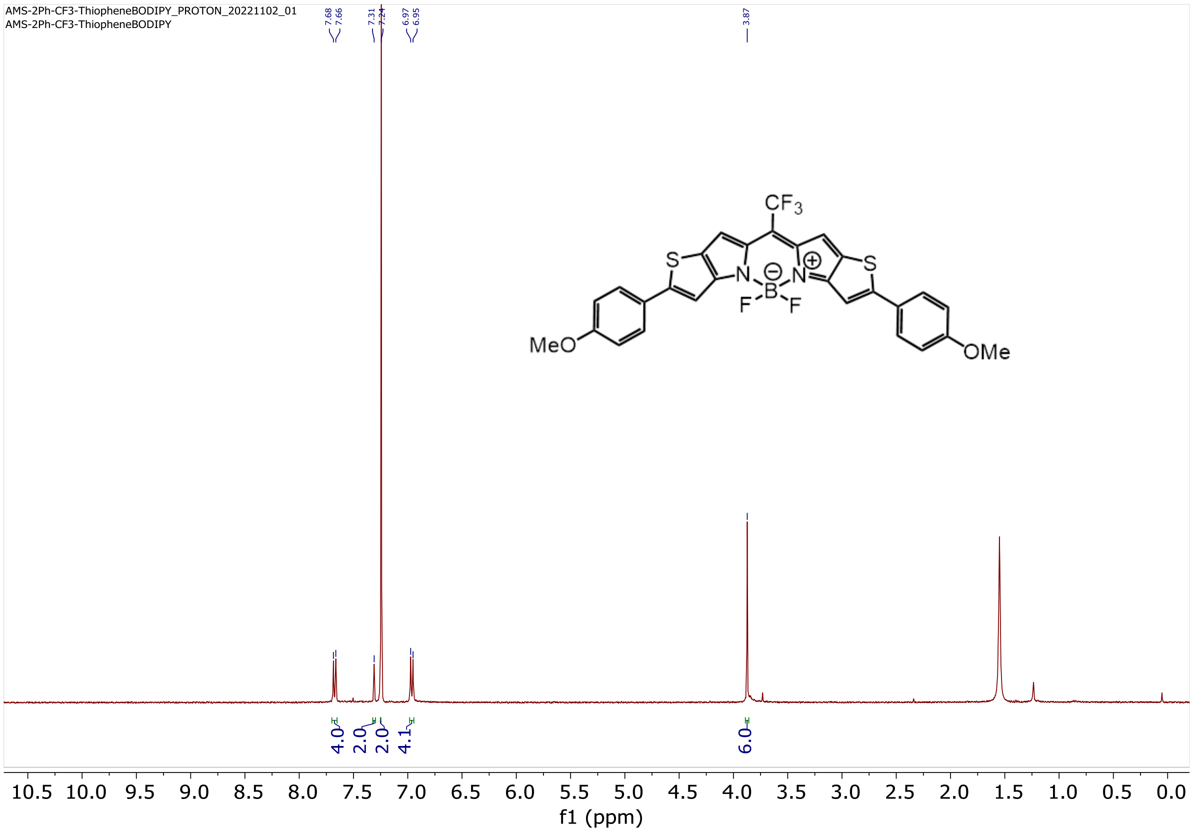

Figure S44: ^{1}H NMR of **BODIPY-H-H** in $CDCl_3$

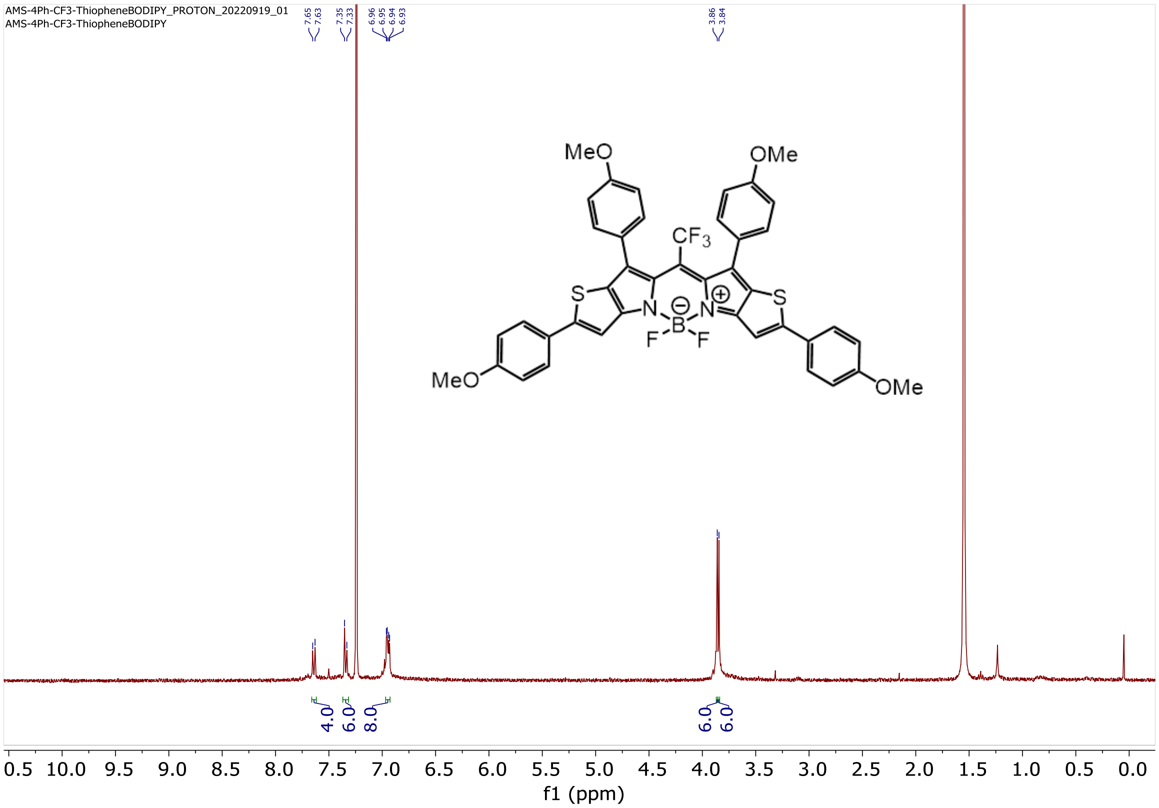

Figure S45: ^{1}H NMR of **BODIPY-Ph-H** in $CDCl_3$

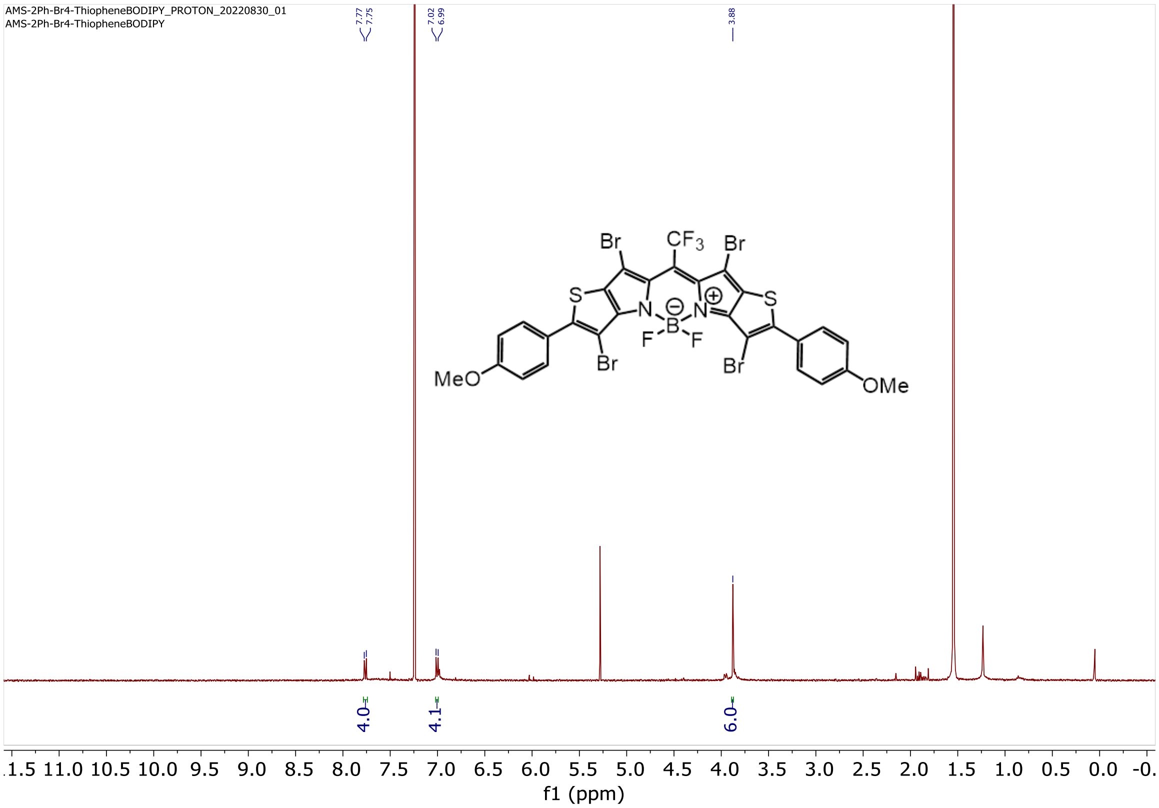

Figure S46: ^{1}H NMR of **BODIPY-Br-Br** in $CDCl_3$

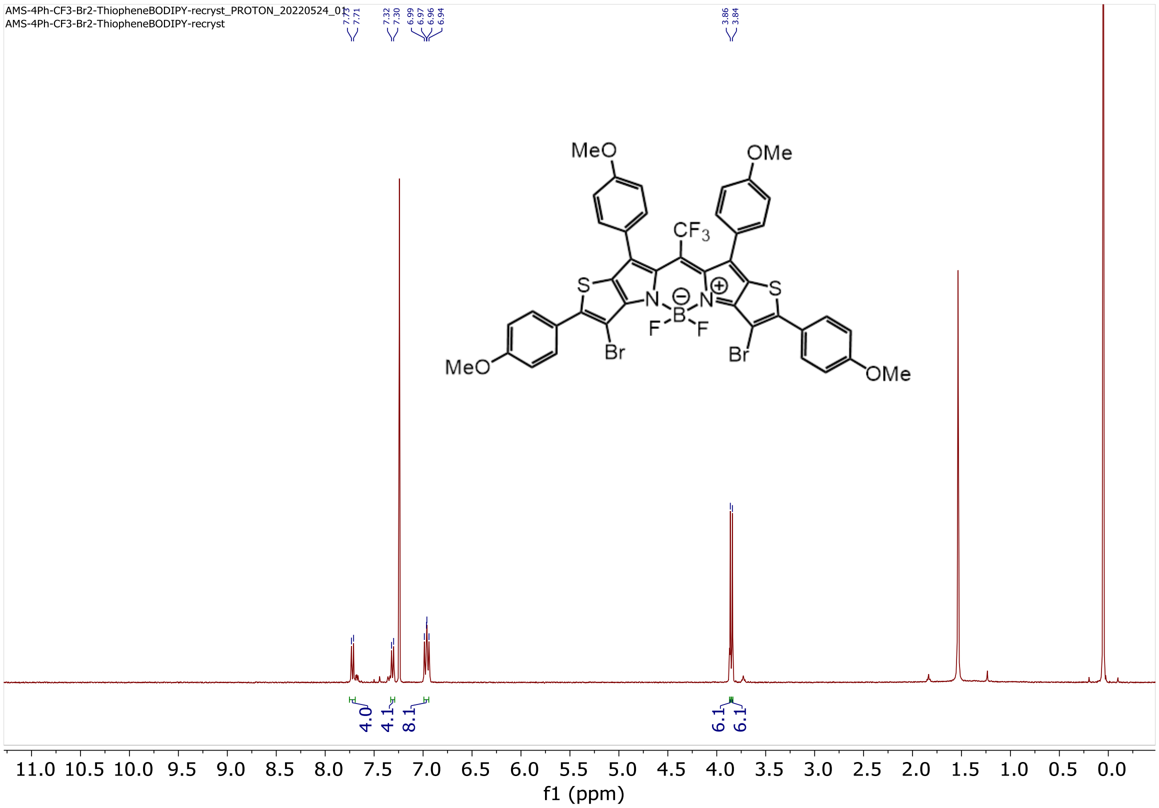

Figure S47: ^{1}H NMR of **BODIPY-Ph-Br** in CDCl$_3$

^{13}C NMR Data

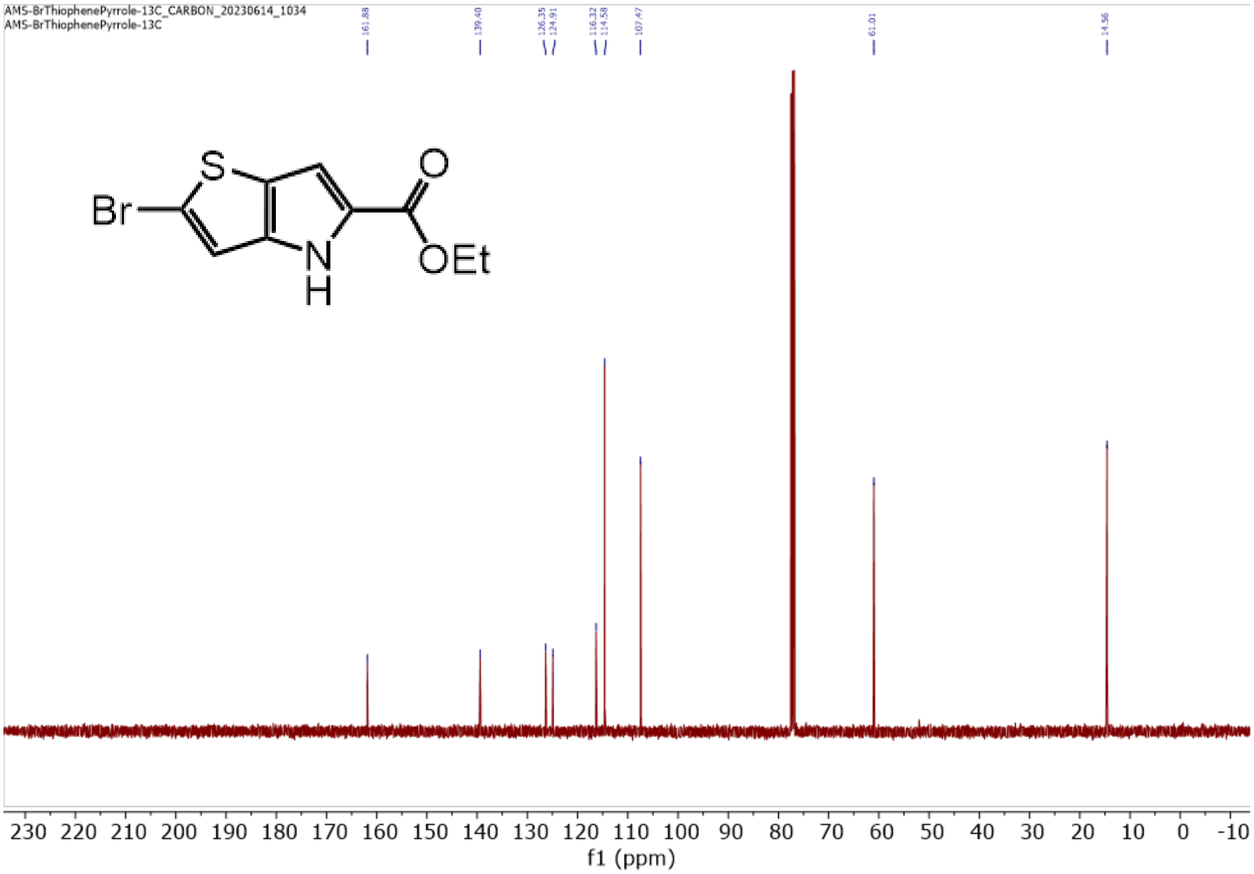

Figure S48: ^{13}C NMR of compound **S1a** in $CDCl_3$

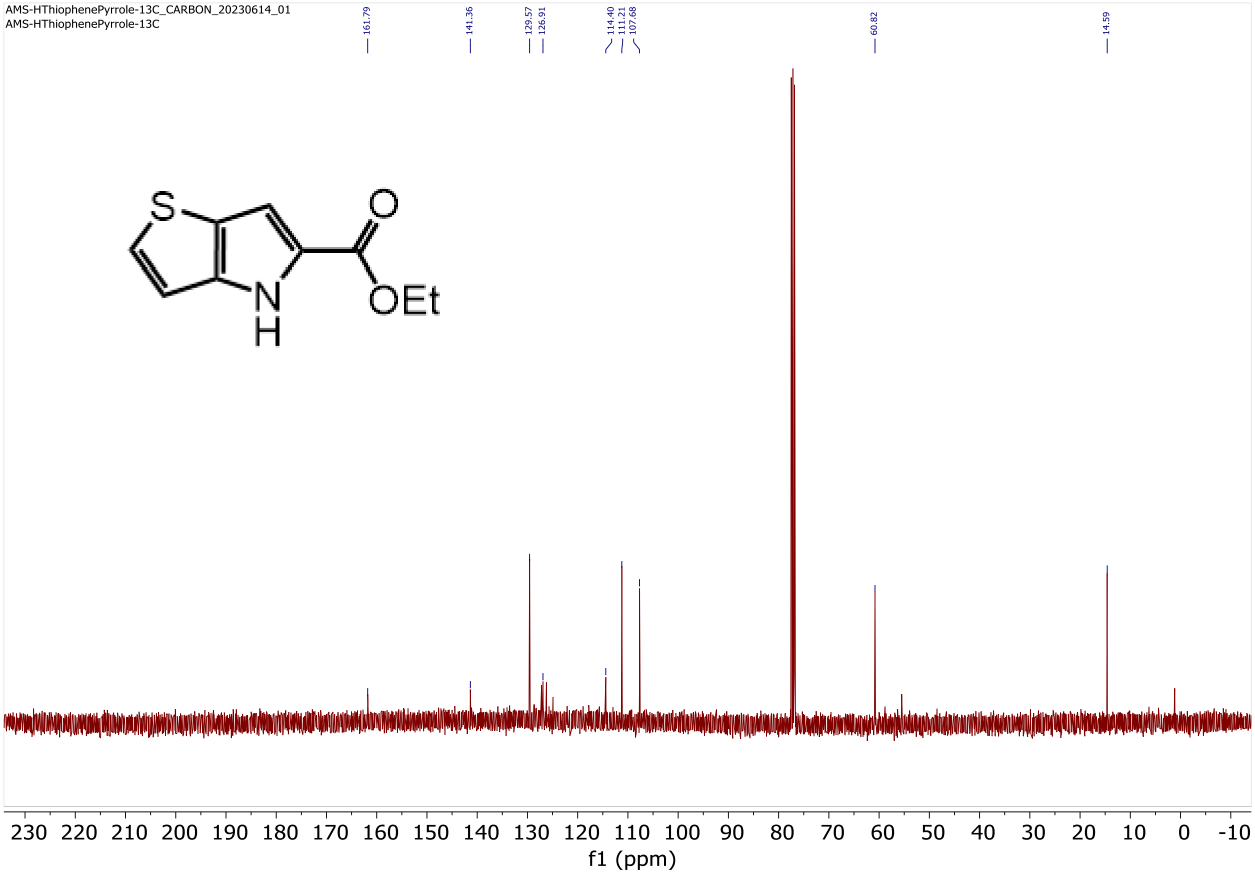

Figure S49: ^{13}C NMR of compound **S2a** in $CDCl_3$

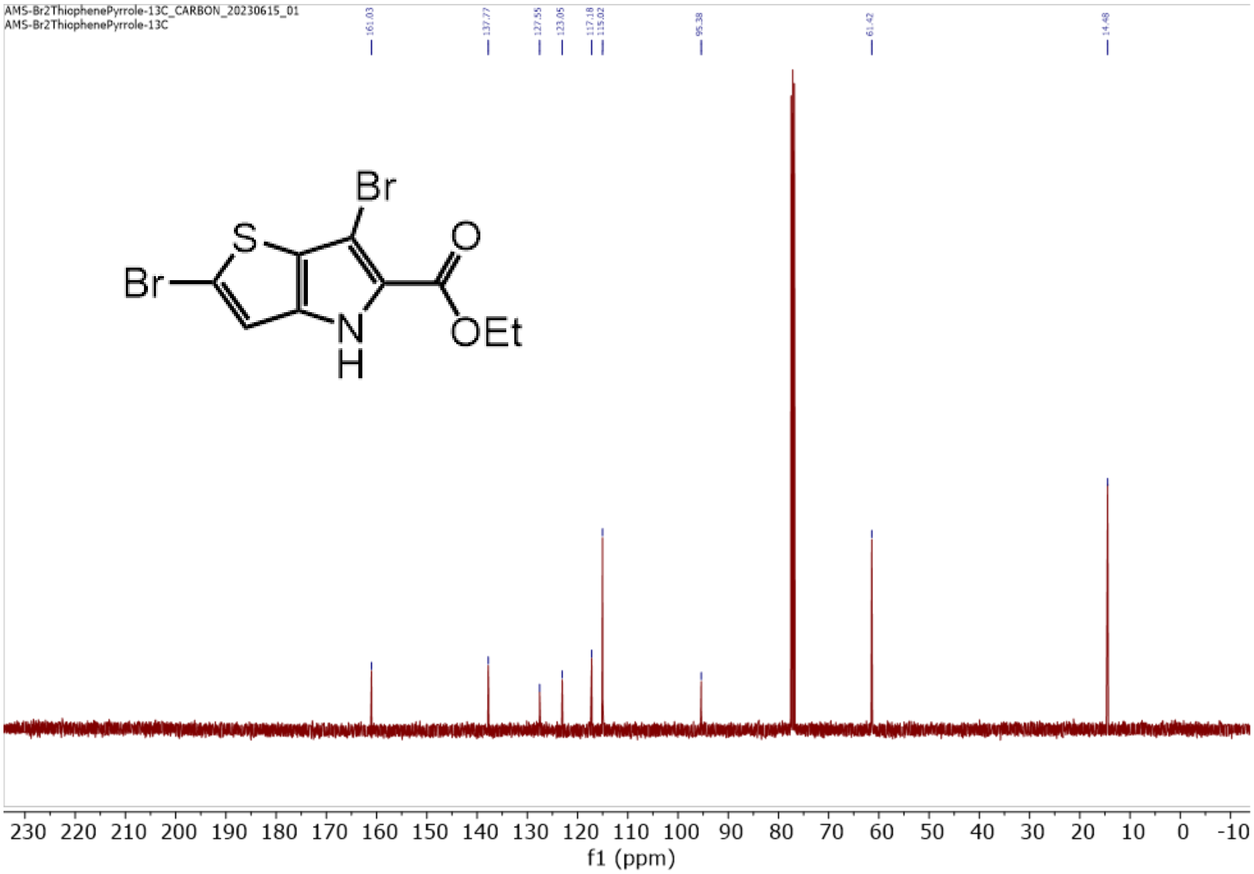

Figure S50: ^{13}C NMR of compound **S2b** in $CDCl_3$

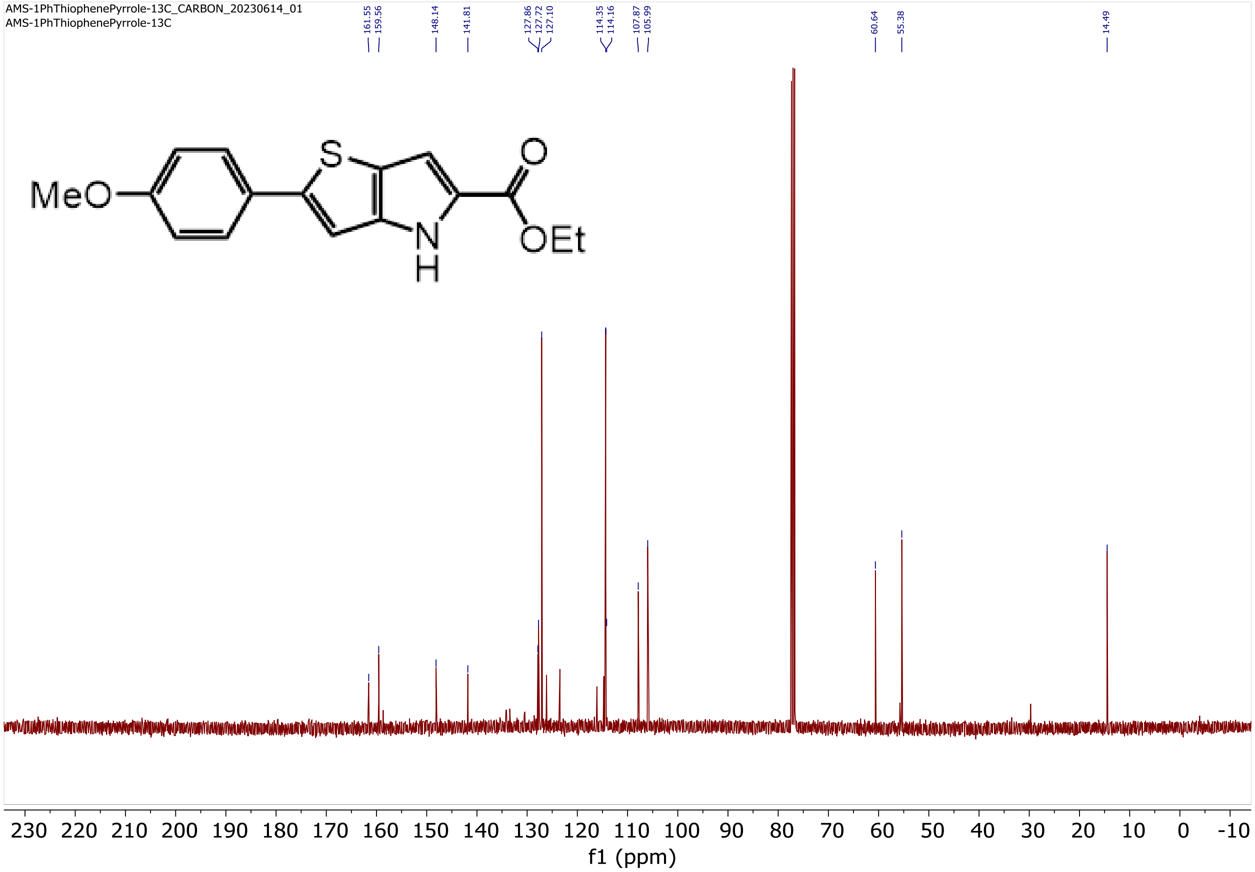

Figure S51: ^{13}C NMR of compound **S1b** in $CDCl_3$

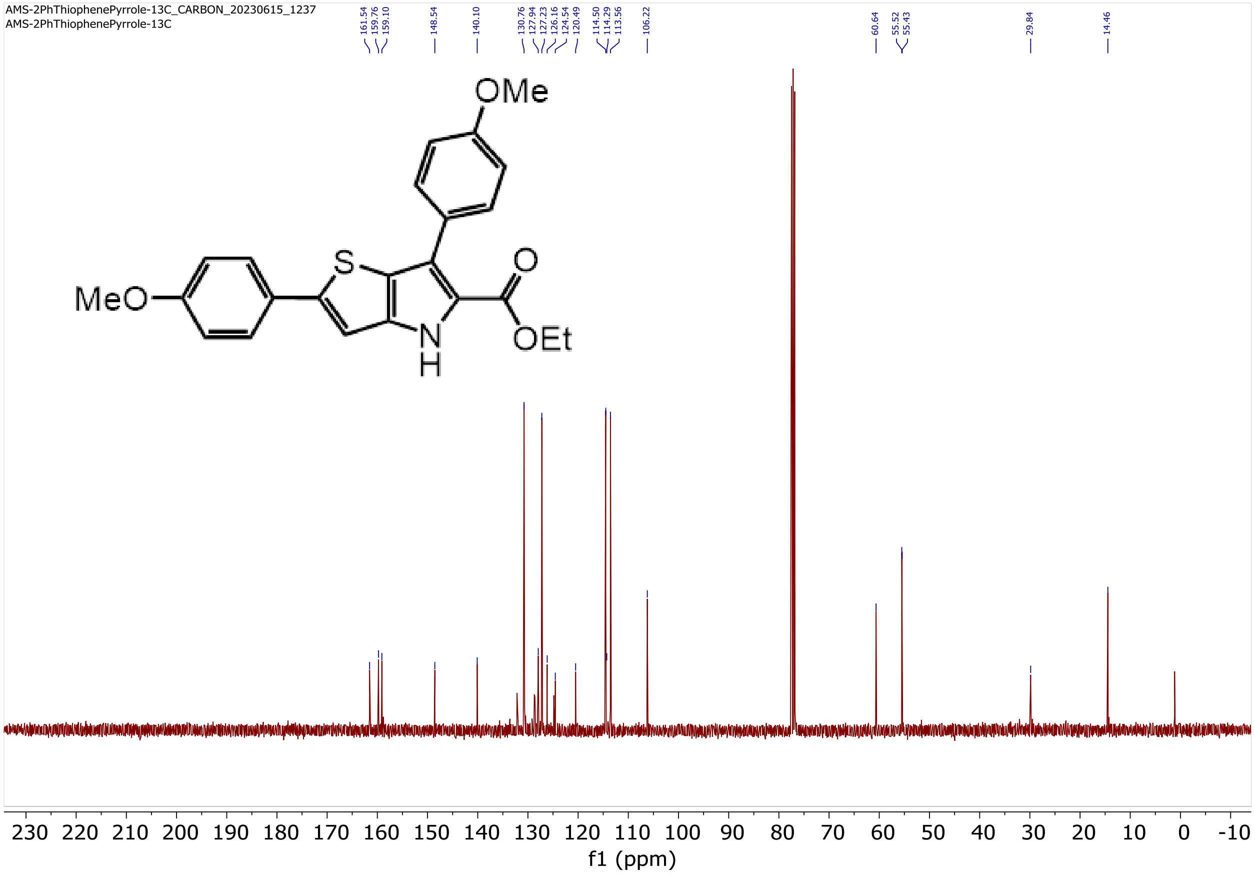

Figure S52: ^{13}C NMR of compound **S2c** in $CDCl_3$

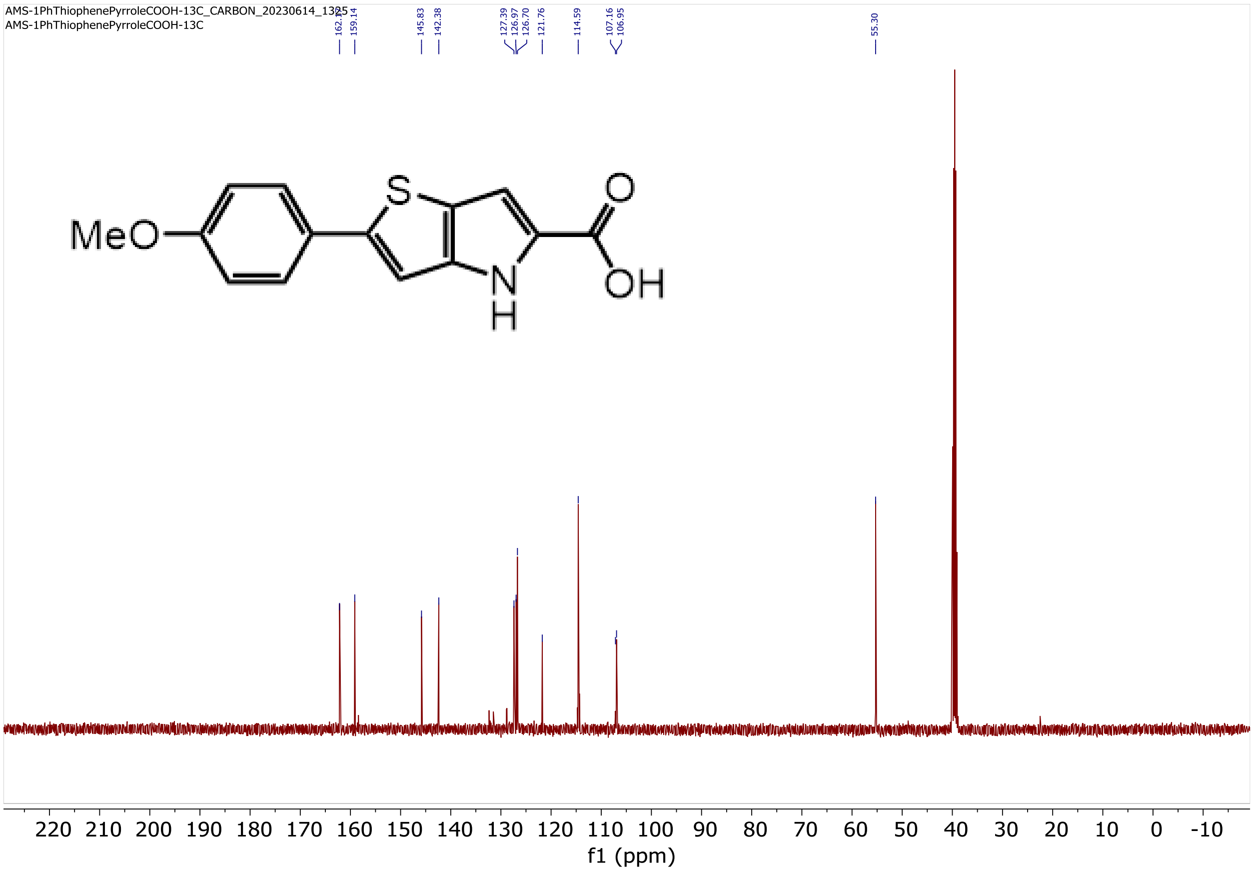

Figure S53: ^{13}C NMR of compound **S1c** in DMSO

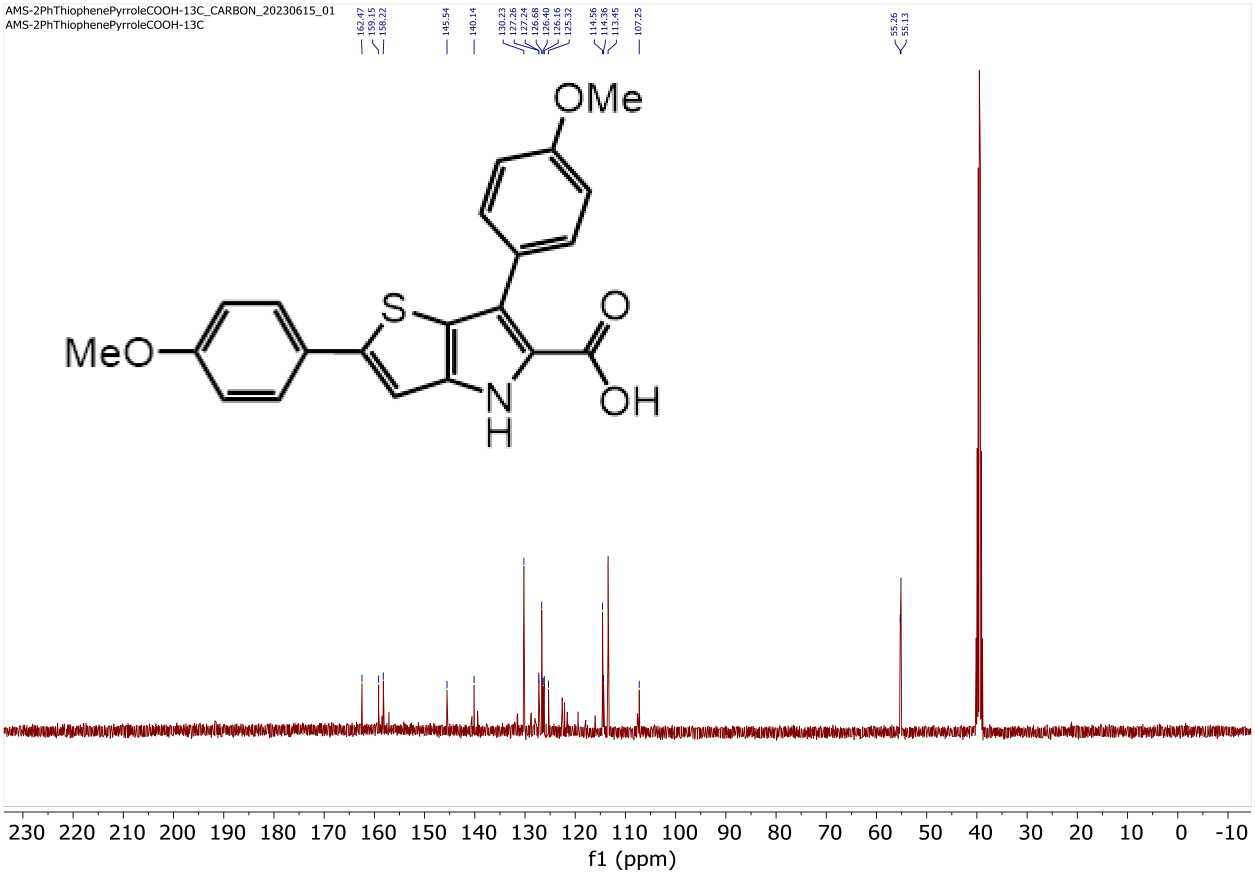

Figure S54: ^{13}C NMR of compound **S2d** in DMSO

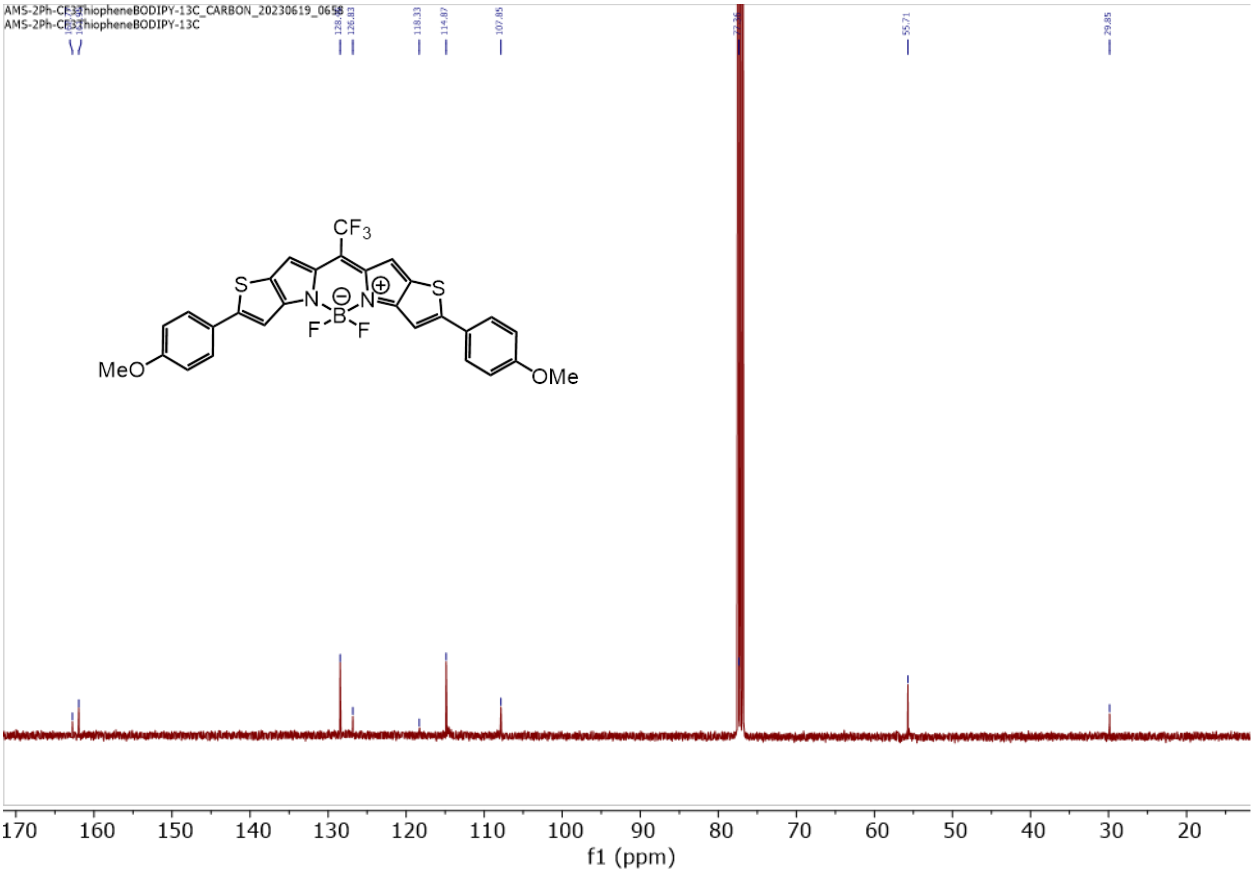

Figure S55: ^{13}C NMR of **BODIPY-H-H** in $CDCl_3$

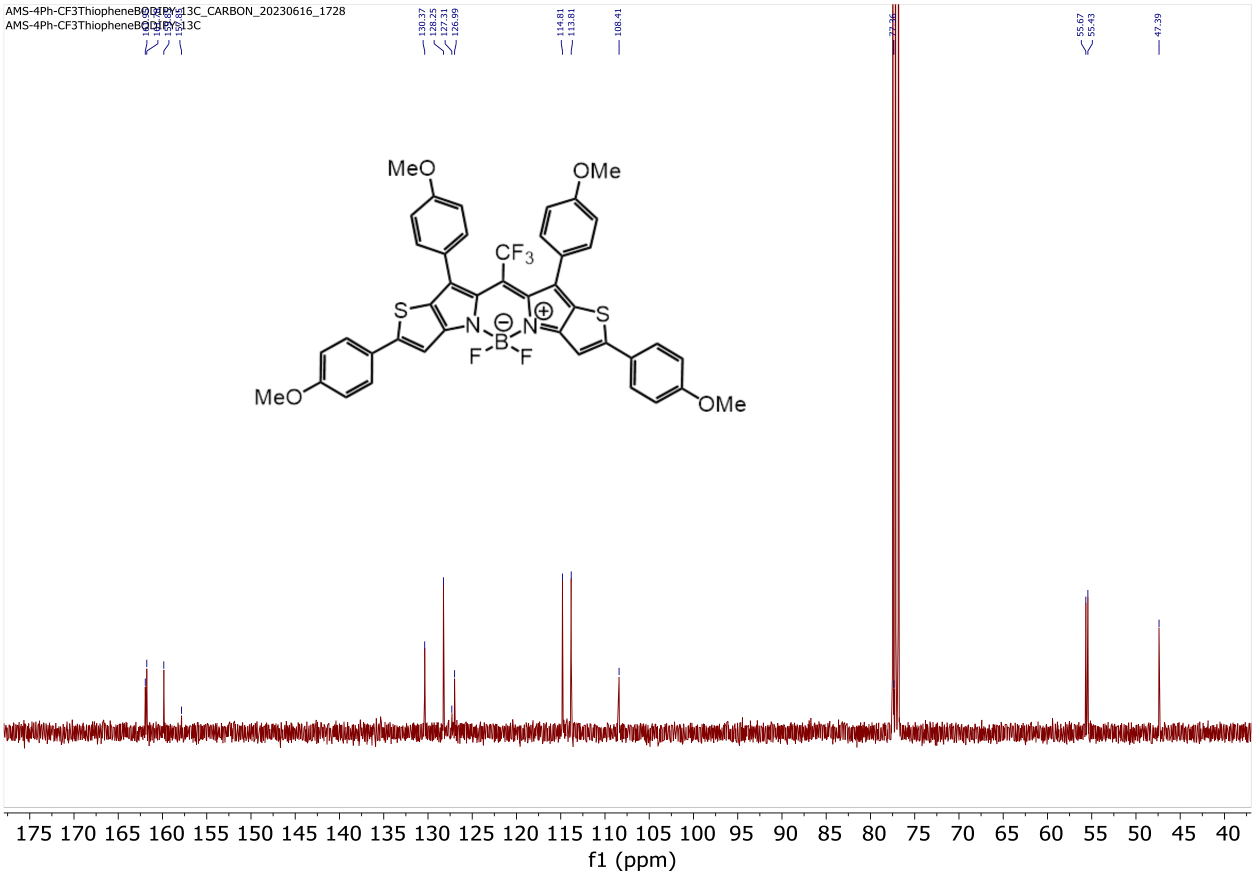

Figure S56: ^{13}C NMR of **BODIPY-Ph-H** in $CDCl_3$

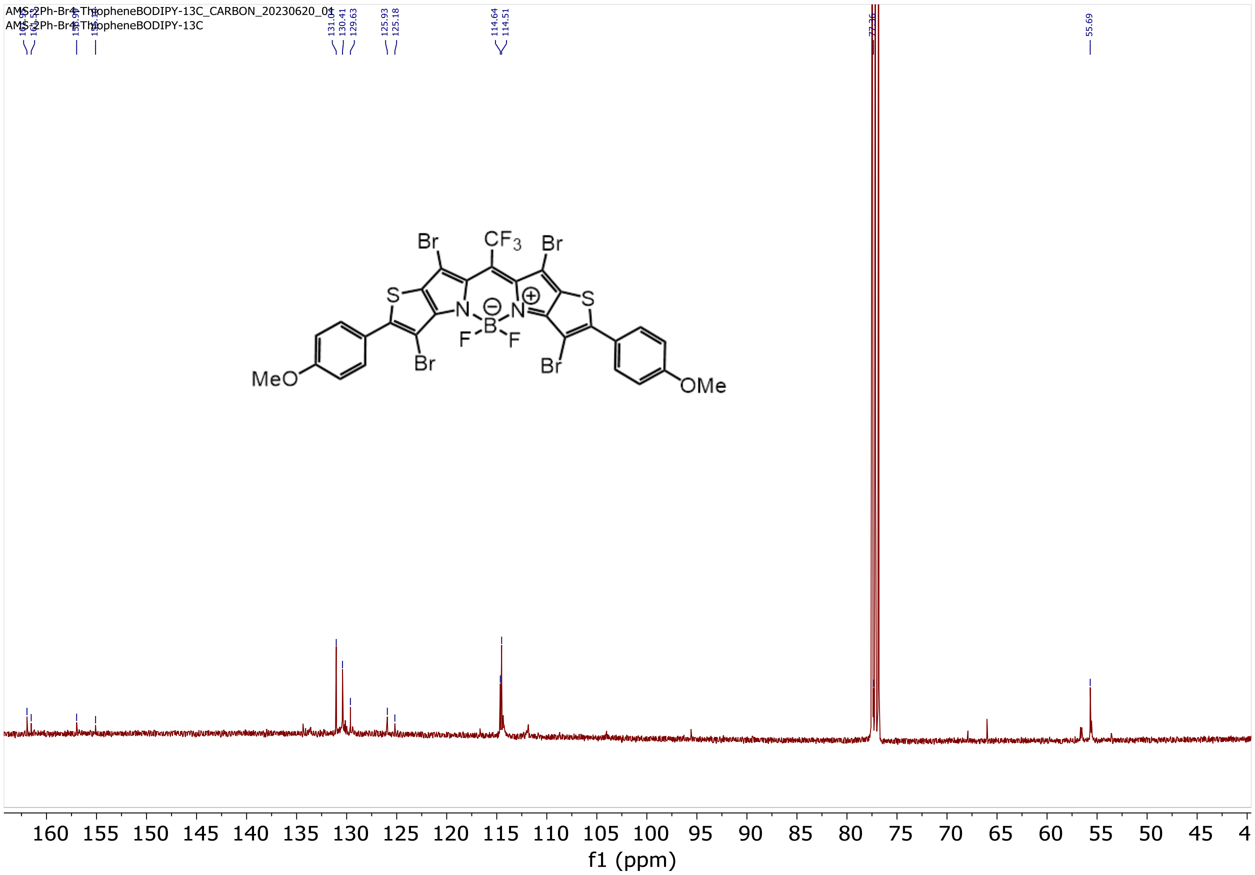

Figure S57: ^{13}C NMR of **BODIPY-Br-Br** in $CDCl_3$

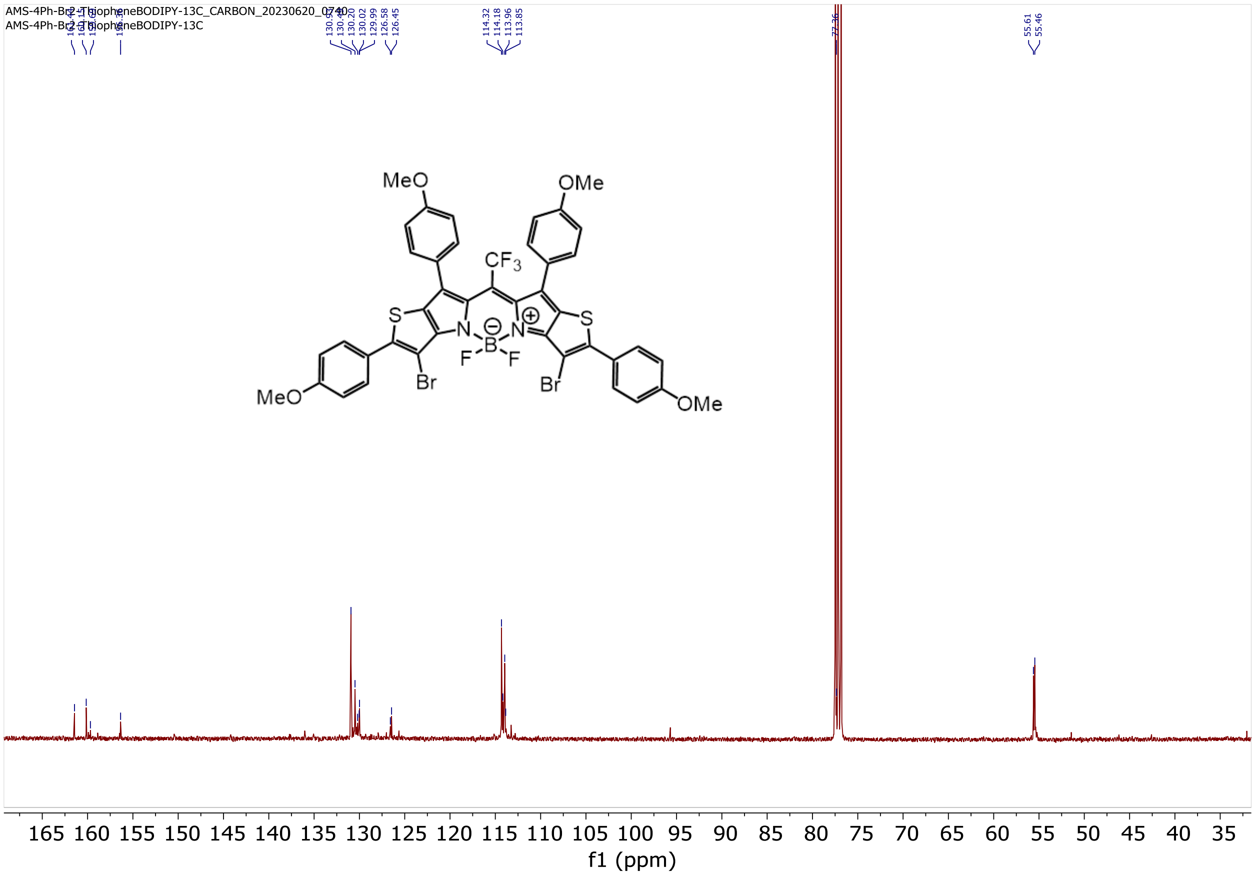

Figure S58: ^{13}C NMR of **BODIPY-Ph-Br** in $CDCl_3$

REFERENCES

S1. Pang, Y., Fan, S., Wang, Q., Oprych, D., Feilen, A., Reiner, K., Keil, D., Slominksy, Y., Popov, S., Zou, Y., Strehmel, B. Ange. Chem. .Int. Ed. 2020, 59, 11440

S2. Bonardi, A., Bondardi, F., Noirbent, G., Dumur, F., Dietlin, C., Gigmes, D., Fouassier, J., Lalevée, J. Polym. Chem. 2019, 10, 6505

S3. Zhou, J.; Pitzer, L.; Ley, C.; Rölle, T.; Allonas, X.. Polym. Chem. 2022, *13*,47, 6475–6483.

S4. Stafford, A., Ahn, D., Raulerson, E., Chung, K., Sun, K., Cadena, D., Forrister, E., Yost, S., Roberts, S., Page, Z. *J. Am. Chem. Soc.* 2020, *142*, 34, 14733

S5. Stafford, A., Ahn, D., Raulerson, E., Chung, K., Sun, K., Cadena, D., Forrister, E., Yost, S., Roberts, S., Page, Z. *J. Am. Chem. Soc*. **2020**, *142*, 14733

S6. Narayanan, M., Kodali, G., Singh, V., Velvadupa, V., Stanley, R. *Journal of Photochemistry and Photobiology A: Chemistry* **2012**, 249, 9–14

S7. Allen, M. J.; Page, Z. A. Tracking Photocuring via ATR-FT-IR with Illumination through the ATR Element. *Spectrosc. Appl. Noteb*. **2020**, *35*, 78.

S8. Thorat, K. G.; Kamble, P.; Ray, A. K.; Sekar, N. Novel Pyrromethene Dyes with N-Ethyl Carbazole at the Meso Position: A Comprehensive Photophysical, Lasing, Photostability and TD-DFT Study. *Phys. Chem. Chem. Phys*. **2015**, *17*, 17221–17236.

S9. Le, A. K.; Bender, J. A.; Arias, D. H.; Cotton, D. E.; Johnson, J. C.; Roberts, S. T. Singlet Fission Involves an Interplay between Energetic Driving Force and Electronic Coupling in Perylenediimide Films. *J. Am. Chem. Soc*. **2018**, 140, 814–826.

S10. Azzaro, M. S.; Le, A. K.; Wang, H.; Roberts, S. T. Ligand-Enhanced Energy Transport in Nanocrystal Solids Viewed with Two-Dimensional Electronic Spectroscopy. *J. Phys. Chem. Lett*. **2019**, 10, 5602–5608.

S11. Java-Based Graphical User Interface for the R Package TIMP. *Journal of Statistical Software* **2012**, *49*, 1–22. https://doi.org/10.18637/jss.v049.i03.

S12. Van Stokkum, I. H. M.; Larsen, D. S.; van Grondelle, R. Global and Target Analysis of Time-Resolved Spectra. *Biochimica et Biophysica Acta (BBA) - Bioenergetics* **2004**, *1657*, 82–104. https://doi.org/10.1016/j.bbabio.2004.04.011.

S13 Baluschev, S.; Yakutkin, V.; Wegner, G.; Minch, B.; Miteva, T.; Nelles, G.; Yasuda, A. Two Pathways for Photon Upconversion in Model Organic Compound Systems. *Journal of Applied Physics* **2007**, *101*, 023101.

S14 Roberts, S. T.; Schlenker, C. W.; Barlier, V.; McAnally, R. E.; Zhang, Y.; Mastron, J. N.; Thompson, M. E.; Bradforth, S. E. Observation of Triplet Exciton Formation in a Platinum-Sensitized Organic Photovoltaic Device. *J. Phys. Chem. Lett.* **2011**, *2*, 48–54.

S15. PIKE Technologies. PIKECalc ATR Calculation. https://www.piketech.com/pikecalc/